Multiphase Flow Loop for the Near Horizontal Hydrodynamics Parameters Measurement: Design, Construction, and Commissioning

by

Thiago Sauma Gomes, B.Sc.

A Thesis

In

Petroleum Engineering

Submitted to the Graduate Faculty
of Texas Tech University in
Partial Fulfillment of
the Requirements for
the Degree of

MASTER OF SCIENCE

Approved

Dr. Ekarit Panacharoensawad
Chair of Committee

Dr. Lloyd Heinze

Mr. Denny Bullard

Mark Sheridan
Dean of the Graduate School

August, 2016

ACKNOWLEDGMENTS

My most sincere gratitude goes to my advisor Dr. Ekarit Panacharoensawad for his incredible patience and support throughout all the stages of this work. Without him, none of this would be possible. I came to his office countless times and he was always willing to help me with everything.

I would also like to thank Denny Bullard, PE and Lloyd Heinze, PhD to serve as my committee members.

God, my girlfriend Thais and my family also played a key role in this project giving me moral support during all this stage of my life.

I am also thankful to Mr. Joe Mcinerney for his help in various laboratory technique and operation; Mr. Enrique Torres and Mr. Raymond Eghorieta, for their collaboration during the building and testing of the facility; Mr. Yeqin Wang for his help on the electronic circuit and wiring; Mr. Scott Graham for his kind suggestion in various construction and measurement techniques; Ms. Yawei Cheng and Ms. Ruonan Wu for their participation in some laboratory operation. Last but not least, I would like to emphasize that this work has been done successfully with a great teamwork from Mr. Gabriel Carestiato who participate in almost all the steps in the facility design, construction, and conducting tests.

I also would like to thank the Brazilian Government, under CAPES sponsorship, which provided me financial assistance throughout my stay in the United States.

TABLE OF CONTENTS

ABSTRACT

The state-of-the-art laboratory scale flow loop was designed and constructed in this study. The flow loop allows the measurement of two-phase gas-liquid and three-phase gas-oil-water hydrodynamics and heat transfer characteristic through visualization and heat transfer sections. The inner pipe diameter of 38.1-mm (1.5 in) and length of 6.70-m (21.98-ft) is selected to allow a capability on up-scaling the laboratory results to the related multiphase flow phenomena in horizontal well, subsea, and on-shore pipeline. The well-thought-out design of the flow loop allows convenient operation of 1) liquid holdup measurement, 2) stable temperature control of the test fluid in the range of 5 to 60 °C (41 to 140°F), 3) precise flow rate measurement and control, 4) absolute pressure inside the test section, and 5) Taylor bubble speed measurement.

This flow loop is designed to be capable of conducting hydrodynamics and heat transfer tests for air/high viscosity oil/water three-phase flow, air/oil and air/water two-phase flow, and single-phase flow of air, water, or oil in a pipe. To ensure that the constructed flow loop is capable of the hydrodynamics test of various flow pattern, the hydrodynamics test on air-water two-phase flow are conducted and compared to the existing theories. The flow pattern map for air-water cases are checked against Taitel and Dukler (1976) model prediction. The measured liquid holdup, slug frequency, translational velocity, slug liquid holdup, drift velocity and slug length are compared against available theoretical calculations. The comparison results show that the developed testing procedures and data analysis methods are reliable and can be used as based cases for further research.

LIST OF TABLES

LIST OF FIGURES

NOMENCLATURE

Variables

A	*Area* [m^2]
C_o	*Flow Distribution Coefficient* [-]
D	*Pipe Diameter* [m]
D	*Pipe Hydraulic Diameter* [-]
$\vec{F}$	*Sum of the Body Forces Applied to the Phase* [N]
F	*Fanning Friction Factor* [-]
f_S	*Slug Frequency* [Hz]
h_F	*Liquid Film Height* [m]
g	*Gravitational Acceleration* [m/s^2]
H_L	*Average Liquid Holdup* [-]
H_{LLS}	*Liquid Holdup in Slug Body* [-]
H_{LTB}	*Liquid Holdup in Taylor-Bubble Region* [-]
L	*Pipe Length* [m]
L_S	*Slug Length* [m]
$\dot{m}$	*Mass Flowrate* [kg/s]
P	*Pressure* [Pa]
q	*Volumetric Flowrate* [m^3/s]
r	*Pipe Radius* [m]
S	*Length* [m]
T	*Temperature* [°F]
t	*Time* [s]
T_U	*Slug Unit Time Period* [s]
u	*Velocity in x-Direction* [m/s]
$\vec{V}$	*Velocity Vector* [m/s]
v	*Velocity in y-Direction* [m/s]
v_d	*Drift Velocity [m/s]*
v_m	*Mixture Velocity [m/s]*

v_t	*Translational Velocity [m/s]*
v_{SG}	*Gas Superficial Velocity* [m/s]
v_{SL}	*Liquid Superficial Velocity* [m/s]
x	*Liquid Pick-up Rate* [kg/s]
w	*Velocity in z-Direction* [m/s]
z	*Coordinate of the z-axis*

Greek Symbols

α	*Gas Void Fraction* [-]
ε	*Pipe Roughness* [m]
λ_L	*No-Slip Liquid Holdup* [-]
μ	*Dynamic Viscosity* [Pa.s]
ρ	*Density* [kg/m^3]
τ	*Wall Shear Stress* [Pa]

Subscripts

α	*Relative to the Phase*
F	*Liquid Film*
G	*Gas*
GLS	*Gas in Slug Body Region*
I	*Gas-Liquid Interface*
L	*Liquid*
LLS	*Liquid in Slug Body Region*
LTB	*Liquid in Taylor Bubble Region*
o	*Oil*
P	*Pipe*
S	*Slug Body*
U	*Slug Unit*

Dimensionless Number

Re	*Reynolds Number* [-]

CHAPTER I

INTRODUCTION

Gas-liquid two-phase flow and Gas-oil-water flow phenomena play important roles in many industries including the petroleum, chemical and nuclear industries. For oil and gas industry, multiphase flow phenomena are observed in various parts of petroleum production and transportation. These parts include the multiphase flow in horizontal and vertical well, subsea pipeline system, onshore flow line, and cross-country gas pipeline system. Slug flow is one of the most common flow pattern occurring on various type of multiphase flow, especially on the slightly upward inclined pipe, horizontal well, and vertical well. The hydrodynamics of slug flow are complicated and can be affected by various parameters. Several flow variables including gas and liquid flow rates, pipe geometry and fluid properties such as gas and liquid densities, viscosities, and surface tension affect the flow behavior significantly.[1] Precise understanding of two-phase flow characteristics is crucial for the optimal operation of pipeline and downstream facilities.

In the past, the majority of the gas-liquid two-phase flow studies were conducted for low viscosity liquids (mainly water) since heavy oil reserves were almost ignored due to the high production cost and the lack of a proper technology to exploit the resource. Many oil companies started to pay more attention on the extraction of heavier oil during the time where the crude oil price was more than $100 per barrel. The crude oil price dropped starting at the end of 2014 caused the research funding on the high viscosity oil production to be decreased. Yet, petroleum is a non-renewable resource and the exponential growth of the world population demand is inevitably outweighing the available petroleum reserve. Therefore, there is a need to exploit the unconventional petroleum reserve, eventually. One of the global abundance of those reserves, as can be seen from Figure 1, is heavy oil together with extra heavy oil. Along with bitumen and oil sands, they constitute 70% of oil resources worldwide (more than twice of conventional light crude oil).

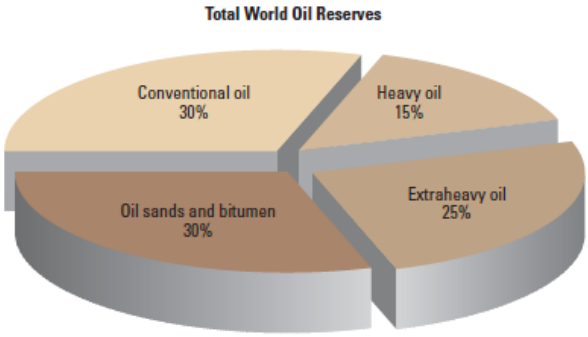

Figure 1.1 Total world oil reserves[2]

Lately, as the interest towards heavy oil production has been expanding, studies and efforts on the effect of viscosity on gas-liquid slug flow has been increasing as well. Recent experimental studies showed the differences in flow behavior between low viscosity oils (< 0.02 Pa.s) and high viscosity oils (> 0.2 Pa.s) for two-phase gas-liquid flow. However, only a few data for medium oil viscosity (between 0.02 Pa.s and 0.2 Pa.s) have been disclosed in the literature so far. Thus, there is a need for the experimental investigation of medium viscosities oils in order to characterize accurately the two-phase flow behavior for the entire range of viscosities. Therefore, the state-of-the-art flow loop is designed and constructed to enable the experimental study on gas/medium viscosity oil two-phase flow and gas/oil/water three-phase flow. The predominant flow pattern for upward and downward inclined flows are intermittent and stratified flows, respectively. Thus, the facility is designed to accommodate these flow patterns. The abilities to measure pressure drop, slug frequency, slug length, and slug liquid hold up are incorporated with the newly constructed facility.

1.1. Main Objective

The main objective is to design, construct and commission the state-of-the-art flow loop that is capable of conducting hydrodynamics and heat transfer experiment for multiphase flow studies including the test on a medium viscosity oil. This work mainly focus on the hydrodynamics testing and design parts of the facility. The facility has been

constructed together with another team member (Mr. Gabriel Carestiato) whose study is mainly focus on the heat transfer part of the facility construction and testing. This thesis[3] along with the Excel file[4] used in the calculation procedures can be downloaded freely from the internet.

1.2. Scope of Work

The scope of this work is to design, construct, and commission the flow loop facility built in the laboratory room 101 of the Department of Petroleum Engineering at Texas Tech University. The design will allow the medium viscosity oil (specifically designed for 0.039 Pa.s < μ_o < 0.166 Pa.s) to be tested with gas and water to generate two/three-phase flow in a horizontal and near horizontal pipe. A Computational Fluid Dynamics (CFD) commercial software (Fluent) is used to provide the calculation and the design of drift velocity experiment. The construction process is considered as the main contribution of this work. The commissioning process was performed by using water to show that common hydrodynamics parameter for air-water flow can be measured and conform to well-known theoretical models.

The most common two-phase flow parameters are pressure gradient, slug unit liquid holdup, slug frequency, slug length, drift velocity, and film profile in the Taylor bubble zone. The reliability of the facility is assessed by comparing the air/water two-phase flow parameter against literature data and the available mechanistic model.

1.3. Thesis Overview

This thesis is divided into six chapters. Chapter I makes a short introduction to the subject covered in this thesis and describes the boarder impact and the importance of this research.

Chapter II covers the theory behind fluids dynamics and its fundamental equations. A review on two-phase gas-liquid flow patterns is performed. The in-depth literature review on gas-liquid slug flow is provided. The previous works have been

reviewed to show the current status of the subject matter and to show the limitation on the experimental data currently available for slug flow hydrodynamics research.

Chapter III explains the calculations procedure used in the two-phase flow hydrodynamics estimation for the facility design. The drift velocity simulation (from CFD software) steps used in the design of the test section is also reported in this chapter.

Chapter IV presents all the details of the flow loop facility design and operating procedure. Chapter V explains the commissioning process, with air/water two-phase flow test result. The theoretical calculation and CFD result based on the procedure explained in chapter III is used to validate the reliability of the constructed flow loop.

Chapter VI describes the conclusions and future recommendations based on this study results.

CHAPTER II

LITERATURE REVIEW

This chapter addresses the main aspects of single-phase flow and its related governing equations. Then, the two-phase gas-liquid flow patterns are briefly discussed. Finally, slug flow model and the experimental data from the literature are reviewed to provide the background for designing the state-of-the-art multiphase-flow loop facility.

2.1. Single-Phase Flow Overview

Single-phase flow phenomena understanding should be the first step to comprehend the main features of multiphase flow. The current status of research of single-phase flow is well developed and dealing with this kind of flow is relatively easy in most of cases. Methods to predict and measure pressure drop, fluid behavior and properties are quite advanced,[1] making the design and the operation of single-phase pipelines simpler.

Other than that, several formulas and correlations used in two-phase flow arise from modifications of single-phase flow. That is the case of superficial velocities, friction factor calculation, Lockhart and Martinelli pressure drop approach- where the total pressure drop is given separately by the contribution of each phase- and the pseudo-phase approach, where the two-phases are mixed together and considered to be just one.

Fluid travelling alone along a pipe can be either laminar or turbulent, depending on the geometry, surface roughness, flow velocity, surface temperature and type of fluid.[1] Laminar flow happens mostly for high viscous fluids at lower velocities and the particles travelling along the pipe flow as individual layers without experiencing mass interaction among them. In addition to that, they tend to maintain their characteristics constant throughout the pipe. On the other hand, in turbulent flow regimes, particles do

not follow a clear path line. There is a random 3-D macroscopic movement of those particles and it occurs mainly for lower viscous liquids, like water.[5]

The nature of turbulent flow is characterized by the fluctuation of the velocity fields chaotically over time.[6] It leads to a mixing and fluctuation of the transported quantities, such as momentum and energy.[7] Besides, pressure drop for turbulent flow correlates stronger with mass flow rate than for the case of laminar flow. This behavior can be explained by the need to provide more energy to keep the violent eddies in motion in the fluid.[6]

Turbulent flow characterization is much harder than laminar flow due to its randomness. Some variables are defined to better understand and analyze it. One of them is the eddy viscosity, also known as turbulent viscosity. The eddy viscosity, different from the actual absolute viscosity, which is a fluid property, depends on the flow, namely the turbulence intensity and the pipe position.[6] Closer to the pipe wall (laminar sublayer), eddy viscosity is negligible (much lower than absolute viscosity). However, it becomes much bigger than the absolute viscosity as it approaches to the center of the pipe, in the turbulent zone. This variable is described as the result of the momentum exchange among particles of adjacent layers caused by turbulent eddies.[8]

The flow regime can be predicted by the Reynolds number, which means, the ratio between inertial forces and viscous forces in the fluid. Expressing it for an internal flow in a circular pipe:

$$Re = \frac{Inertial\ Forces}{Viscous\ Forces} = \frac{\rho v D}{\mu} \tag{2.1}$$

In order to determine in which regime the flow is, Reynolds verified through his experiments that, for circular pipes, laminar flow occurs for $Re < 2000$ and, for turbulent flow, $Re > 2400$. Any value in between those limits falls in the transition between laminar and turbulent flow regimes.[5]

In spite of the current research towards single-phase flow is much more developed than two-phase flow, some gaps still need to be filled to provide more

accurate results. The most used friction factor formulas, for example, should be only used for steady-state flow, whereas, for transient flow, those calculations turn out to be highly inaccurate. Colebrook friction factor formula, one of the most used correlations, does not take into account the effect of the surface's uniformity, which is known to play a major role. In addition, no such regime as completely turbulent flow takes place. Most of times, even a small region next to the pipe wall can develop laminar flow features. It can lead to misleading results when considering turbulent flow as a whole.[9] Thus, more research is still needed on this area.

The governing equations describing single-phase flow- including the continuity equation (mass conservation, Eq. 2.2) and momentum conservation (Navier-Stokes equation, Eq.2.3) -for incompressible, constant density and viscosity fluids in Cartesian coordinates are given as follows:[6]

$$\frac{\partial u}{\partial x}+\frac{\partial v}{\partial y}+\frac{\partial w}{\partial z}=0 \tag{2.2}$$

$$\begin{aligned}
\rho\left(\frac{\partial u}{\partial t}+u\frac{\partial u}{\partial x}+v\frac{\partial u}{\partial y}+w\frac{\partial u}{\partial z}\right) &= \rho g_x-\frac{\partial P}{\partial x}+\mu\left(\frac{\partial^2 u}{\partial x^2}+\frac{\partial^2 u}{\partial y^2}+\frac{\partial^2 u}{\partial z^2}\right)\\
\rho\left(\frac{\partial v}{\partial t}+u\frac{\partial v}{\partial x}+v\frac{\partial v}{\partial y}+w\frac{\partial v}{\partial z}\right) &= \rho g_y-\frac{\partial P}{\partial y}+\mu\left(\frac{\partial^2 v}{\partial x^2}+\frac{\partial^2 v}{\partial y^2}+\frac{\partial^2 v}{\partial z^2}\right)\\
\rho\left(\frac{\partial w}{\partial t}+u\frac{\partial w}{\partial x}+v\frac{\partial w}{\partial y}+w\frac{\partial w}{\partial z}\right) &= \rho g_z-\frac{\partial P}{\partial z}+\mu\left(\frac{\partial^2 w}{\partial x^2}+\frac{\partial^2 w}{\partial y^2}+\frac{\partial^2 w}{\partial z^2}\right)
\end{aligned} \tag{2.3}$$

One of the purpose of these fundamental laws is to obtain the velocity field of the fluid particles. Understanding them is crucial because they are also applied for multiphase flow phenomena. For example, the momentum balance equation for stratified two-phase gas liquid flow is derived from those equations. In addition, the origin of Navier-Stokes equations arises from the application of Newton's second Law together with a pressure term and a fluid stress term caused by viscosity. Moreover, it

can be applied to Newtonian fluids and to both kinds of flows: inviscid- zero viscosity- and viscous flows.

However, it is not possible to solve those fundamental equations analytically for most engineering problems. Nevertheless, it is still possible to get an approximate computer-based solution to the governing equations for a wide range of most robust problems. This is the subject matter of Computational Fluid Dynamics (CFD), which will be briefly discussed later in this work. Pressure gradient calculation for single-phase flow, whose expression is also derived from the fundamental laws, is shown with details in Chapter III.

2.2. Gas-Liquid Two Phase Flow Overview

The occurrence of gas-liquid two-phase flow in the petroleum industry may arise during the production and transportation of oil and gas either in the horizontal, inclined or vertical pipes configuration. Thus, in order to better design separation facilities and flowlines, some important parameters are needed, like the liquid holdup, gas/liquid volume fraction and pressure drop. The reader is referred to Appendix A to review those main two-phase flow variables.

Two-phase flow covers a much higher number of flow variables, different from single-phase flow. Besides, the flow configuration is more complex, harder to comprehend and model. Because of that, the empirical, exact-solution and the numerical simulation approaches are almost impractical or too complicated.[1] Therefore, usual single-phase features like velocity profile, turbulence and boundary layer, are not capable to describe the behavior of such flows.[10]

Among all kinds of two-phase flows (Gas-Liquid, Gas-Solid, Liquid-Liquid and Liquid-Solid), gas-liquid flows are known to be the most complex ones. This difficulty can be explained by the combination of some important features, such as the existence of a deformable interface and the compressibility of one of the phases (gas).[11] Furthermore, quantifying the spatial distribution between the phases is a complex task

because the gas-liquid interface presents most of times a random motion and a complicated shape.[12] The unicity and complexity related to this kind of flow is also due to the use of bigger diameters and longer lengths of the pipes, and many times the hostile environments.[13]

One more complicating factor inherent to gas-liquid flow is related to the influence of one of the phases on the flow of the other one. Consequently, the local variables of each phase, such as velocity and pressure, might fluctuate with time considerably. Thus, measuring an average value of a variable for two-phase flow requires more complicated procedures than the ones applied to the single-phase flow variables.[12]

Another situation that should be dealt when it comes to multiphase flow is related to turbulence. For single-phase flow, this matter is already complex and still considered as an unsolved science issue. Turbulence is still much harder to analyze and model when more than one phase is present in the flow.[14] The larger number of terms to be modeled in the momentum equations enhances this complexity.[15]

The difference related to single-phase flow becomes still more problematic when it comes to the technology involving multiphase flow. All kinds of flowmeters, for example, pose some uncertainty, even for single-phase flow. Measurement of the flow stream is more complicated when there is a mixing of air in a liquid stream. Coriolis flow meter is known to be one of the best solutions for that, even though they still present some accuracy problems. [16]

Not only flow meters but also differential pressure transmitters pose several complications when dealing with multiphase flows. On one hand, both the flow structure and the relationship between pressure and flow rate in the measurement devices for single-phase flow are known, providing accurate results. On the other hand, those relationships are more complicated when more than one phase is present. This can be explained by the input of new parameters to the flow, such as the phase's velocities and volumetric fraction of each phase. Most of times solutions adapted from single-phase

measurements are still implemented, even though a lot of effort has been made towards the developing of multiphase flow technologies recently.[17]

2.2.1. Flow Pattern Classifications

Interaction between surface tension and gravitational forces causes gas-liquid two-phase flow to present several patterns.[18] Flow patterns can be understood as the several configurations that each of the phases flowing simultaneously in the pipe can geometrically be set.[1]

These flow regimes are dictated by the pipeline configuration (e.g. diameter, inclination) and by the operating conditions (e.g. superficial gas and liquid velocities, pressure and temperature).[19]The next figures show the flow patterns encountered in horizontal and slightly inclined pipes and in vertical and sharply inclined pipes, respectively:

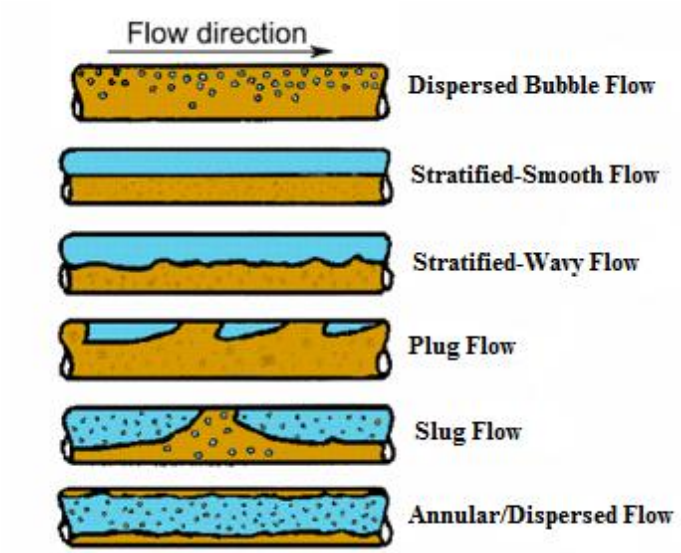

Figure 2.1 Flow Pattern Existent in Two-Phases Liquid-Gas Horizontal Flow[11]

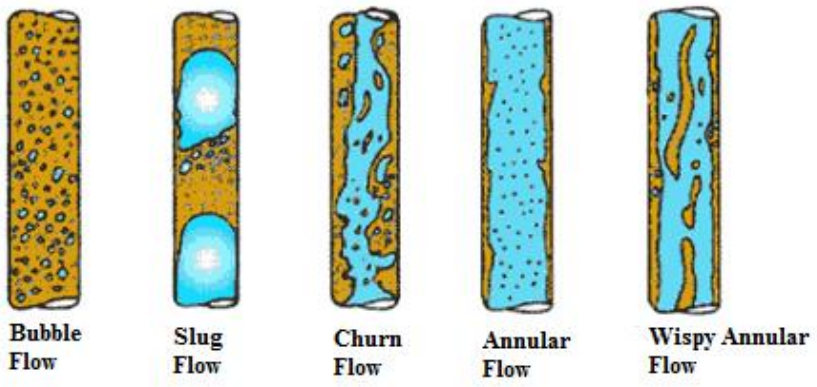

Figure 2.2 Flow Pattern Existent in Two-Phases Liquid-Gas Vertical and Sharply Inclined Flow[11]

A powerful model, developed in 1976, to calculate the gas-liquid flow pattern for horizontal and near horizontal flow ($\pm 10°$) was implemented by Taitel and Dukler.[20] Superficial gas velocity (v_{SG}) and superficial liquid velocity (v_{SL}) are plotted to define the transition boundaries between the flow regimes. In the next figure, the transitions between dispersed bubble flow, annular flow, stratified flow and intermittent flow are shown:

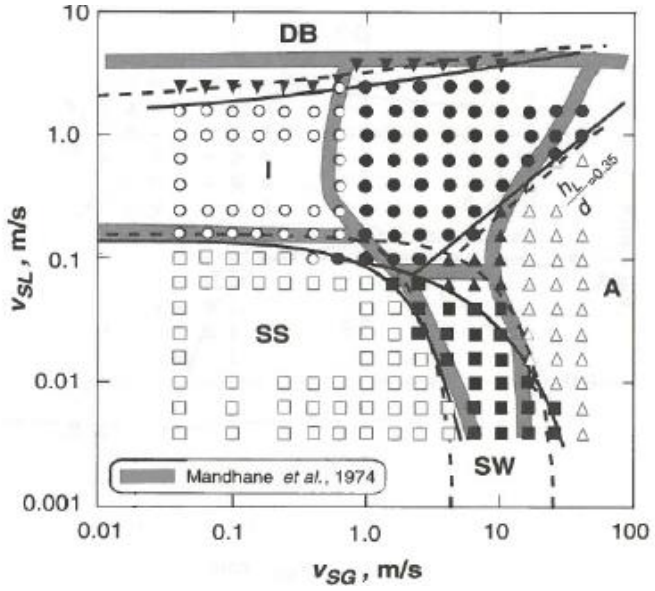

Figure 2.3 Taitel and Dukler (1976) Flow Pattern Map for Horizontal Flow[1]

2.2.2. Horizontal and Near-Horizontal Flow Patterns

Prediction of flow patterns for horizontal and inclined flows is a harder task than for vertical flow. This might be explained due to the asymmetry caused by gravity, acting perpendicularly to the pipe[17] and differences in density, which makes the phases to separate. The heavier phase (liquid) accumulates at the bottom of the pipe, underneath the gas phase. Under those circumstances, the appearance of a form of stratified flow becomes very common.[18] Below, the flow patterns for horizontal and near-horizontal flow are briefly described:

Stratified Flow: this flow pattern is associated with lower gas and liquid flow rates. The phases involved are separated by a horizontal interface, where gas stays on the top and liquid on the bottom of the pipe. Gravity is the drive force of this regime. At lower gas velocities, the gas-liquid interface is smooth and the Stratified Smooth regime takes place. As the gas flow rate goes up, stable waves form at the interface and the Stratified Wavy pattern occurs.[1,17]

Intermittent Flow: this flow pattern takes place at higher gas velocities. A rupture of the gas-liquid interface occurs at some points of the flow and droplets can be observed inside the gaseous phase**.**[17] This regime is characterized by alternate flows of gas pockets and liquid slugs bridging the entire cross sectional area of the pipe. A film region underneath the gas pocket is present. The liquid slug, which travels at a much higher speed, overruns the slow liquid film region ahead of it. [1] Intermittent flow is split into Slug and Elongated-Bubble flow patterns. Their flow mechanism are the same, but the Elongated-Bubble is considered a threshold of Slug Flow, when there are no entrained bubbles in the liquid slug.[1]

Annular Flow: this flow regime occurs at very high gas flow rates. A liquid film forms around the pipe periphery whereas a gas core flows at very high velocities in the center. The liquid film height is bigger at the bottom of the pipe than at the top. The interface is unstable and a considerable amount of droplets is kept suspended in the gas core.[21]

Dispersed-Bubble Flow: it occurs at very high liquid velocities. The gas phase is dispersed as discrete bubbles uniformly across the pipe cross sectional area in the liquid phase (the continuous phase).[18] As a consequence of the high liquid flow rates, the dispersed bubbles are carried out by the liquid phase and both phases flow at the same speed.[1]

2.2.3. Vertical and Sharply Inclined Flow Patterns

The flow patterns for the vertical case will not be covered in depth since the focus of this work is on horizontal and near-horizontal flows. As an informative note, the flow patterns for those kinds of flow are the following: Bubble Flow, Slug flow, Churn Flow and Annular Flow. They can be seen in Figure 2.2.

2.3. CFD Overview

The governing equations describing fluid mechanics- continuity equation (mass conservation, Eq. 2.2) and momentum conservation equations (Navier-Stokes equation, Eq. 2.3) – are too complicated to deal with. They, together with the energy equation, constitute a set of nonlinear, coupled, second order partial differential equations.

An analytic solution for those equations is a hard task, even though it is possible to limit a physical problem to incompressible and inviscid flows (which seldom happens in real life). Nevertheless, this can be overcome by obtaining approximate computer-based solutions to the governing equations. This is the major role of Computational Fluid Dynamics (CFD).

The basic functioning of CFD is to work based on a discrete domain, by transferring the actual continuous problem to a selected grid. In CFD simulations, the software interpolates the values at the grid points to get the solutions for each flow parameter throughout the domain.

The majority of the commercial CFD codes uses the finite-volume or finite-element methods for discretization purposes. For example, the FLUENT code, the one used in this work for drift velocity calculation, applies the finite-volume method.

When it comes to multiphase flow, three different models are available in FLUENT: the volume of fluid (VOF) model, the mixture model, and the Eulerian model. In this work, only the major topics featuring the VOF model and its assumptions will be discussed. For further information regarding the others methods, the reader is referred to the ANSYS Fluent Theory Guide.[7]

As it will be discussed later in this chapter, drift velocity can be obtained from the simultaneous penetration of air into an initially horizontal pipe filled with liquid and the drainage of this liquid.[22] The model that better represents this problem is the Volume of Fluid model, also known as VOF model.

The VOF model works by applying the finite volume method, bringing the original continuous domain problem to a discretized domain, represented by a grid or mesh. This model is best suit for two immiscible fluids where the location surface of study is their interface, which is tracked by the model. In addition, the momentum equations are applied for each fluid simultaneously. Besides, the volume fraction is accounted for at every single point in the computational domain. This model can be also applied to stratified flows, to the motion of large bubbles in a liquid stream and to the tracking of any liquid-gas interface (such as drift velocity).

The volume fraction of a particular phase is added in the computational cell whenever an additional phase is introduced to the problem. The total sum of all volume fractions of each cell throughout the domain should yield the unity. The volume fraction of the gas phase (ratio of the gas volumetric flow rate with respect to the total volumetric flow rate) can be named by α. There are only three possible conditions for a cell inside the computational domain. Either the cell is liquid-full (α=0); it is full of gas (α=1) or it contains both phases ($0<\alpha<1$).

For a gas-liquid flow, the effective viscosity (μ) and density (ρ) at each cell are given respectively by:

$$\mu = \mu_G + \mu_L(1-\alpha) \tag{2.4}$$

$$\rho = \rho_G + \rho_L(1-\alpha) \tag{2.5}$$

Where, μ_G, μ_L, ρ_G and ρ_L are the dynamic viscosities and the density of the gas and the liquid phases, respectively.

The tracking of the interface between the liquid and gas phases is carried out by the solution of a continuity equation of the gas phase. Expressing it in vector form:

$$\frac{\partial}{\partial t}(\alpha\rho_\alpha) + \nabla.\left(\alpha\rho_\alpha\vec{V}\right) = 0 \tag{2.6}$$

The resulting predicted velocity field is shared among the phases once a single momentum equation is solved throughout the domain. The momentum equation for a transient Newtonian liquid, based on the volume fractions of all phases through the density and viscosity properties can be represented in vector form as follows:

$$\frac{\partial}{\partial t}\left(\rho\vec{V}\right) + \nabla.\left(\rho\vec{V}\vec{V}\right) = -\nabla.\left[\mu\left(\nabla.\vec{V} + \nabla.\vec{V}^T\right)\right] + \rho\vec{g} + \vec{F} \tag{2.7}$$

Where $\vec{F}$ represents the sum of other body forces applied to the phases and $\vec{g}$ is the gravity vector.

2.4. Slug Flow Overview

Slug flow is the flow pattern most focused on this work because it is the dominant flow pattern in upward inclined flow and it also occurs in horizontal and vertical pipes over a several set of gas-liquid flow rates.[23] In horizontal and inclined slug flow configurations, gas flows in the topmost part of the pipe due to buoyancy whereas liquid flows in the bottom. There are alternate flows of liquid slugs and gas pockets. The majority of the gas phase can be found in large bullet-shaped gas pockets (named Taylor bubbles). Much faster liquid slugs bridging the entire cross sectional area of the pipe separate them. These slugs also contain small entrained gas bubbles.[1]

Slugs are usually undesired in the field because they can cause significant pressure fluctuations. This might lead to an uneven arrival of gas and liquid at the

processing facilities, causing flooding of the receiving tanks. Separators must be capable of handling the largest possible slugs without significant liquid carry-over in the gas stream.[24] Furthermore, this flow pattern is known to create increases of hydrates deposits and corrosion of the facilities if the flow contains sand.[25] Its intermittent behavior also provokes vibrations and a high-pressure drop along the pipe. This enhances the chance of damaging the pipe supports and bend.[26] Thus, the operator should avoid working at the flowline exit with gas and liquid velocities that fall into the range of slug flow occurrence. This can be done with the aid of flow pattern maps.

The complex nature of this kind of flow is associated to its unstable and random nature in a periodically steady-state condition. This complication makes its hydrodynamics variables harder to analyze. The time averaged velocity profile is well-defined and liquid and gas flow rates remain steady. However, the component mass flow rates, phase velocities and pressures present large variations over time at any pipeline cross sectional area. Furthermore, the instantaneous velocity of slug flow is chaotic, like turbulent flow.[26] A lot of mechanistic models and experimental studies have been carried out in order to achieve a better understanding of the mechanism of slug formation.

The pioneer work to study the unsteady nature of liquid-gas hydrodynamics was conducted in 1975 by Dukler and Hubbard[27] for horizontal and near-horizontal tubes. They created the concept of a slug unit (see Figure 2.4). Slug flow can be represented by a sequence of those slug units with same characteristics traveling at a constant translational velocity. Their model needs two additional input parameters, namely the slug frequency and the liquid holdup in the slug body. They also assume homogeneous no-slip flow in the slug body, which means, gas and liquid in the slug body travel at the same velocity.

Their model is capable of predicting several slug hydrodynamics parameters, such as translational velocity, film velocity as function of time and distance, slug length and surface shape of the film region. The mechanics behind it is based on the observation that the much faster slug body overrides and accelerates the slow liquid film

in motion. The film region is accelerated to the full slug velocity, creating a mixing eddy region located at the front of the slug body.

The pushing gas pocket sheds liquid behind at the same time that liquid from the film is picked up by the slug. A new film zone which decelerates over time is created.[27] Thus, a constant slug length is reached because the rate of picking up and shedding is supposed to be the same for steady-state flow conditions. Pressure drop is caused by losses along two different zones. The first one is the wall friction loss within the slug body region (the frictional loss in the mixing zone is neglected). The second one is the acceleration pressure loss caused by the increase of velocity of the film to the slug body speed.[28]

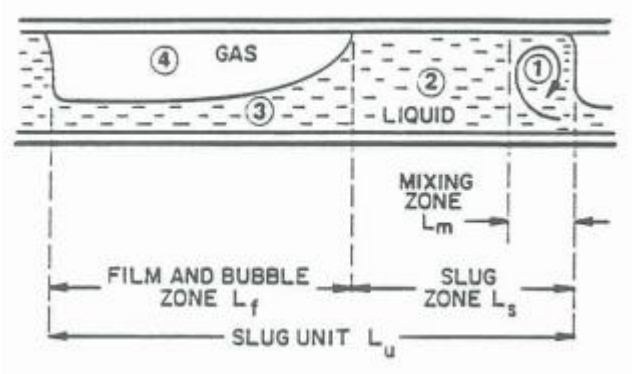

Figure 2.4 Representation of a Slug Unit[29]

An attempt to extend the application of Dukler and Hubbard model to the entire intermittent regime was performed by Nicholson et al.[30] They developed a semi-mechanistic model for horizontal slug flow. It was suggested that the liquid holdup in the front of the film has not necessarily to be the same as in the previous slug body. The length of the slug body is required to predict the average pressure gradient and liquid holdup in the slug unit.

Later on, a unified model that could work for all range of inclination angles was developed by Taitel and Barnea[31] through a comprehensive analysis of slug flow. An interfacial shear stress term (neglected in the previous models) was introduced to account for the gas-liquid interactions along the film zone. They developed two different

methods to predict the pressure gradient across a slug unit. This could be done by applying a force balance along two different zones. The first option is to apply it only on the liquid slug zone (neglecting the pressure drop in the film zone). The second one is to consider the entire slug unity (yielding more accurate results). Liquid and gas velocities in the slug body are not the same in this model, differently from Dukler and Hubbard approach.

Xiao et al.[32] came up with a comprehensive mechanistic model to combine slug flow models for horizontal and near-horizontal pipes. A uniform film thickness along the film zone was adopted to avoid numerical integration. Global pressure drop across a slug unit was taken into account. Correlations for slug length, translational velocity and liquid holdup in the slug body were used as input parameters for the model.

2.5. Slug Flow Hydrodynamic Parameters Literature Review

The review about to be showed tells about the current development on the field of the main slug flow parameters. One of the major gap in gas-liquid two-phase flow research is the uncertainty in several models for calculating hydrodynamics of the high and medium viscosity oil cases. The majority of the existing correlations was only tested for low viscous fluids in horizontal and near-horizontal pipes. Besides, these models do not take into account the combined effect of viscosity and higher pipe inclinations. The exception is the drift velocity.

However, any drift velocity experiment using medium viscous liquid in long inclined pipes has been performed so far. All experiment only calculate drift velocity at one single location. Such experiment could explain how drift velocity behaves along the pipe length for medium viscosity liquids. Furthermore, pressure gradient, slug length, slug frequency and film shape have not been tested for medium and high viscous liquids at higher inclination angles and for downward flow yet. For high viscous oils, tests have been conducted only for near-horizontal pipe angles and for vertical flow.

The motivation to build the state-of-the-art multiphase facility is to produce experimental data needed to fill those gaps of data. Results collected could be used to test the current correlations and models existing in the literature as well. A larger set of data would contribute to expand the understanding of slug flow phenomena.

2.5.1. Slug Length

Many studies carried out in the literature analyzed the slug length for low viscous liquids.[24,33,34,35, 36,37] For flows under such conditions, the mixture velocity shows to have no significant impact on slug length and it can be neglected.[33,34] The generally accepted value for fully developed stable slug length adopted by many authors as being 30D does not work properly for pipe sizes bigger than 50.8-mm (2-in) ID.[34] Furthermore, several researchers identified the statistical distribution of the slug length to be well-fitted by a lognormal distribution.[24 35,36]

Experimental studies conducted on air and water slug flow for near-horizontal pipes show that the superficial liquid and gas velocities affect slug length. It decreases when the superficial liquid velocity increases because the liquid holdup becomes higher. On the other hand, the slug length increases with an increase in the gas superficial velocity for the same liquid superficial velocity.[37]

Recently, experimental studies performed in high viscous oil suggested that slug length decreases as liquid viscosity goes up.[38, 38, 39] Besides, Gokcal[38] claimed that slug lengths observed in his tests turned out to be much shorter than 32D as proposed in previous studies.[40,41] In addition, the slug length decreases for near-horizontal pipe inclinations when the mixture velocity increases.[42] Statistical analyses proved that liquid phase viscosity played a major role on slug length distribution. It deviates from the log-normal distribution observed for low viscous liquids to a truncated positively skewed distribution.[39] For medium viscosity oil, none of the models existing in the literature seems to give a satisfactory result to predict slug length. It might be explained by the fact that none of them consider all possible variables affecting slug length, such as pipe geometry, flow conditions, and fluid properties.[43]

2.5.2. Slug Frequency

Slug frequency phenomenon is random in nature due to flow complexity of slug formation. Poisson probability model is found suitable to model the slug frequency phenomenon.[44] Extensive studies on prediction of slug frequency for low viscous liquids in horizontal and near-horizontal pipes have been reported in the literature.[45,46,47,48, 49, 50,51,52,53,37] Experimental investigation showed that slug frequency does not change with pipe length except in certain slug flow sub-regimes. That is the case of high liquid flow rate and low gas flow rate, and low liquid flow rate and high gas flow rate.

Furthermore, pipe diameter, actual and superficial liquid velocity and the ratio of slip to mixture velocities were found to strongly correlate with slug frequency.[51,53] For near-horizontal pipes, slug frequency increases with increasing the superficial liquid velocity. On the other hand, the frequency of slugs decreases by increasing the gas superficial velocity. This trend can be due to the higher void fraction.[37,54]

Slug frequency experiments conducted in high viscous oil for horizontal and inclined pipes showed that this parameter increased for higher liquid viscosity. [38,42,55,54] For medium viscous oil, the same trend was observed.[43] Inclined pipes present higher slug frequencies due to inclination effects when compared to horizontal flow. Slug frequency increases, attains a peak and then goes down at higher superficial gas velocities.[42] Smaller pipe diameter also affects slug frequency. A higher value of slug frequency is observed when compared to larger pipe sizes.[56]

2.5.3. Translational Velocity

The translational velocity is the speed of the slug unit or interface. It is composed of a superposition of the bubble velocity in a stagnant liquid (namely drift velocity) and the maximum velocity in the slug body.

Nicklin [57] proposed an equation for translational velocity, v_t, as:

$$v_t = C_o v_m + v_d \tag{2.8}$$

Where, C_o is the flow distribution coefficient, v_m is the mixture velocity, and v_d is the drift velocity. Flow coefficient C_o is defined as the ratio of the maximum to the mean velocity of a fully developed velocity profile[43]. It is related to the contribution of the slug mixture to the translational velocity.[1] C_o is approximately 1.2 for turbulent flow and 2 for laminar flow.[57] The flow coefficient and drift velocity are both a function of pipe inclination.

Several experimental studies on slug translational velocity have been carried out for low[28,52,58] and high[38] viscous liquids in horizontal and upwards pipe configurations. For high viscous liquid flow, translational velocity goes up as mixture velocity increases.[38,42] Yet, translational velocity was found to go up as medium liquid viscosity increases for a constant mixture velocity.[43]

2.5.4. Drift Velocity

Drift velocity's importance is strongly related to the fact that it is one of the components needed to calculate the slug's interface velocity. One of the best physical meaning that describes this phenomenon was given by Benjamin.[22] He assumed a stagnant column of liquid initially closed at all edges. This column was suddenly opened at one boundary to the atmosphere, allowing gas to go inside the column. At the same time, liquid inside is drained out due to the gravity force. The bubble propagation speed in the liquid column is known as drift velocity. The potential for the bubble injection depends on the draining of the liquid. The higher the potential, the faster the bubble will move.

Drift velocity is affected by the physical properties of the fluids, including viscosity and surface tension and pipe geometry.[38] The next figure depicts this phenomenon:

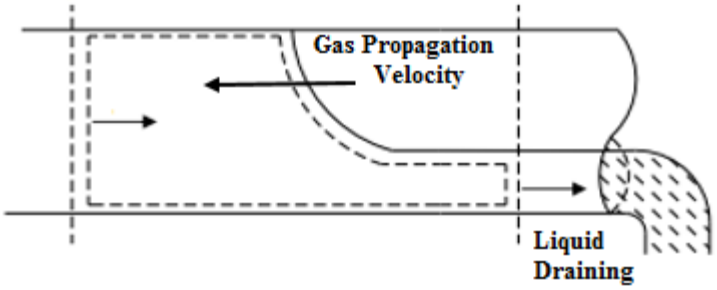

Figure 2.5 Propagation of Gas Pocket in Draining Horizontal Pipe (Adapted from Gokcal[38])

Several studies existing in the literature investigated drift velocity for liquids with low viscosity at all sorts of pipe inclinations.[59,60,22,61,62,63,64,65] In addition, observations show that bubble velocity for low viscous liquids reaches a steady value after some point along the pipe and remains constant thereafter.[59] Other than that, the behavior of the drift velocity for inclined flow is found to display a convex parabolic trend with respect to the inclination angle[66]. It goes up as angle increases and then it starts dropping to its lowest value (for vertical flow). It reaches its maximum value at an intermediate angle of inclination around 40º to 60º from the horizontal.[59,61,62,63,64] Furthermore, the effect of surface tension on drift velocity seems to be negligible when pipe ID is $\geq$ 50.8 mm (2 in).[38] Pipe diameter is also known to affect drift velocity because the larger drainage area for bigger pipes increases the gravitational potential. Therefore, drift velocity increases.[42,66]

Experimental studies on drift velocity have been also carried out for high[64,38,42] and medium[66] viscous liquids. The nose region of the bubbles becomes blunter and results in lower drift velocities when viscosity or surface tension goes up. [64,38,42,66] The bubble speed is less dependent on inclination for viscosity dominated conditions. This can be explained by the slow drainage of fluid around the nose.[64]

Jeyachandra[42] observed that there is a clear effect of inclination on drift velocity for high viscous oil. Drift velocity goes up as the inclination angle gradually increases from the horizontal. The gravitational potential increases, leading to a stronger drive

force for the bubble to penetrate the pipe. This trend reaches a peak at an inclination around 30 and 50º, where the gravitation potential is at its maximum value. Any further increase on inclination angle reduces the area available for drainage. A resistance for the air bubble to penetrate into the oil effectively is created, reducing the drift velocity. More information on this subject is found on Jeyachandra's Thesis.[42]

CFD simulations on high viscous oils analyzed the film thickness behind the penetrating gas bubble. The height of this film tends to increase as liquid viscosity goes up. Besides, it is not constant throughout the pipe during the drainage of liquid. As for low viscous liquids, the drained liquid height is almost constant and it can be easily averaged.[67]

Another feature caught by CFD simulations on high viscous liquids showed that drift velocity decreased over time.[68,69,70,71] The probable reason why this tendency had not been reported previously may be due to the fact that the slug bubble velocity had been only measured at one location in a fairly short pipe.[68] The physical explanation for that may be related to the frictional losses that become higher when the height of the liquid layer beneath the bubble increases.[69]

Moreover, simulations show that the viscous bubble slows down to a standstill for an increasing time. [70] Also, the bubble length only affects the bubble velocity when the length of the bubble is very small. Bubbles with a length of 3D were observed to have the same velocity as bubbles that can grow indefinitely. Only bubbles with lengths of a single pipe diameter or smaller were found to have a lower velocity.[71]

2.5.5. Slug Liquid Holdup and Average Liquid Holdup

Several studies have been performed to predict the slug liquid holdup (the fraction of liquid inside the slug body) for low[72,73,74,75] and high viscous fluids[76,42] in both horizontal and near horizontal pipes. Viscosity is believed to have only impact in slug liquid holdup when liquid viscosity goes up at higher mixture velocities.[76,43,77] However, slug holdup decreases when the oil viscosity increases for liquid medium viscosities between 0.108 Pa.s (108cP) and 0.166 Pa.s (166cP). Brito[43] explains this

trend by some possible factors: "*more gas entrainment owing the momentum exchange at the slug front; the amount of gas entrained in the liquid film increases owing to the gas separation difficulties; less gas coalesces to the Taylor bubble*".

2.5.6. Liquid Film/Taylor Bubble Shape

Experimental investigations show that the liquid film height in the stratified zone increases for high liquid viscosity.[58] It is significantly larger and more aerated than for lower viscous liquids. Other than that, a thin film has been reported for high viscous oil flow at the top of the pipe due to the low drainage of the oil.[39,76] A numerical analysis of the shape of this film has not been characterized yet.

Laboratory studies showed that Taylor bubble shape changes as the mixture velocity increases. At lower velocities, the bubble has a well-defined nose and tail. As the fluid velocity goes up, the nose points towards the center of the pipe and the tail is full of small gas bubbles.[78] For lower liquid viscosities, Taitel and Barnea[31] model seems to match well the film profile. It suggests that the gas-liquid interaction in the stratified region must be taken into consideration.[28]

2.5.7. Pressure Gradient

Several studies existing in the literature show that pressure drop is affected when inclination angle and viscosity changes. Taitel and Barnea[31] model seems to be one of the best ones to predict pressure drop for high viscous liquids.[58] On the other hand, Dukler and Hubbard[27] model shows to be more appropriate for low viscous liquids.[28] It was reported that an increase in liquid viscosity leads to an increase in pressure gradient.[79,42,43] This trend is more evident at higher superficial oil and gas velocities.[79] Furthermore, pressure gradient monotonically increases as liquid viscosity goes up in downward inclined flow. Moreover, pressure gradient is lower when compared to horizontal flow due to the negating effect of gravitational pressure gradient.[42]

A decrease in pressure gradient is observed at low gas velocities for upward inclined flow at lower liquid velocities. Also, an increasing trend is observed for larger gas velocities.[42] According to Jeyachandra, [42] "*this phenomenon owed to the competing*

effects of gravitational and frictional pressure gradient". Besides, the total pressure gradient is higher when compared to horizontal flow. It could be explained by the additional effect of gravitational pressure gradient.

2.5.8. Literature Review Summary Tables

The next tables summarize the available experimental data conducted in the literature for slug flow. They include the kind of test fluids, pipe geometry, range of liquid viscosity and parameters that each one of the authors analyzed. This serves as basis for building and developing the state-of-the-art facility. These gaps of data discussed can be filled with the experiments to be performed in the future, especially for medium viscous oil.

Table 1. Overall Slug Parameters Experimental Data Review

Authors Name (Year)	**Test Fluids**	**Inclination Angles (°)**	**Liquid Viscosity (cP)**	**Parameters Analyzed**	**Pipe Diameter (m)**
Gregory and Scott (1969)	Carbon Dioxide and Water	Horizontal	1	f_S	0.019
Gregory et al. (1978)	Air and Light Oil	Horizontal	6.75	H_{LLS}	0.0258 and 0.0512
Heywood and Richardson(1979)	Air and Water	Horizontal	1	f_S, L_S, H_{LTB}, H_{LLS}	0.042
Brill et al. (1981)	Air and Oil	Horizontal	1	L_S	0.3048 and 0.4064
Nydal et al. (1992)	Air and Water	Horizontal	1	L_S; v_{TB}	0.0529 and 0.090
Nadler and Mewes (1995)	Air and Oil/Water	Horizontal	14 to 37	H_L	0.059

Table 1. Continued

Cook et al. (1995)	Air and Water	Horizontal	1	dP/dL; $v_{TB;}$ f_S; L_S, h_F; H_{LLS}	0.032 and 0.050
Marcano et al. (1998)	Air and Kerosene	Horizontal	Not Disclosed	dP/dL; $v_{TB;}$ f_S; L_S	0.077
Gomez et al. (1999)	Air, Nitrogen, Kerosene, Oil, Diesel, Freon and Water	Horizontal to Vertical	1 to 6.5	H_{LLS}	0.051, 0.076,0.178, 0.203
Zabaras (1999)	Air and Water	Horizontal to 11	1	f_S	0.0254 to 0.2032
Abdul-Majeed (2000)	Air, Nitrogen, Kerosene, Light Oil, Freon and Water	-10 to 9	1 to 7	H_{LLS}	0.0258 to 0.2032
Colmenares et al. (2001)	Air and Lube Oil	Horizontal	480	dP/dL; $v_{TB;}$ f_S; L_S; H_{LLS}	0.0508
Rosa (2004)	Air, Glycerin and Water	Horizontal	1 and 27	f_S; L_S; v_{TB}; H_L; L_F	0.026
Gokcal (2008)	Air and Oil	Horizontal	178 to 598	dP/dL; v_D; f_S; L_S; v_{TB}	0.0508
Al-Safran (2009)	Air and Oil	Horizontal	10.2	f_S	0.0508
Perez et al. (2010)	Air and Water	Horizontal to Vertical	1	f_S	0.038 and 0.067

Table 1. Continued

Jeyachandra (2011)	Air and Oil	-2; +2	181 to 585	dP/dL; H_{LTB} f_S; L_S; H_L; H_{LLS}; H_L	0.0508
Kora et al. (2011)	Air and Oil	Horizontal	181 to 587	H_{LLS}; h_F; H_{LTB}	0.0508
Schulkes (2011)	Air, Water and Oil	-1 to 80	1 to 589	f_S	0.019 to 0.1
Brito (2012)	Air and Oil	Horizontal	39 to 166	dP/dL; H_L; H_{LTB}; L_S; H_{LLS}	0.0508
Al-Safran et al. (2013)	Air and Oil	Horizontal	180 to 587	H_{LLS}; L_S	0.0508
Wang et al. (2013)	Air, Oil and Kerosene	-30 to Vertical	1.6 to 589	H_{LLS}	0.0508 to 0.1
Zhao et al. (2013)	Air and Oil	Horizontal	1000 to 7500	f_S	0.026 and 0.074
Okezue (2014)	Air and Oil	Horizontal	1100 to 4000	H_{LLS}; f_S	
Siddiqui et al. (2015)	Air and Water	1.16	1	H_{LLS}; f_S; L_S	0.074

Table 2. Drift Velocity Experimental Data Review

Authors Name (Year)	**Test Fluids**	**Inclination Angles (°)**	**Liquid Viscosity (cP)**	**Pipe Diameter (m)**
Davies and Taylor (1950)	Air, Water and Nitrobenzene	Vertical	Not Disclosed	0.0254

Table 2. Continued

Zukoski (1966)	Carbon Tetrachloride, Water, Glycerin, Mercury and Ethyl alcohol	Horizontal	Not Disclosed	0.005 to 0.0178
Bendiksen (1984)	Air and Water	-30 to 90	1	0.0242
Weber et al. (1986)	Air, Water, Methanol, Glycerin, Sucrose and Corn Syrup	0, 15, 30, 45, 60, 75 and 90	1 to 6120	0.006 to 0.0373
Hasan and Kabir (1989)	Air and Water	68 to 90	1	0.048, 0.057 and 0.087
Alves et al. (1993)	Air and Kerosene	Horizontal to Vertical	1.6	0.051
Gokcal (2008)	Air and Oil	0, 10, 20, 30, 40, 50, 60, 70, 80 and 90	1; 104 to 1287	0.0508
Jeyachandra (2011)	Air and Oil	0, 10, 30, 50, 70 and 90	154 to 574	0.1524
Moreiras et al. (2014)	Air and Oil	0, 10, 20, 30, 40, 50, 60, 70, 80 and 90	39 to 166	0.0508

CHAPTER III

CALCULATION PROCEDURE FOR FACILITY DESIGN

This chapter provides the calculations procedures used in the single-phase and two-phase flow hydrodynamics estimation for the facility design. The drift velocity simulation (from CFD software) modelling used in the design of the test section is also reported here.

3.1. Single-Phase Water Pressure Drop Calculations

The first hydrodynamic parameter to be calculated in the facility is the pressure drop for water single-phase flow. It works as the base line for pressure drop when more than one phase is present on the flow. For fully developed flow, the total pressure drop along the pipe includes the frictional, gravitational and accelerational pressure-gradient components, as given respectively, by:

$$-\frac{dP}{dL} = -\frac{dP}{dL})_F - \frac{dP}{dL})_G - \frac{dP}{dL})_A \tag{3.1}$$

For single-phase flow, the total pressure gradient of the three components above can be obtained from momentum and mass conservation laws, yielding:

$$-\frac{dP}{dL} = \frac{2}{d} f_F \rho v^2 + \rho g \sin\theta + \rho v \frac{dv}{dL} \tag{3.2}$$

Where, f_F is the Fanning friction factor.

Accelerational and gravitational pressure gradient can be neglected because velocity does not change much along the pipe and the test was conducted in the horizontal. Thus, the formula above can be reduced to:

$$-\frac{dP}{dL} = \frac{2}{d} f_F \rho v^2 \tag{3.3}$$

The friction factor *f* is defined based on Reynolds number and pipe roughness. Colebrook equation was selected to give friction factor as follows:

$$\frac{1}{\sqrt{f}} = -2log\left(\frac{\varepsilon/D}{3.7} + \frac{2.51}{Re\sqrt{f}}\right) \tag{3.4}$$

The given relationship between pressure drop and the liquid velocity can be used in the case of the pipe viscometer to back calculate the fluid viscosity based on the measured DP data.

3.2. Gas-Liquid Stratified Pressure Drop, Liquid Height and Holdup

The next parameters to be calculated are pressure drop, liquid height and liquid holdup for stratified flow. According to Taitel and Dukler[20] model, liquid film was assumed to be constant throughout the pipe. Momentum balance equations were applied on gas and liquid phase, separately as:

$$-A_L \left.\frac{dP}{dL}\right|_L - \tau_{WL} S_L + \tau_I S_I - \rho_L A_L g sin\theta = 0 \tag{3.5}$$

$$-A_G \left.\frac{dP}{dL}\right|_G - \tau_{WG} S_G - \tau_I S_I - \rho_G A_G g sin\theta = 0 \tag{3.6}$$

The combined-momentum equation for both phases is obtained next to eliminate the pressure drop term:

$$\tau_{WG}\frac{S_G}{A_G} - \tau_{WL}\frac{S_L}{A_L} + \tau_I S_I\left(\frac{1}{A_L} + \frac{1}{A_G}\right) - (\rho_L - \rho_G) g sin\theta = 0 \tag{3.7}$$

The liquid height is needed to solve it, which makes this equation implicit for h_L. Calculation of the different geometrical and forces variables is carried out with the single-phase flow method. The hydraulic diameter of the liquid and gas phases are given by:[20]

$$d_L = \frac{4A_L}{S_L} and\ d_G = \frac{4A_G}{(S_G + S_I)} \tag{3.8}$$

Reynolds number, friction factor and wall shear stress, for turbulent flow of the liquid phase are given by:

$$f_L = C_L(Re_L)^{-0.2} = 0.046\left(\frac{d_L v_L \rho_L}{\mu_L}\right)^{-0.2} \tag{3.9}$$

$$\tau_{WL} = f_L \frac{\rho_L {v_L}^2}{2} \tag{3.10}$$

The same applies to the gas phase. Shear stress for the gas-liquid interface is obtained from:

$$\tau_I = f_I \frac{\rho_G (v_G - v_I)^2}{2} \tag{3.11}$$

Taitel and Dukler[20] assumed an existence of a smooth interface so that the friction factor of the gas and of the interface are approximately the same. The interface friction factor may be neglected because interface velocity is much smaller than gas velocity. The wall shear stress of the interface can be considered equal to the gas one by doing those approximations.

It is possible to substitute the parameters obtained into equation 3.7 to get the liquid level by either trial and error, bi-section method, or Newton-Raphson method. The final solution for that is given in the dimensionless form. Length, area, and velocities variables are scaled up by pipe diameter, d^2 and by the superficial velocities of the corresponding phase, respectively. The dimensionless form of the momentum-combined equation is obtained next for stratified-smooth flow by substituting the dimensionless parameters into equation 3.7:

$$X^2\left[(\tilde{v}_L \tilde{d}_L)^{-0.2} {\tilde{v}_L}^2 \frac{\tilde{S}_L}{\tilde{A}_L}\right] - \left[(\tilde{v}_G \tilde{d}_G)^{-0.2} {\tilde{v}_G}^2 \left(\frac{\tilde{S}_G}{\tilde{A}_G} + \frac{\tilde{S}_I}{\tilde{A}_L} + \frac{\tilde{S}_L}{\tilde{A}_L}\right)\right] + 4Y = 0 \tag{3.12}$$

The two dimensionless group parameters defined as X and Y are given as follows:

$$X^2 \equiv \frac{\frac{4C_L}{d}\left(\frac{\rho_L v_{SL} d}{\mu_L}\right)^{-0.2}\frac{\rho_L v_{SL}^2}{2}}{\frac{4C_G}{d}\left(\frac{\rho_G v_{SG} d}{\mu_G}\right)^{-0.2}\frac{\rho_G v_{SG}^2}{2}} = \frac{-\frac{dp}{dL}\Big)_{SL}}{-\frac{dp}{dG}\Big)_{SG}} \tag{3.13}$$

$$Y \equiv \frac{(\rho_L - \rho_G) g\ sin\theta}{\frac{4C_G}{d}\left(\frac{\rho_G v_{SG} d}{\mu_G}\right)^{-0.2}\frac{\rho_G v_{SG}^2}{2}} = \frac{(\rho_L - \rho_G) g\ sin\theta}{-\frac{dp}{dG}\Big)_{SG}}$$

All dimensionless variable on the combined momentum balance equation are dependent on the dimensionless liquid level ($\tilde{h}_L = h_L/D$) as given:

$$\tilde{A}_L = 0.25\left[\pi - cos^{-1}\left(2\tilde{h}_L - 1\right) + \left(2\tilde{h}_L - 1\right)\sqrt{1 - \left(2\tilde{h}_L - 1\right)^2}\right], \tag{3.14}$$

$$\tilde{A}_G = 0.25\left[cos^{-1}\left(2\tilde{h}_L - 1\right) - \left(2\tilde{h}_L - 1\right)\sqrt{1 - \left(2\tilde{h}_L - 1\right)^2}\right],$$

$$\tilde{S}_L = \pi - cos^{-1}\left(2\tilde{h}_L - 1\right),$$

$$\tilde{S}_G = cos^{-1}\left(2\tilde{h}_L - 1\right),$$

$$\tilde{S}_I = \sqrt{1 - \left(2\tilde{h}_L - 1\right)^2},$$

$$\tilde{v}_L = \frac{\tilde{A}_P}{\tilde{A}_L}, \quad and \quad \tilde{v}_G = \frac{\tilde{A}_P}{\tilde{A}_G},$$

$$\tilde{d}_L = \frac{4\tilde{A}_P}{\tilde{S}_L}, \quad and \quad \tilde{d}_G = \frac{4\tilde{A}_G}{\tilde{S}_G + \tilde{S}_I},$$

The slip-liquid holdup is obtained simply by dividing the dimensionless cross sectional area of the pipe occupied by the liquid phase by the total dimensionless area of the pipe:

$$H_L = \tilde{A}_L / \tilde{A}_P \tag{3.15}$$

Pressure drop can be obtained from the momentum balance equations (Eq. 3.5 and 3.6) of any phase. Both values should yield the same result.

Some adjustments must be made in order to get pressure drop for stratified-wavy flows. The first one is not to consider the interfacial friction factor to be the same as the gas phase friction factor. Instead, the value for that is considered to follow the correlation developed by Cohen and Hanratty[80]. They assumed small-amplitude waves to exist in the interface:

$$f_I = 0.0142 \tag{3.16}$$

Moreover, shear stresses of gas and interface are not the same for stratified-wavy flow. Shear stress on the interface is obtained from Eq. 3.11. The dimensionless combined-momentum balance equation becomes:

$$X^2\left[(\tilde{v}_L\tilde{d}_L)^{-0.2}\tilde{v}_L{}^2\frac{\tilde{S}_L}{\tilde{A}_L}\right] - \left\{(\tilde{v}_G\tilde{d}_G)^{-0.2}\tilde{v}_G{}^2\left[\frac{\tilde{S}_G}{\tilde{A}_G} + \frac{f_I}{f_G}\left(\frac{\tilde{S}_L}{\tilde{A}_L}\right) + \frac{f_I}{f_G}\left(\frac{\tilde{S}_I}{\tilde{A}_L}\right)\right]\right\} + 4Y = 0 \tag{3.17}$$

Other than that, all the remaining procedure to obtain pressure drop and liquid holdup for stratified-wavy flow was the same as the one previously done for stratified-smooth flow.

3.3. Gas-Liquid Slug Flow Hydrodynamic Parameters

The calculation procedures and correlations used to predict the main slug hydrodynamic parameters needed to design and validate the results obtained through the facility are presented next:

3.3.1. Slug Length

Slug length is a needed input parameter for calculating slug pressure drop from Taitel and Barnea[31] model. The first correlation used was developed by Brill et al.[24] Test fluids were air and water. Experiment was conducted in large pipe diameters pipes in the horizontal:

$$Ln(L_S) = -3.851 + 0.059Ln\left(\frac{v_m}{0.3048}\right) + 5.445[Ln\left(\frac{D}{0.0254}\right)]^{0.5} \quad (3.18)$$

The second correlation tested was obtained by Scott et al.[34] They conducted experiment with air/water in horizontal pipes to develop statistical distributions of slug lengths. Their correlation does not account for the mixture velocity, which was found to be negligible:

$$L_S = -26.6 + 28.495[Ln\left(\frac{D}{0.0254}\right)]^{0.1} \quad (3.19)$$

The last equation used was developed by Marcano.[36] He carried out several slug-flow tests over combinations of gas and liquid flow rates in a flow loop consisted of a 77.9-mm (3.068-in) diameter and 420m (1378ft) long horizontal flowline:

$$\frac{L_S}{D} = e^{(\mu+0.5\sigma^2)} \quad (3.20)$$

$$\mu = 4.073 - 0.218Ln(v_{SL}) - 0.178Ln(v_m)$$

$$\sigma = 0.661 - 0.018Ln(v_{SL}) - 0.119Ln(v_m)$$

Superficial velocities are given in *ft/s*.

3.3.2. Slug Frequency

Two different correlations were used to predict slug frequency. Heywood and Richardson[47] developed the following equation for a 42-mm (1.65in) ID horizontal pipe. It depends on the no-slip liquid holdup and the mixture velocity:

$$f_s = 0.0434[\lambda_L\left(\frac{2.02}{D} + \frac{v_m^2}{gD}\right)]^{1.02} \quad (3.21)$$

The second correlation used was developed by Zhao et al.[81] They experimentally investigated slug frequency on liquid viscosities ranging from 1.0 Pa.s (1000cP) to 7.5 Pa.s (7500cP) in 0.026m (1in) ID and 0.074m (3in) ID horizontal pipes. Liquid flow in the tested range was laminar. Turbulent liquid flow was not covered in the correlation. The following correlation was developed by fitting the data obtained:

$$\frac{f_s D}{u_m \Psi(\alpha)} = \begin{cases} 10.836 {Re_{SL}}^{-0.337} \; for \; Re_{SG} \leq 4000 \\ 6.40 {Re_{SL}}^{-0.141} \; for \; Re_{SG} > 4000 \end{cases} \text{ for } Re_{SL} < 4000 \tag{3.22}$$

Where

$$\Psi(\alpha) = 0.016\alpha(2 + 3\alpha)$$

$$Re_{SL} = \frac{\rho_L v_{SL} D}{\mu_L}$$

$$Re_{SG} = \frac{\rho_G v_{SG} D}{\mu_G}$$

3.3.3. Translational Velocity

Slug interface velocity used in this work was based on the correlation developed by Bendiksen[61] for drift velocity. It also considers flow coefficient (C_0) to be 1.2- turbulent flow :

$$v_{TB} = c_0 v_m + 0.54\sqrt{gD}\, cos\theta + 0.35\sqrt{gD}\, sin\theta \tag{3.23}$$

3.3.4. Drift Velocity

One correlation will be tested along with the CFD simulations (shown later on this chapter) for drift velocity prediction. The correlation used was obtained from Bendiksen.[61] He carried out air-water experiment to study the behavior of the velocities of single elongated bubbles in flowing liquids. Inclination angles ranged from downward vertical to upward vertical:

$$v_d = 0.54\sqrt{gD}\, cos\theta + 0.35\sqrt{gD}\, sin\theta \tag{3.24}$$

3.3.5. Pressure Drop

Taitel and Barnea[31] unified model was selected for pressure drop calculation purposes. Some simplifications have been assumed, such as a uniform film thickness in the Taylor bubble zone; no-slip between gas and liquid phase in the slug body; smooth pipe and fluid properties constant throughout the pipe. Fluid properties, superficial velocities and pipe geometry are known. Moreover, slug length is a necessary input for

the model. It can be obtained from Brill et al.[24] correlation. A momentum balance on the entire slug unit was applied. Therefore, the pressure drop along the film zone was not neglected. Pressure gradient for slug flow is calculated from:

$$-\frac{dp}{dL} = -\frac{\Delta p_U}{L_U} = \rho_S g sin\theta L_S + \frac{\tau_S \pi D}{A_P} L_S + \rho_F g sin\theta L_F + \frac{\tau_F S_F}{A_P} L_F + \frac{\tau_G S_G}{A_P} L_F \qquad (3.25)$$

The detailed systematic procedure to get pressure drop is shown in Appendix B.

3.3.6. Film Shape

Film shape was calculated from two different approaches: Dukler and Hubbard[27] and Taitel and Barnea.[31] The same considerations for pressure drop calculation on slug flow were taken into account. The exception is not assuming the film height in the Taylor bubble zone to be constant. Film shape can be calculated from a momentum balance applied to a differential control volume of liquid film from Dukler and Hubbard[27] model. The following first order ODE- Ordinary Differential equation solution yields the film shape:

$$\frac{dh_F}{dz} = \frac{-\tau_F S_F - A_P H_{LTB} \rho_L g sin\theta}{\frac{x^2 H'_{LTB}}{\rho_L A_P H_{LTB}^2} - A_P H_{LTB} \rho_L g cos\theta} \qquad (3.26)$$

This equation must be solved numerically for h_F and the boundary condition is $h_F(z=0) = h_S = H_{LLS} * d$. In a similar way, Taitel and Barnea[31] model gives the following first order ODE to obtain the film shape:

$$\frac{dh_F}{dz} = \frac{\frac{\tau_F S_F}{A_F} - \frac{\tau_G S_G}{A_G} - \tau_I S_I \left(\frac{1}{A_F} + \frac{1}{A_G}\right) + (\rho_L - \rho_G) g sin\theta}{(\rho_L - \rho_G) g cos\theta - \rho_L v_F \frac{(v_{TB} - v_{LLS}) H_{LLS}}{H_{LTB}^2} \frac{dH_{LTB}}{dh_F} - \rho_G v_G \frac{(v_{TB} - v_{GLS})(1 - H_{LLS})}{(1 - H_{LTB})^2} \frac{dH_{LTB}}{dh_F}} \qquad (3.27)$$

Similarly, this equation must be solved numerically for h_F and the boundary condition is: $h_F(z=0) = h_S = H_{LLS} * d$. The liquid holdup in the Taylor-bubble region is obtained from:

$$\frac{dH_{LTB}}{dh_F} = \frac{4}{\pi D}\sqrt{1-\left(2\frac{h_F}{D}-1\right)^2} \tag{3.28}$$

A VBA code written to calculate the film shape for both methods is given in Appendix C.

3.4. Drift Velocity CFD Simulation

This section superficially describes each step taken to modelling drift velocity phenomenon for horizontal and inclined 2D channels using CFD. The results obtained through simulations performed with a commercial package (ANSYS Fluent Version 15.0)[82] provide more support to validate the data obtained through the state-of-the-art multiphase flow loop.

First, the geometry, mesh and the physics equations used to setup the simulations for drift velocity will be presented. A 2D channel with a rectangular section has been used to simulate the drift velocity behavior in a uniform grid spacing ($\Delta x = \Delta y =$ 0.005m) with 11,200 cells. Simulation were performed using an Intel Core i7 64-bit processor with 2.4 GHz. Computational simulation time for that grid size was very acceptable for the purposes of this work. Below, it is depicted a channel with 38.1-mm (1.5in) height representing the geometry and uniform mesh proposed:

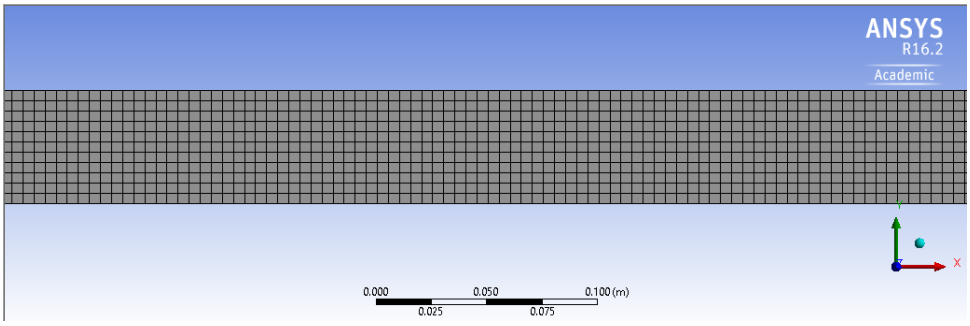

Figure 3.1 Geometry and Mesh View for a 2-inches height 2D Channel

The boundary and initial conditions for this case can be seen next:

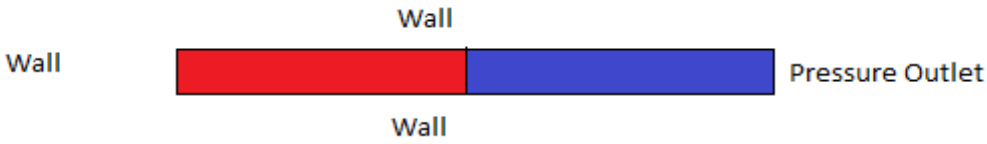

Figure 3.2 Boundary and Initial Condition for the Horizontal Case

A very similar initial and boundary conditions used by Randim[69] was chosen as basis for the simulations performed in this work. At time zero, the left half of the channel was filled with liquid (red) and the other half was filled with gas (blue). Therefore, a diaphragm separated the two immiscible phases. This diaphragm works as a quick operating valve, similar to the one used in the facility. Once the valve is opened (representing the start of the simulation), liquid will start to drain out of the pipe. At the same time, gas from the atmosphere will enter the pipe and propagate.

A wall boundary condition and the no slip condition were applied ($\vec{V} = 0$) at the walls. Besides, a constant pressure condition was specified (atmospheric pressure) at the outlet.

Now the most superficial aspects of the numerical methods chosen to solve the physical problem of the drift velocity will be summarized. For further information regarding the numerical methods behind the software, the reader is referred to ANSYS Fluent Tutorial Guide.[7]

The double-precision version of FLUENT was used in all simulations. Gas was set to be the primary phase in the VOF model, whereas liquid was set to be the secondary phase. Gravity was included in all calculations directed downwards. A pressure-based solver changing with time (transient) rules the simulations. The PRESTO scheme for the pressure interpolation; the PISO scheme for the pressure/velocity coupling; first-order implicit time discretization and first order upwind scheme for the momentum equation along with the geo-reconstruction scheme for representing the interface between the two phases have been selected to better characterize the physical problem.

The Energy Equation is turned off (decoupled by the solver, which means less computational effort) because changes of temperatures have been disregarded in all simulations. Thus, only the momentum and the continuity equations are solved.

Aside from that, a variable time step (it automatically changes the time step when an interface is moving through dense cells or if the interface velocity is high) was chosen, starting always at 0.001s. It would not only minimize numerical errors in the solution but also make it faster. The value of the scaled residual was set to be 10^{-6} as a convergence criterion,.

The next table summarizes some information regarding values used in the simulations:

Table 3. Simulations Information

Inclination Angles Simulated (°)	0; 1 and 5
Pipe Diameter (in)	1.5
Pipe Extension (m)	6.0
Trap Section Extension (m)	1.0
Liquid Density (kg/m^3)	996
Liquid Viscosity (Pa.s)	$1.1*10^{-3}$
Gas Viscosity (Pa.s)	$1.8*10^{-5}$
Gas Density (kg/m^3)	1.4

The drift velocity, which means the time taken by the front of Benjamin's bubble to travel between two fixed points, was calculated according to the following equation:

$$v_d = \frac{x_2 - x_1}{t_2 - t_1} \tag{3.29}$$

Where, x_1 and x_2 are the positions of the stagnation point at an old t_1 and at a new t_2 time level, respectively. In the simulations, $x_1$will be always fixed at the origin ($x_1 = 0$) while x_2 will be moved together with the bubble edge to calculate the drift velocity at some specific locations. Consequently, t_1 represents the initial condition, t_1 = 0. The next figure depicts better those variables involved in the calculation:

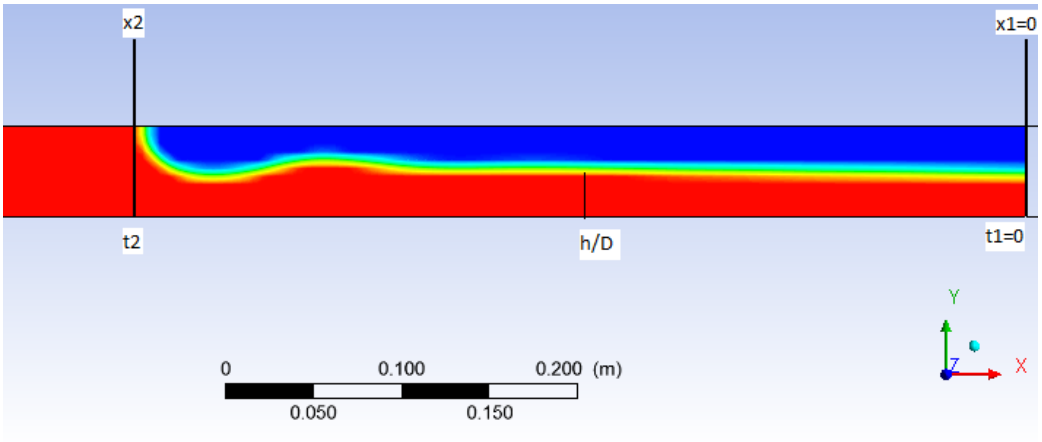

Figure 3.3 Drift Velocity Measurement Technique on Fluent

According to the figure, the drift velocity will be calculated at the point right ahead the nose bubble. For example, in order to find the drift velocity at point x_2:

$$v_{d2} = \frac{x_2}{t_1} \tag{3.30}$$

For a general location n, drift velocity can be calculated from:

$$v_{dn} = \frac{x_n}{t_n} \tag{3.31}$$

CHAPTER IV

EXPERIMENTAL SETUP

The experimental program was carried out in the multiphase flow loop built in lab 101 of Texas Tech Petroleum Engineering Department. The facility can be inclined from -2° to 25° from horizontal. The main components of the flow loop are the pump section, the metering section, the heat exchanger section, storage tanks, pipe viscometer section and the test sections. In addition, a detailed description of test fluids used and the different components of the flow loop are provided in this chapter.

4.1. Test Fluids

RO (Reverse Osmosis) water and compressed air were utilized as the test fluids. RO water from Lubbock's city was selected because this kind of fluid is free of the majority of contaminants usually existing in the water. It could affect its physical properties after some time, yielding misleading results. Compressed air was supplied by an outlet existent in the lab. Gas flow can be controlled through a needle valve placed right after the gas outlet. The properties of the test fluids at standard conditions, 20°C and 101.325 kPa (68°F and 14.696 psia), are given next:

Table 4. Test Fluid Properties

Water Density (ρ_w) [kg/m^3]	996
Gas Density (ρ_g) [kg/m^3]	1.2
Water Viscosity (μ_w) [Pa.s]	1.1×10^{-3}
Gas Viscosity (μ_g) [Pa.s]	1.8×10^{-5}

Water density has been measured using a sensitive scale (the flow meter also provides good results). Kinematic viscosity is obtained through a Cannon-fensk

viscometer. Absolute viscosity can be found once density is measured. Gas viscosity is calculated by performing single-phase test only with gas, so that its viscosity is obtained from the pipe viscometer section. Gas density can be measured from the mass flowmeter readings.

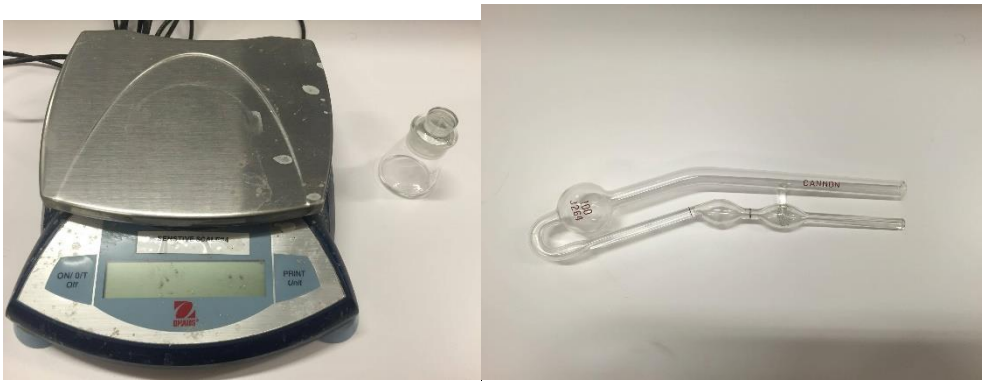

Figure 4.1 Sensitive Scale and Cannon-fensk Viscometer

Shell Omala S2 G 100 is highly recommended for conducting tests with medium viscosity oil in the future. The suggestion of this oil can be addressed to the following properties: it poses a large viscosity range, which is strongly dependent on temperature; it is Newtonian, physically stable and immiscible with water; it is easily visible in acrylic pipe, environmentally safe and reasonable in cost. The oil properties are shown in Table 5.

Table 5 Oil Properties

Properties	**Shell Omala S2 G 100**
Kinematic Viscosity @40°C [mm^2/s]	100
Kinematic Viscosity @100°C [mm^2/s]	11.3
Flash Point [°C]	240
Pour Point [°C]	-24
Density @15°C [kg/m^3]	887

4.2. Test Facility

The Test Section is comprised by two parts: an acrylic one (the one used in this work) and a Heat Transfer one, built to study temperature behavior for two-phase flow. The facility was designed to allow flow at three different configurations: only through the acrylic section; only through the Heat Transfer section and through both test sections. This last configuration allows a better visualization of the phenomena when heat transfer experiments are being conducted. The reader is referred to Carestiato's Thesis[83] for further details on gas-liquid heat transfer topic.

The 6.7-m (21.9-ft) long test section is built in acrylic pipe to make visual observation better. PVC tees (with the low extremity working as ports) are connected to the DP Transmitter to measure the pressure drop along different spots. The end of the test section can be connected directly to the storage tank using a 38.1-mm (1.5-in) ID flexible hose. Tank is made of polyethylene whose upper temperature limit is 65.5°C (150°F), which has never been reached for the purposes of this work.

Liquid is pumped directly from the storage tank to the metering, the heat exchanger, the viscometer and the test sections using a 5-hp PV30B Blackmer Pump Vane Pump. A Variable Frequency Driver (VFD) installed close to the pump provides control of the liquid flowrate. Air is supplied to the facility from a gas outlet existing in

the lab. Liquid and air interact at the mixing tee right after the outlet of the heat exchange section and right before the viscometer section.

Separation of the two phases occurs at the transfer tank due to gravity. A beam supports both test sections and, based on a pivot-support mechanism, the inclination of test section can be tilt from -2° to 25° from the horizontal. Four pipe-in-pipe heat exchangers placed in the liquid line have been designed for obtaining a desired temperature. Liquid viscosity is highly dependent on temperature, especially for oils. Thus, changing temperature leads to the control of viscosity.

The heat exchanger section consists of one water storage tank, one recirculating chiller and a Pipe-in-Pipe heat exchanger consisting of 4 copper pipes (1.5-inches ID) jacketed with PVC (2-inches ID). Water from the tank flows to the recirculating chiller by gravity. Then, the chiller (sets to cool or heat the water) pumps the water to the annulus/jacketed part of the heat exchanger. Test fluid flows inside the copper pipe at the same time. Water returns to the tank after the heat exchanger outlet and the loop starts over until the desired test fluid temperature is achieved after several circulations. A bypass line underneath the heat exchanger was also built when changing the liquid viscosity was not desired.

The viscometer pipe section consists of a PVC pipe of 6.22-m (20.4-ft) and 30.8-mm (1.5-inches) ID diameter. It is divided into two parts: the first one, it is a development region and the second one, the measurement region itself. In the latter, two ports are connected to a Differential Pressure (DP) Transmitter to measure the pressure drop along this section. Viscosity is back calculated from pressure drop equation for single-phase flow.

Stable liquid temperature control is also possible throughout the experiments. It can be tracked by temperature probes placed at different locations. All measuring devices are connected to a data acquisition system, which is logged in round-the-clock. Data for temperature, pressure drop and flowmeter readings gathered by the system are instantaneously sent to a computer. There, they can be accessed through an Excel

spreadsheet automatically generated. Pump speed is controlled by the VFD, which can be done remotely from the computer as well.

An overall picture of the multiphase flow loop facility is given in Figure 4.2. A schematic CAD drawing of the facility is also provided in Figures 4.3 and 4.4.

Figure 4.2 Multiphase Flow Loop Overall Picture

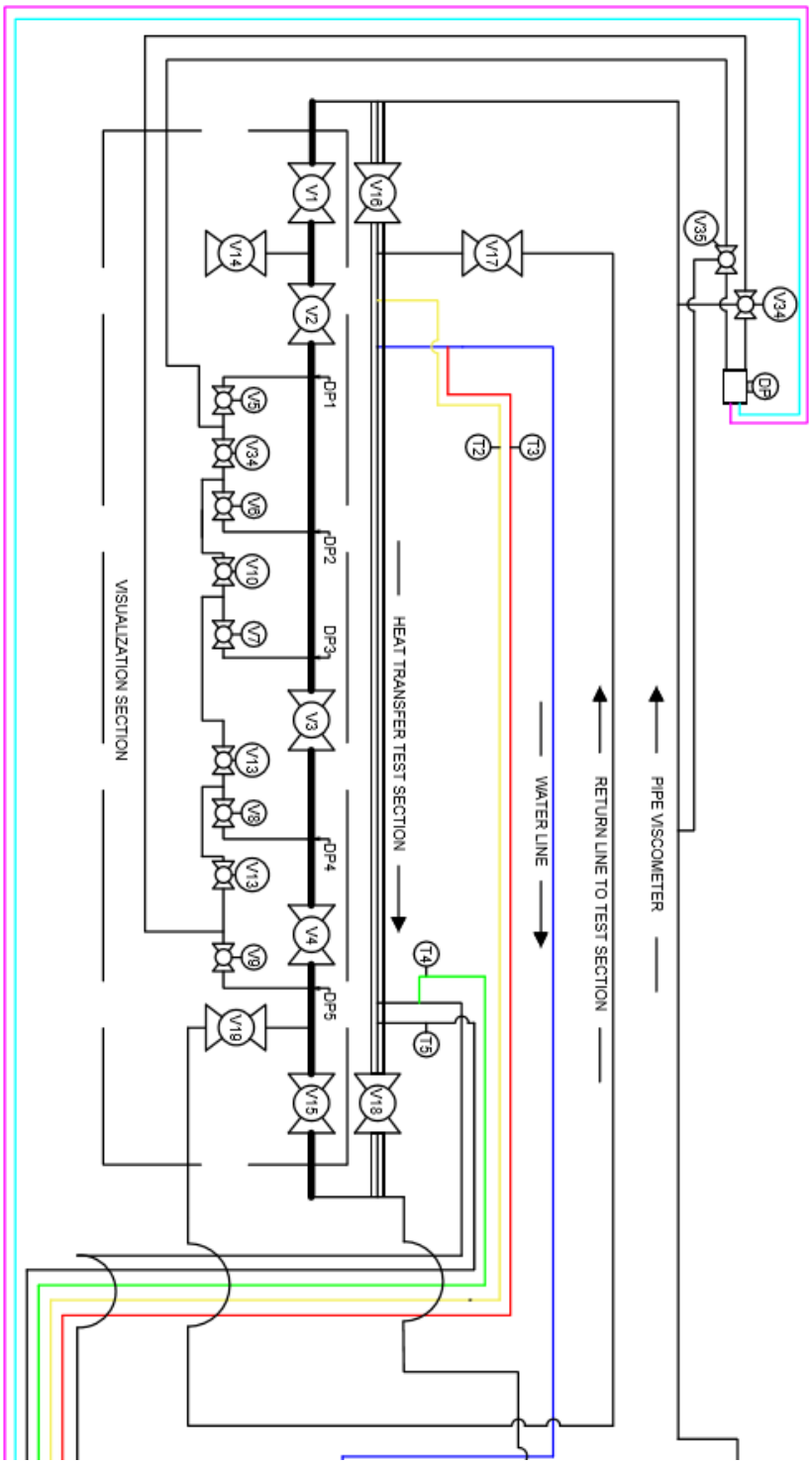

Figure 4.3 Schematic Facility Drawing Part 1

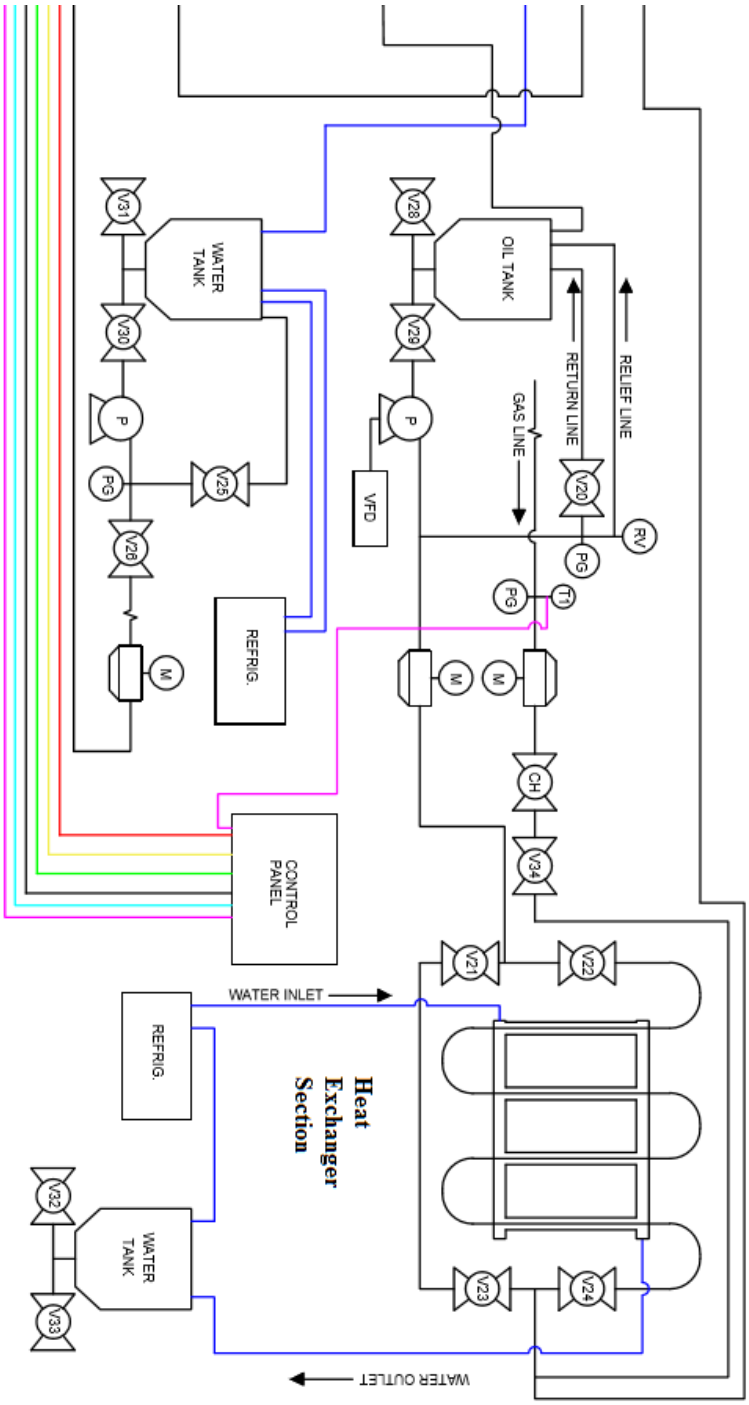

Figure 4.4 Schematic Facility Drawing Part 2

The loop can be divided into four main sections:

1. ***Metering section***
2. ***Heat Exchanger section***
3. ***Pipe Viscometer section***
4. ***Test sections***

4.2.1. Metering Section

Physical and flow properties of gas and liquid are measured separately by Micro Motion™ Coriolis mass flow meters before they mix . Two Micro Motion™ mass flow meters (CMF25 and CMF300) are used to record the mass flow rate, volumetric flow rate and density of liquid and gas, respectively.

Gas temperature and pressure are necessary inputs to calculate the superficial air velocity from the gas mass flow rate. They should be measured before the mixing with liquid. A picture of the metering system is shown next:

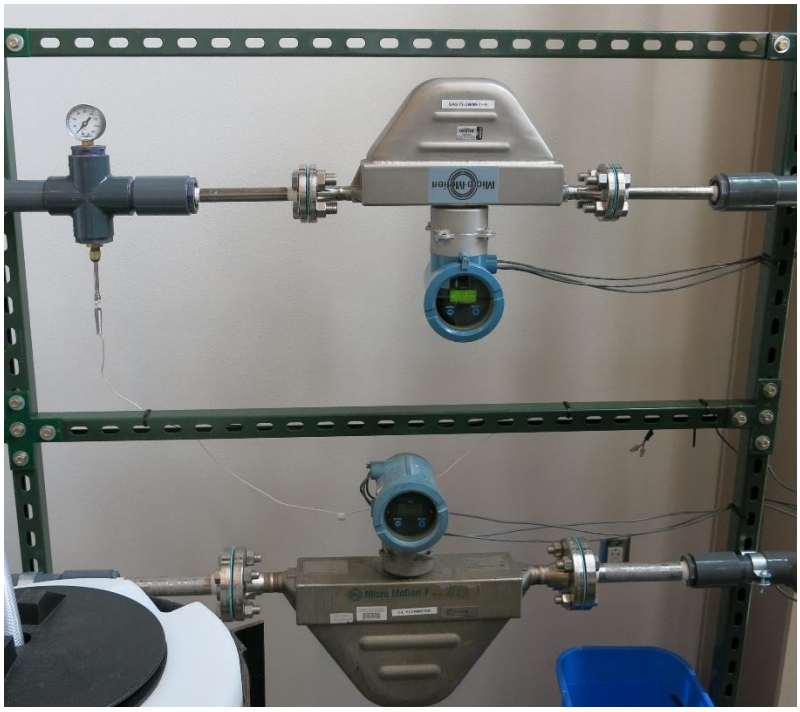

Figure 4.5 Metering Section

4.2.2. Heat Exchanger Section

The heat exchanger section consists of a 11.35 L (3 gallons) water storage tank, one recirculating chiller and four Pipe-in-Pipe heat exchangers. They form a closed loop system. This section is depicted in the schematic and in the pictures taken next:

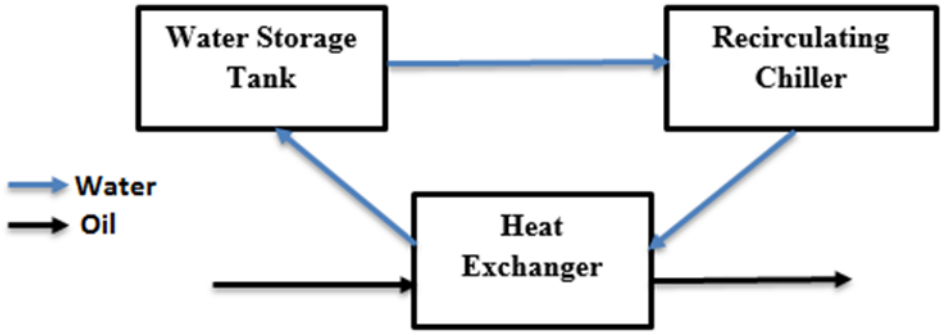

Figure 4.6 Heat Exchanger Section Schematic

Figure 4.7 Recirculating Chiller and Heat Exchanger

The main purpose of this section is to change the liquid viscosity by either heating or cooling it. A Cole-Parmer™ recirculating chiller was selected because it provides a rapid cool-down and heat-up times. Thus, it is capable of maintain temperature to ±0.1°C. Powerful force/suction pump provides flow rates up to 21 L/min (5.55 gpm) at pressures up to 80.7 kPa (11.7 psi).

Water in the storage tank goes to the recirculating chiller by gravity action. After passing through the chiller (where it is heated or cooled), it is pumped into the heat exchanger. There, this water meets the fluid test pumped from the main storage tank. Water circulates in this loop (from the tank to the chiller, from the chiller to the heat exchanger and from the heat exchanger back to the tank) several times until the test fluid reaches the desired temperature.

The heat exchanger is a Pipe-in-Pipe Heat Exchanger kind. Four PVC pipes (2-inches ID, 7-m long, each) jacket four copper pipes (1.5-inches ID, 6-m long, each). Test fluid pumped from the storage tank flows inside the copper pipes in series. Cool/warm water flows in the PVC/Copper annulus in parallel. Additionally, the water coming from the chiller is diverted into the four PVC pipes at the inlet of the heat exchanger. Then, it is diverted back into just one pipe at the outlet of the heat exchanger. After that, it goes back to the water tank, closing this loop.

The heat exchanger efficiency is higher when the fluids flow counter-currently (counter flow). Thus, it is desired to set the Copper/PVC Jacketed pipes this way. However, design issues when building the facility allowed only two sets of pipes to be constructed like these (the others ones were set concurrently- parallel flow). The valves right before and after the heat exchanger should remain closed when there is no need to change the fluid test viscosity. These valves allow the fluid to go through the bypass line instead. Moreover, self-heating of the test fluid is negligible because the test fluid pump almost does not add heat to it.

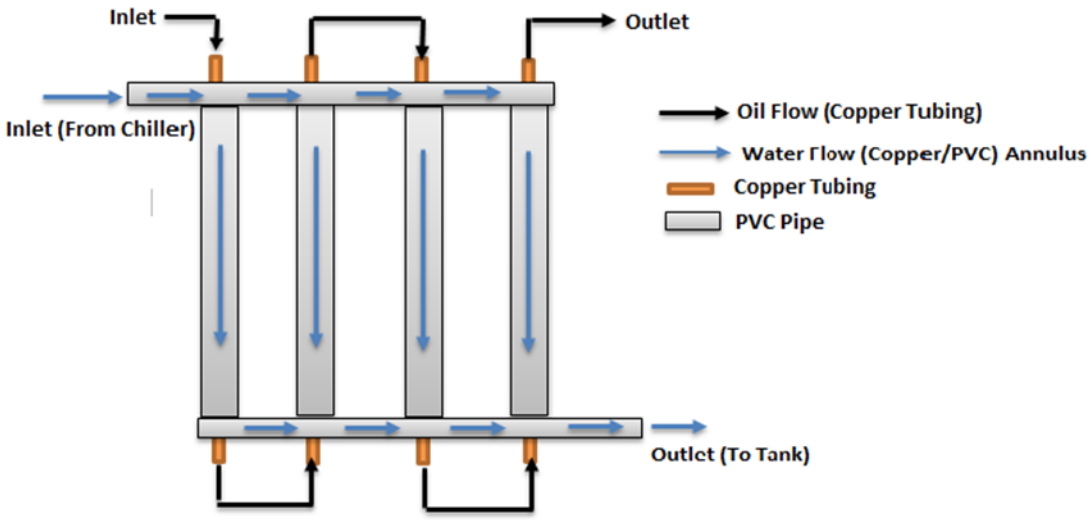

Figure 4.8 Heat Exchanger Schematic

4.2.3. Pipe Viscometer Section

Single-phase liquid flow is pumped into this section with the main objective to calculate the test fluid viscosity from pressure drop measurements (performed by a Differential Pressure Transmitter). Viscosity can be back calculated from pressure drop equation for single-phase flow once pressure drop is known. The pipe viscometer is made of a 6.22-m (20.4-ft) long 30.8-mm (1.5-in) ID PVC pipe. It consists of two separate pipe sections.

The first one, the developing section, has 3.22-m (127-in) long. It lets the single-phase flow to be fully developed. The following section, the Pressure Drop Measurement Section, has 3.0-m (118-in) long. It measures the pressure drop through two tees, one at the inlet and the other one at the outlet of this section. They are connected from the bottom part to the Differential Pressure Transmitter through a 3.175-mm (1/8-in) ID Clear Flexible PVC tubing. This way, fluid from the first tee (at the inlet) goes into the high-pressure side of the Differential Pressure Transmitter. Similarly, fluid from the second tee (at the outlet) flows into the low-pressure side. Therefore, the device can measure pressure drop along this pipe extension. Furthermore, two thermistors located at the Heat Transfer section can be used to measure liquid

temperature. Temperature measurement is crucial to determine the viscosity of the test fluid during experiments. The schematic of this section is shown next:

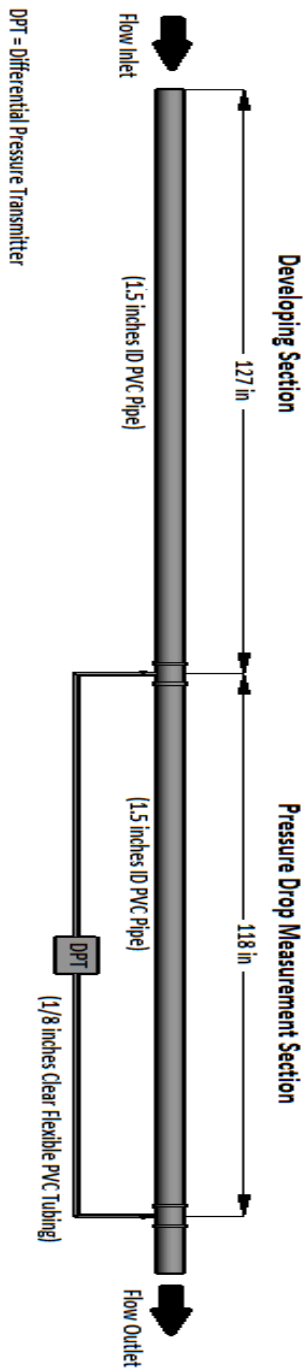

Figure 4.9 Schematic of Pipe Viscometer Section

4.2.4. Test Section

A schematic of the acrylic test section is shown Figure 4.12. For the detailed schematic drawing of the Heat Transfer Test Section, the reader is referred to Carestiato's thesis.[83] Test section built for hydrodynamics measurements consists of a 6.70-m (21.98-ft) long transparent acrylic pipe with a 38.1mm (1.5in) ID. The reason for choosing this diameter can be explained by the fact that no experiment on medium/high viscous oils for gas-liquid two-phase flow has been performed so far with this pipe size to this author's knowledge. Besides, the acrylic pipe should be long enough to allow slug flow to approach fully developed flow as much as possible. A longer dimension for that pipe could not be used due to budget limitations.

Transparency of the acrylic pipe improves visual observations of the flow behavior. Both test sections are installed on a horizontal beam supported by four stands and one pivot. The inclination of the test section can be adjusted manually by changing the height of a horizontal stand located halfway under the horizontal beam. The acrylic test section is instrumented with one differential pressure transmitter (the same one used for the pipe viscometer section).

For drift velocity experiment, a 63.5-cm (0.21-ft) long trap section at the inlet of test section was built to allow trapping and drainage of liquid. Therefore, a gas bubble was allowed to fill the space left by the drained liquid and be injected into the pipe. This length was chosen to allow an amount high enough of gas to penetrate the stagnant column of liquid during drift velocity experiment.

Pressure drop along this section can be measured at different locations. Five PVC tees are used to connect the acrylic pipes to make that possible. At each connection point, the lower extremity of the tees has been used to connect to a clear and flexible 3.175mm (1/8in) ID size PVC capillary tubing. The other end of the tubing will be connected to the DP Transmitter through a scheme of small ball valves. The schematic drawing (Figure 4.12) shows that, valves 5 through 13 can be closed or open, according to the location where pressure drop should be measured. This scheme with valves and

the capillary tubing was hung on the horizontal beam to make operations easier (see Figures 4.10 and 4.11).

For example, pressure drop along the inlet and outlet of the test section is be measured (trap section not included). Only valves 5 and 9 should be opened, while all the others valves must remain closed. This way, liquid at a higher pressure (upstream of the test section) flows through the capillary tubing into the high-pressure side of the pressure transmitter. Liquid at a lower pressure (downstream of the test section) flows into the low- pressure side of the pressure transmitter. In case of measuring the pressure drop along the Pressure Drop Span 3 region, valves 7,8,10,11 and 13 must be opened, while all the others should stay close.

A trap section was built at the upstream of the test section to allow drainage of the trapped liquid from a short piece of pipe. Besides, it should allow air to fill it for drift velocity experiments. This can be performed by first closing valves 1 and 2. Then, drain valve (valve 14) underneath this section must be opened.

Figure 4.10 Part of Pressure Measurement Apparatus

Figure 4.11 Capillary Tubing connected to both ends of Ball valve hung on the beam

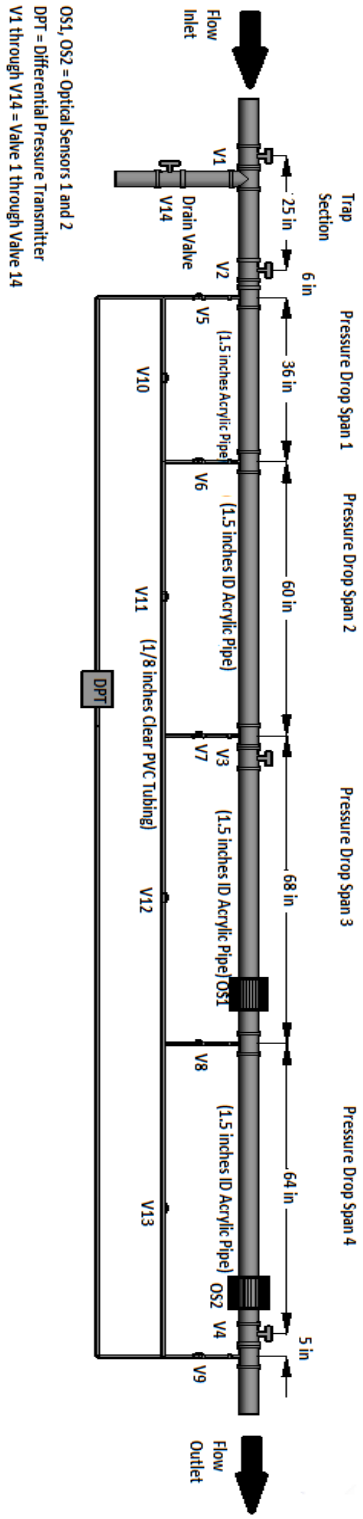

Figure 4.12 Schematic of Test Section

4.3. Instrumentation

One differential pressure transmitter, five Resistance Temperature Detector (RTD) temperature transducers, one Variable Frequency Drive and two Micro Motion™ mass flow meters are used in this study.

4.3.1. Thermistors

Two Omega™ Transition Joint-Style Thermistor probes are used for measuring liquid and gas temperatures. They work for immersion applications: the device should be put all the way inside the pipe so that it can contact the flow thoroughly. It yields a more accurate temperature measurement. Temperature accuracy for these instruments is in the range of $^{+}$/- 0.28°C (0.5°F).

Calibration of those devices was conducted using a Fluke™ Temperature Calibrator. It provides a temperature reading range of 35°C to 375°C (95°F to 707°F). The probe was insert into the device and after a couple minutes, the calibrated reading was displayed.

Figure 4.13 Temperature Calibrator Device

4.3.2. Mass Flow Meters

Two Coriolis Micro Motion™ F-Series mass flow meters are used to measure liquid and air mass flow rates, and densities. The manufacturer performed the flow meters calibration. The systematic uncertainty for the gas and liquid flow rates is reported as ±0.5 % and ± 0.1% for the gas and liquid, respectively. Density accuracy is

2.0 kg/m^3 (0.12 lb/ft^3). Both devices can also measure fluid temperatures with an accuracy of ±1°C (1.8°F) ± 0.5% of the reading.

4.3.3. Differential Pressure Transmitter

One Azbil™ AT9000 Advanced Transmitter Differential Pressure Transmitter (GTX31D series) was used to measure pressure drop. It provides high accuracy of ±0.04 % along with long-term stability (zero drift of only ±0.1% over 10 years), greatly reducing calibration work after installation. The manufacturer provided calibration.

This Differential Pressure Transmitter was employed to measure the pressure drop along both pipe viscometer and the acrylic test sections. Two three way-valves were placed to divert the flow into the Differential Pressure Transmitter from those two different locations as it can be seen in the next figure. Thus, just one equipment can be used for two purposes.

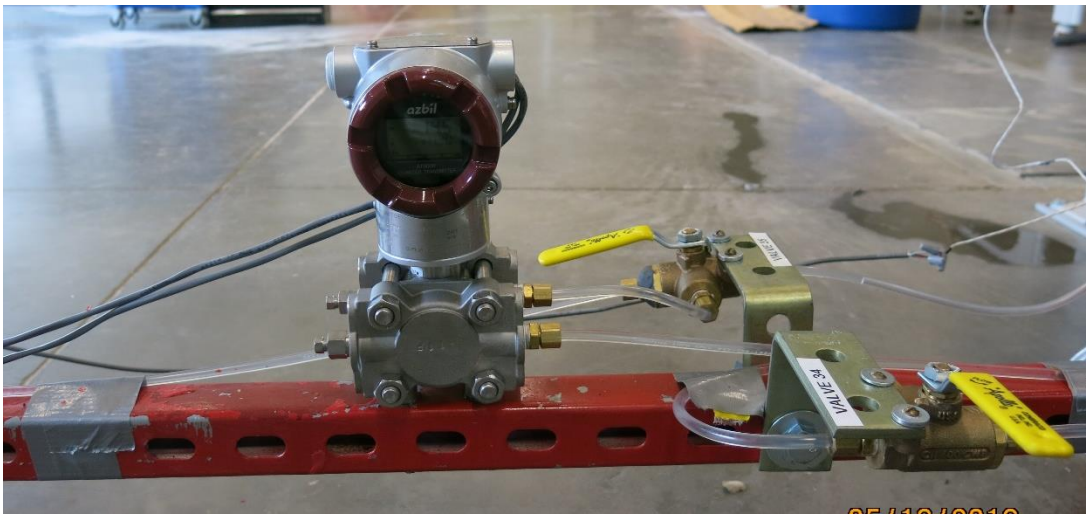

Figure 4.14 DP Transmitter and Three-way valves

4.3.4. VFD – Variable Frequency Drive

A VFD- Automation Direct™ GS2 ac drive series- was used for controlling the pump and providing a good control of the liquid flow rate. It allows configuration of the drive, setting the speed, starting and stopping the drive, commanding forward and reverse direction of motor shaft. It is also possible to monitor specific parameters during

operation. Moreover, the VFD should be housed inside a designed enclosure with a proper ventilation to avoid damaging the device.

Figure 4.15 VFD inside the enclosure with ventilation

4.4. Data Acquisition System and Data Processing

A Red Lion™ Data Acquisition System was installed so that all the operational parameters measured by the instruments could be recorded in real time. Data is automatically sent to the software installed in the lab computer to be analyzed through an Excel spreadsheet format.

It is not necessary to login and logout from the software because the data logging is recorded twenty-four hours a day. Moreover, it is also possible to control the pump speed via VFD manually from the computer. The picture of the data acquisition module inside the proper enclosure is depicted next:

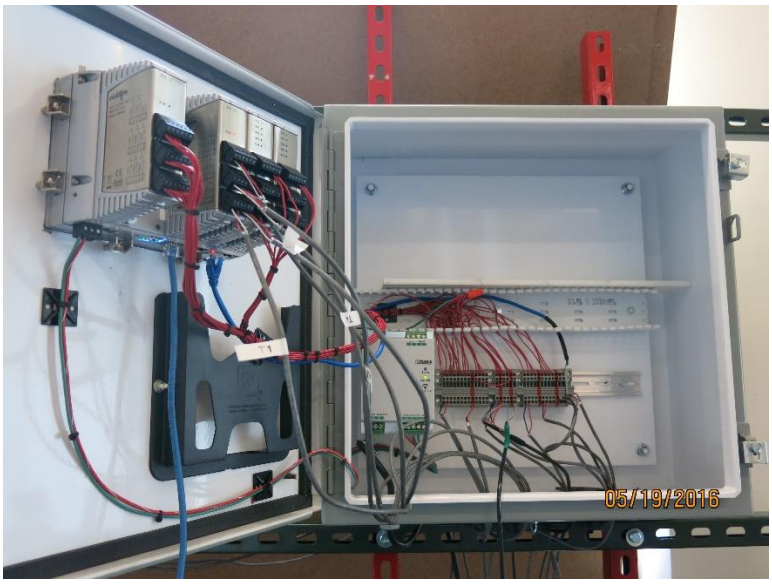

Figure 4.16 Data Acquisition System inside the Enclosure

4.5. Experimental Procedure and Hazard Analysis

An experimental procedure is detailed next to avoid any hazard damage and to achieve the best performance of the facility. The operator should wear safety glasses and head hat at all time. Other than that, the pressure regulator for the gas line should not exceed 50 psi. A pressure relief valve for the liquid line was installed close to the tank to avoid breaking the line for overpressure. This valve allows a maximum operation pressure in the line of 50 psi.

1. Set the desired flow inclination angle by lowering or raising up the beam with a jack;
2. Turn on the power for the pump and the VFD;
3. Check all the valves to assure whether the test fluids will be circulated through the correct path or not and to avoid buildup of pressure inside the pipes;
4. By operating the valves, decide which way the fluids should circulate: only through the acrylic section, only through the heat transfer test section or through both test sections;
5. Close the ball valve right after the check valve at the gas line;

6. Turn on the test fluid pump and control the speed through the VFD to obtain the desired liquid flowrate and velocity;

7. When it is desired to heat up or cool down the liquid, circulate it through the heat exchanger with the chiller turned on; otherwise, circulate it through the bypass line;

8. After the set temperature is reached, single phase measurements can be taken along the pipe viscometer section and both test sections;

8.1 For liquid viscosity calculations, set both three-ways valve accordingly to divert the flow from the pipe viscometer into the DP Transmitter. With the pressure drop obtained, back calculate viscosity from pressure drop equation;

8.2 For drift velocity experiments:

8.2.1 Turn on the pump to fill completely the acrylic section with liquid;

8.2.2 Turn off the pump and immediately close the valves at the inlet and at the outlet of test section to have liquid trapped there;

8.2.3 Close the valve at the inlet of the trap section and open the drain valve – liquid will start to drain out of the pipe and the trap section will have only gas inside;

8.2.4 Open the valve at the inlet of the acrylic section to allow both drainage of the liquid inside the pipe and entrance of gas from the trap section and the atmosphere to continuously penetrate through the liquid column;

8.2.5 The time taken by the bubble to travel along different points across the pipe is recorded and it is used to calculate the drift velocity;

9. For two-phase flow experiments, open the needle valve and the ball valve at the gas line to let gas flows into the facility. Gas velocity is controlled by setting the correct gas mass flow rate and then gas velocity is obtained from ideal gas law;

10. Let fluids circulate for a few minutes until steady flow is obtained before measuring the hydrodynamics parameters;

11. For pressure drop calculations along the test section, accordingly set the three-ways valves to divert the flow from the acrylic section into the DP Transmitter. Before doing that, open the bleed valve at the DP Transmitter to bleed any gas bubble trapped inside the DP line. Pressure drop between different ports along the pipe are obtained when setting the valves underneath the test section accordingly;

12. Observe flow hydrodynamics parameters, use a video camera and the data acquisition system - installed on the laboratory computer and which runs throughout the day- to analyze the results obtained;

13. Shut down the pump, the VFD and the electricity power provided to them.

14. Close the needle valve to stop the supply of gas to the system;

Before conducting single-phase liquid tests, some gas bubbles coming from the gas line might be entrained in the liquid. It is recommended to wait for a few minutes before starting the test and turn on the pump at lower speed to remove those bubbles. This would avoid any misleading results caused by the bubble's presence.

4.6. Experimental Range

Forty-six tests have been carried out with water and air as test fluids to evaluate the main hydrodynamics parameters of gas-liquid two-phase flow. Liquid viscosity and density almost did not change because all tests were performed at standard conditions. The values for them were considered the same as the ones obtained in Section 4.1. As for the gas density, the calculation procedure is shown in Section 4.7.4 through the gas ideal law. Gas viscosity was obtained from pressure drop measurement from the pipe viscometer section for single-phase gas measurement (viscosity is back calculated with pressure drop known, as shown in Section 3.1). The following table summarizes the range of the operational parameters, such as gas and liquid velocities, densities and viscosities and pipe inclination angles used throughout the tests:

Table 6. Operational Range

Pipe Inclination (θ= 0°)						
Test#	**ρ_G [kg/m^3]**	**μ_G [Pa.s]**	**μ_L [Pa.s]**	**v_{LS} [m/s]**	**ρ_L [kg/m^3]**	**v_{GS} [m/s]**
1	1.074	1.8×10^{-5}	1.1×10^{-3}	0.03	996.1	0.238
2	0.998	1.8×10^{-5}	1.1×10^{-3}	0.03	996.1	2.148
3	1.002	1.8×10^{-5}	1.1×10^{-3}	0.03	996.1	9.924
4	1.011	1.8×10^{-5}	1.1×10^{-3}	0.03	996.1	13.04
5	1.130	1.8×10^{-5}	1.1×10^{-3}	0.20	996.1	0.226
6	1.065	1.8×10^{-5}	1.1×10^{-3}	0.20	996.1	2.013
7	1.123	1.8×10^{-5}	1.1×10^{-3}	0.20	996.1	8.854
8	1.195	1.8×10^{-5}	1.1×10^{-3}	0.20	996.1	12.37
9	1.125	1.8×10^{-5}	1.1×10^{-3}	0.50	996.1	0.227
10	1.168	1.8×10^{-5}	1.1×10^{-3}	0.50	996.1	1.836
11	1.414	1.8×10^{-5}	1.1×10^{-3}	0.50	996.1	7.036
12	1.518	1.8×10^{-5}	1.1×10^{-3}	0.50	996.1	8.683
Pipe Inclination (θ= +1°)						
Test#	**ρ_G [kg/m^3]**	**μ_G [Pa.s]**	**μ_L [Pa.s]**	**v_{LS} [m/s]**	**ρ_L [kg/m^3]**	**v_{GS} [m/s]**
1	1.447	1.8×10^{-5}	1.1×10^{-3}	0.10	996.1	0.177
2	1.514	1.8×10^{-5}	1.1×10^{-3}	0.50	996.1	0.966
3	1.550	1.8×10^{-5}	1.1×10^{-3}	0.50	996.1	1.383
4	1.740	1.8×10^{-5}	1.1×10^{-3}	0.50	996.1	3.739
5	2.009	1.8×10^{-5}	1.1×10^{-3}	0.50	996.1	6.560
6	1.406	1.8×10^{-5}	1.1×10^{-3}	0.20	996.1	1.040
7	1.410	1.8×10^{-5}	1.1×10^{-3}	0.20	996.1	1.520
8	1.443	1.8×10^{-5}	1.1×10^{-3}	0.20	996.1	4.509
9	1.547	1.8×10^{-5}	1.1×10^{-3}	0.20	996.1	8.522
10	1.321	1.8×10^{-5}	1.1×10^{-3}	0.04	996.1	1.107
11	1.322	1.8×10^{-5}	1.1×10^{-3}	0.04	996.1	1.621
12	1.307	1.8×10^{-5}	1.1×10^{-3}	0.04	996.1	4.977
13	1.332	1.8×10^{-5}	1.1×10^{-3}	0.04	996.1	9.899

Pipe Inclination (θ= +5°)						
Test#	**ρ_G [kg/m^3]**	**μ_G [Pa.s]**	**μ_L [Pa.s]**	**v_{LS} [m/s]**	**ρ_L [kg/m^3]**	**v_{GS} [m/s]**
1	1.540	1.8×10^{-5}	1.1×10^{-3}	0.50	996.1	0.475
2	1.580	1.8×10^{-5}	1.1×10^{-3}	0.50	996.1	1.358
3	1.745	1.8×10^{-5}	1.1×10^{-3}	0.50	996.1	3.730
4	1.989	1.8×10^{-5}	1.1×10^{-3}	0.50	996.1	6.632
5	1.460	1.8×10^{-5}	1.1×10^{-3}	0.20	996.1	0.501
6	1.419	1.8×10^{-5}	1.1×10^{-3}	0.20	996.1	1.511
7	1.458	1.8×10^{-5}	1.1×10^{-3}	0.20	996.1	4.463

Table 6. Continued

8	1.558	1.8×10^{-5}	1.1×10^{-3}	0.20	996.1	8.460
9	1.423	1.8×10^{-5}	1.1×10^{-3}	0.10	996.1	0.514
10	1.380	1.8×10^{-5}	1.1×10^{-3}	0.10	996.1	1.553
11	1.384	1.8×10^{-5}	1.1×10^{-3}	0.10	996.1	4.701
12	1.431	1.8×10^{-5}	1.1×10^{-3}	0.10	996.1	9.213
Pipe Inclination (θ= -1°)						
Test#	**ρ_G [kg/m^3]**	**μ_G [Pa.s]**	**μ_L [Pa.s]**	**v_{LS} [m/s]**	**ρ_L [kg/m^3]**	**v_{GS} [m/s]**
1	1.083	1.8×10^{-5}	1.1×10^{-3}	0.05	996.1	0.236
2	0.998	1.8×10^{-5}	1.1×10^{-3}	0.05	996.1	2.147
3	1.028	1.8×10^{-5}	1.1×10^{-3}	0.05	996.1	12.824
4	1.116	1.8×10^{-5}	1.1×10^{-3}	0.20	996.1	0.229
5	1.051	1.8×10^{-5}	1.1×10^{-3}	0.20	996.1	2.039
6	1.171	1.8×10^{-5}	1.1×10^{-3}	0.20	996.1	11.256
7	1.209	1.8×10^{-5}	1.1×10^{-3}	1.00	996.1	0.212
8	1.370	1.8×10^{-5}	1.1×10^{-3}	1.00	996.1	1.565
9	2.066	1.8×10^{-5}	1.1×10^{-3}	1.00	996.1	6.384

4.7. Building and Design Challenges

Several obstacles had to be overcome to allow the proper functioning of the experiment and to produce high quality data throughout the process of building the state-of-the-art multiphase flow loop facility. Some of these challenges are discussed next:

4.7.1. Leaking Test

A subject of major importance and that was too much time-consuming during the building process of the facility was the treatment of gas leaking. It occurred mainly through very small gaps left at the pipe fittings connection spots. The reason for that in most of the cases arose from an insufficient use of glue or Teflon tape in those points. In addition, connections between materials of different kinds, like brass-plastic and copper-PVC, led to gas leaking when a suitable pipe fitting did not exist. Tracking of this problem was performed by spraying a water-detergent solution at every connection spot existent in the facility when the system was pressurized with gas. Detection of a

leaking happened when bubbles came out of the solution and started growing continuously.

A solution that proved to work for this problem consisted in a J-B Weld Steel-Steer™ epoxy putty stick. After mixing, it forms an industrial-strength polymer compound that can be molded into shapes, filling the left spots responsible for the leaking. Moreover, it is rated at a tensile strength of 6.2 MPa (900 psi) and withstands temperatures up to 149°C (300ºF), more than enough for the purposes of this work.

A pressure test was carried out to check whether the facility was losing or not too much pressure and gas volume to the environment due to the gas leaking. Gas was supplied to the system and the valve at the outlet of the test section was closed. Thus, the whole facility was pressurized. Initial pressure exerted by the compressed air was 377 kPa (54.69 psi). Several records of pressure and percentage of gas mass loss were taken at time steps of 30min. Pressure was measured by the pressure gauge close to the gas outlet. This kind of test (lasting 8h each) was repeated several times after each gas leaking found was fixed. After correcting as many leaking as possible, the final test results that yielded a minimum amount of pressure and percentage of gas mass lost to the environment, plotted against time, are as follows:

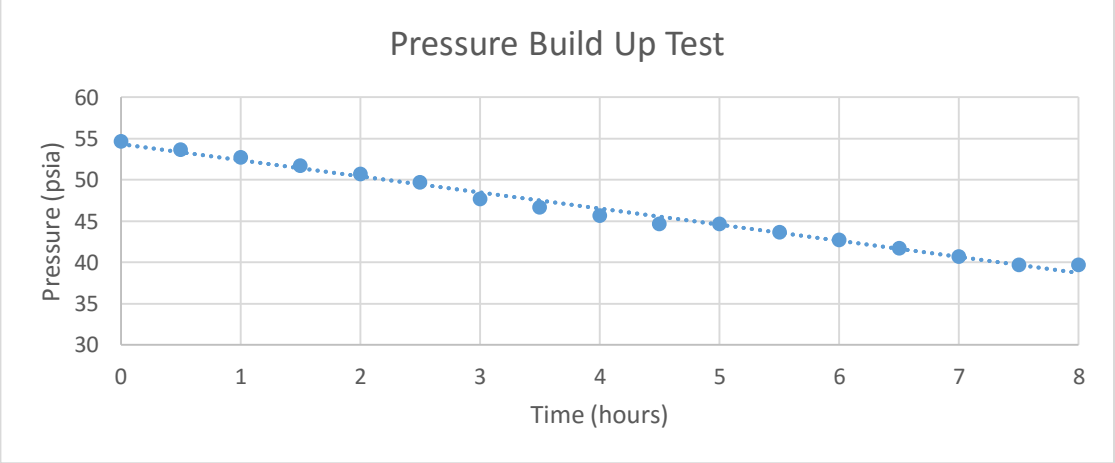

Figure 4.17 Buildup Test

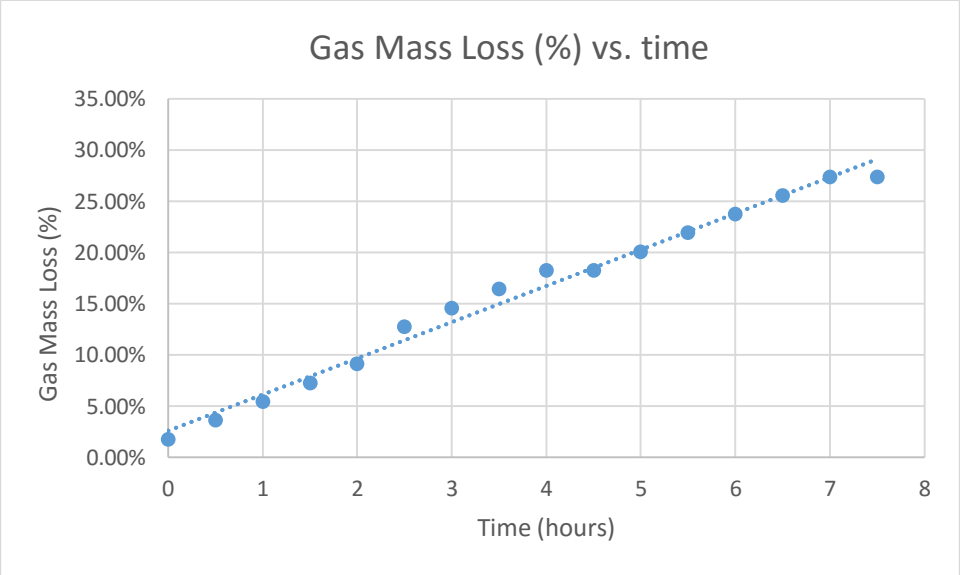

Figure 4.18 Percentage of Gas Mass Lost

The last test took 48 hours and a residual value for pressure and fraction of gas mass lost were found to be 136 kPa (19.69 psia) and 63.99%, respectively. The results above suggest that any gas leaking still existent is not capable to affect the results because the hydrodynamics tests take less than 10 minutes.

4.7.2. Backflow of Liquid in the Gas Line

Gas and liquid were designed to mix at the wye fitting at the very end of each separate streamline. However, no valve at the gas line was installed at first place to control the flow close to the gas outlet.

It was noticed that the gas density read by the flow meter was completely off the expected value after conducting two-phase flow experiment. The reason for that was explained by the backflow of liquid into the gas side at the mixing wye spot. A check valve, which only allows flow in one direction, was installed to avoid liquid to invade the gas line. The gas outlet pipe was also slightly tilted so that liquid would not have enough pressure to overcome gravity. Moreover, a ball valve was installed right after the check valve for single-phase liquid tests. It ensures that liquid would not cause back flow at all.

4.7.3. Acrylic Pipe Fittings and Connections

Acrylic pipe connections posed some troubles. The major of them was related to the connection between each part. The acrylic test section has an extension of more than 6.1-m (20-ft) long and each part only comes in lengths of 5-ft long. Thus, it was necessary to connect four pipe sections together. However, most of the acrylic pipe fittings are too complicated to find in the correct size. The solution found was to buy PVC fittings (tees) and use them as connectors for the acrylic.

A drawback of doing this is associated with the different sizes of the acrylic pipe and the PVC fittings. Acrylic follows a different size rule specification, whereas PVC is in line with the NPT specifications. Therefore, it was necessary to machine the acrylic outer diameter, so that it could slide all the way into the PVC tee properly.

Another complication arises when it is necessary to glue different materials. It is not appropriate to use any kind of glue. Otherwise, some leaking problems may turn up. After a thorough analysys, a glue, friendly for both acrylic and PVC, was selected. It showed to be capable of doing the job.

4.7.4. Gas Superficial Velocity Measurement

Gas superficial velocity measurement was not straightforward. The mass flowmeter does not provide this value directly. Instead, gas velocity can be set by controlling the mass flow rate. Calculation of the former is obtained basing on the gas density and the pipe cross sectional area, as follows:

$$v_{SG} = \frac{\dot{m}}{\rho A_P}$$

However, gas density changes throughout the pipe because pressure and temperature change as well. The value read in the flow meter is not capable of distinguish that. Pressure at the inlet and at the outlet of the acrylic test section were recorded to calculate density at the inlet and at the outlet, respectively. Calculation is based on the ideal gas law as follows:

$$\rho = \frac{P}{R_{specific}T}$$

The constant $R_{specific}$ is the ratio between the constant of the gases R and the air molecular weight. Results for each test show that density do not change much between the inlet and the outlet. Thus, an average of density between those values was taken into account.

4.8. Facility Limitations

The next table shows, respectively, the operational limits of the facility for temperature, the maximum liquid flow rate provided by the pump, the maximum pressure allowed inside the pipes, the range of possible pipe inclination angles for the test section and the maximum safe gas velocity developed by the gas outlet:

Table 7 Facility Limitations

Temperature Range [°C]	5-60
Maximum Liquid Flowrate [gpm]	35
Maximum Operational Pressure [psi]	50
Pipe Inclination Angles [°]	-2 to 25
Maximum Safe Gas Velocity [m/s]	13.84

CHAPTER V

TEST RESULTS AND ANALYSIS

This section provides the results obtained during the commissioning of the facility for single-phase and two-phase pressure drop, slug flow hydrodynamic parameters (slug length, slug frequency, film profile and translational velocity) and flow pattern map. The reliability of the data obtained is validated against some closure relationships and mechanistic models existing in the literature. Furthermore, drift velocity data is compared to results obtained through CFD software.

5.1. Flow Pattern

Different flow pattern maps have been generated by changing the gas and liquid flow rates and pipe inclination. Additionally, several flow patterns could be developed in the new multiphase flow loop. All kinds of flow patterns existing in horizontal and near-horizontal pipes could be produced and studied. The exception was the dispersed bubble flow, where pump limitations did not allow higher liquid flow rates. Several tests were recorded and the video files were uploaded to a Youtube channel[84] with the purpose to encourage the spread of the education on the multiphase flow phenomena.

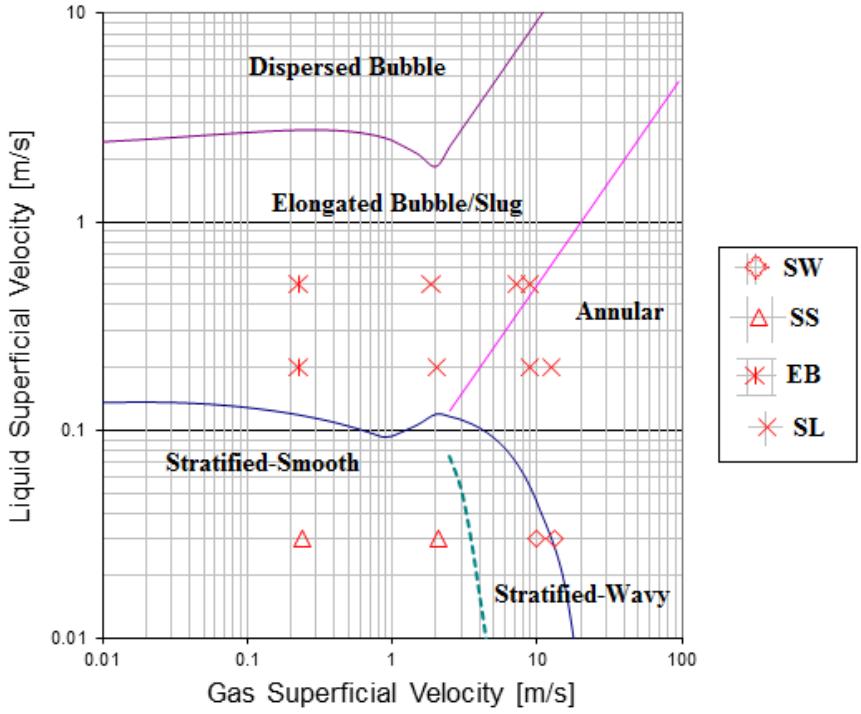

Figure 5.1 Flow Pattern Map for Horizontal Pipe. Line are from Shoham[1] flow pattern prediction software. Symbols are the experimental observations

For horizontal flow, the observed flow patterns agreed very well with the mechanistic model prediction as expected (see Figure 5.1). The next two pictures show the main differences between stratified-smooth and stratified-wavy flow. The latter displays a wavy interface with small amplitudes. The former has a smooth interface and most of times a higher liquid level as well.

Figure 5.2 Stratified Smooth Flow Pattern

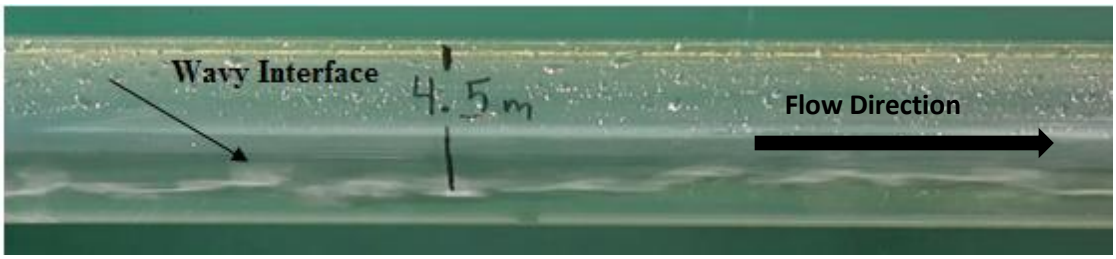

Figure 5.3 Stratified-Wavy Flow Pattern

Slug flow is depicted in the next figure. It shows clearly the distinction between the two main regions existing in that kind of flow. The white region represents the slug body close to the mixing front with some entrained bubbles. At the right half of the figure, the tail of the Taylor bubble characterizes the stratified region.

Figure 5.4 Slug Flow in Horizontal Pipes

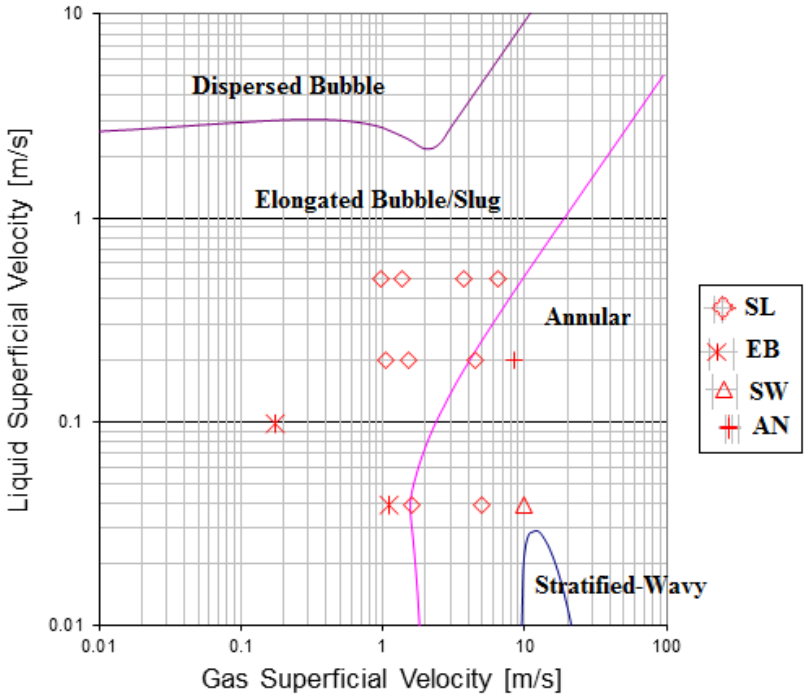

Figure 5.5 Flow Pattern Map for 1 degree Upwards Pipe

A fully developed annular flow could not be achieved in any inclination angle tested because too high gas velocities were needed to develop this kind of flow. A transition between slug, stratified-wavy and annular flows (called sometimes as Proto Slug Flow) was observed instead. The next figure depicts this flow pattern for one degree upwards inclination angle:

Figure 5.6 Proto-Slug Flow Pattern

This transition displays aerated unstable waves being swept around the pipe periphery. These waves wets the upper pipe wall occasionally. “It is not stratified-wavy because liquid is swept around and wets the upper pipe wall with a thin film. In addition, it is not slug flow because “there is no liquid body bridging the entire pipe cross-sectional area. Furthermore, it is not fully developed annular flow because there is no stable film around the pipe periphery. [1]

The physical mechanism of elongated bubble and slug flow are similar. Both flow patterns are intermittent flow. The differences between these flow patterns are the entrainment of gas phase inside the liquid phase and the speed of the gas-liquid interface. The elongated bubble flow shows the absence of entrained bubbles in the slug body. Figure 5.7 (representing an elongated bubble flow) shows a single-phase liquid body, which is completely free of air. A significant amount of gas is entrained in liquid phase for Slug flow as shown in Figure 5.4. The gas-liquid interface is well-defined and very smooth for the case of the elongated bubble compared to slug flow.

Figure 5.7 Front of Taylor Bubble for Elongated Bubble Flow

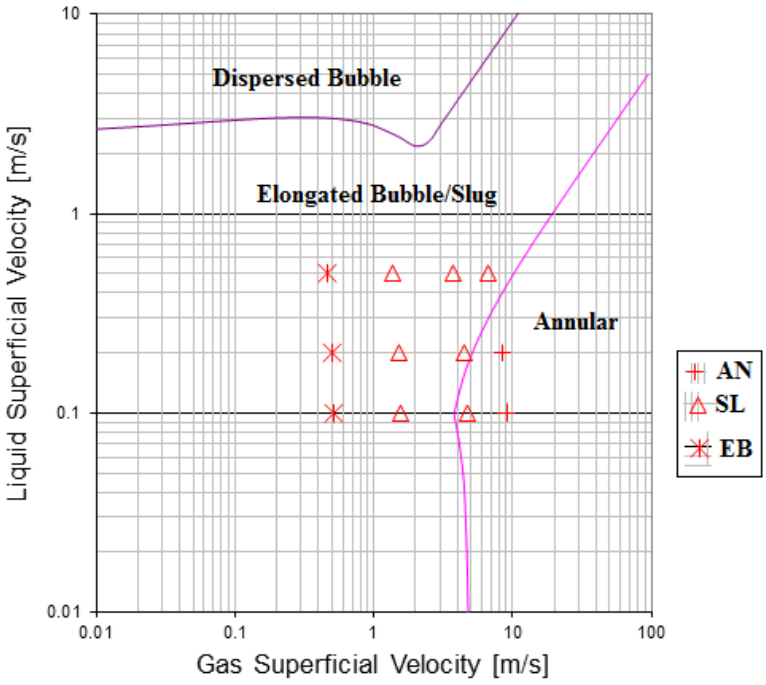

Figure 5.8 Flow Pattern Map for 5 degrees Upwards Pipe

The flow pattern map becomes more dominated by intermittent flow as pipe inclination starts to increase more from the horizontal, as Figure 5.8 shows. The next picture shows an occurrence of slug flow for that pipe inclination:

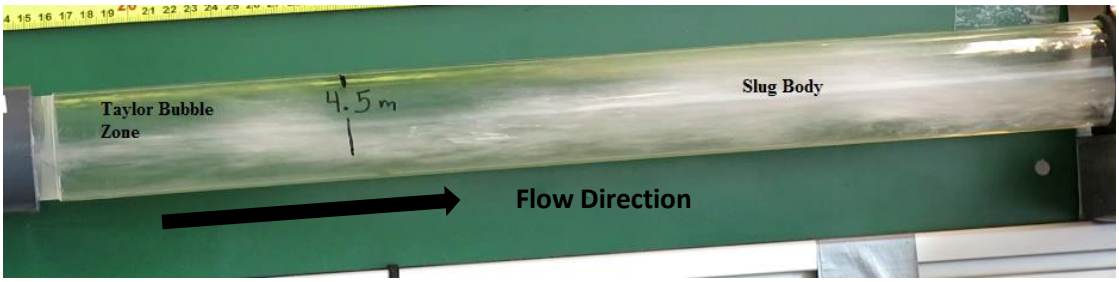

Figure 5.9 Slug Flow for 5 degrees upwards pipe

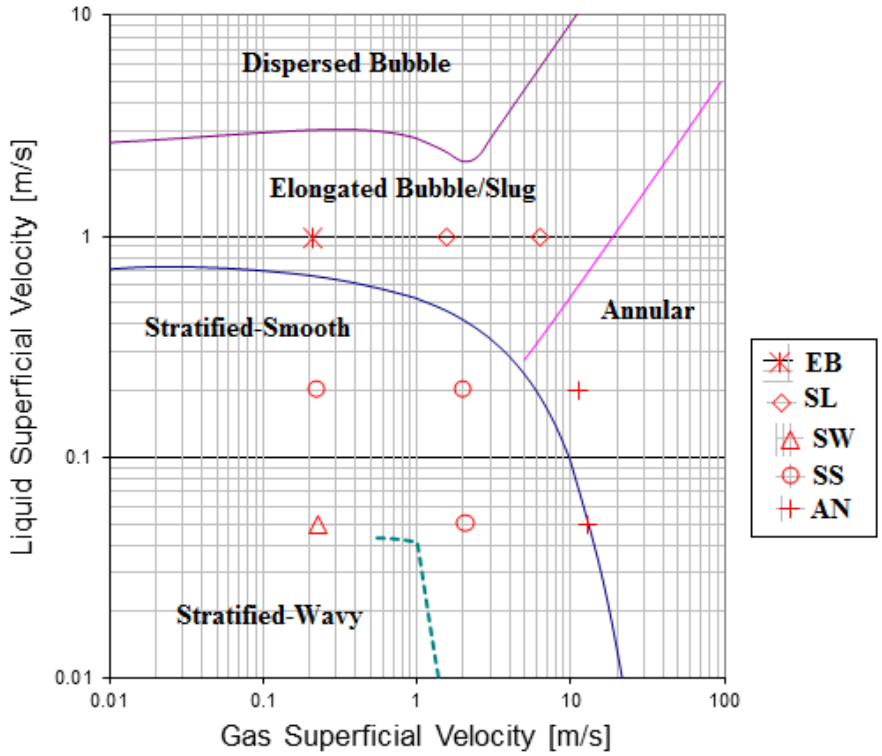

Figure 5.10 Flow Pattern Map for 1 degree downwards Pipe

The dominant flow pattern for downwards flow is stratified flow, as it can be observed from the last plot. The next picture shows a stratified-wavy flow for an inclination angle of one degree downwards:

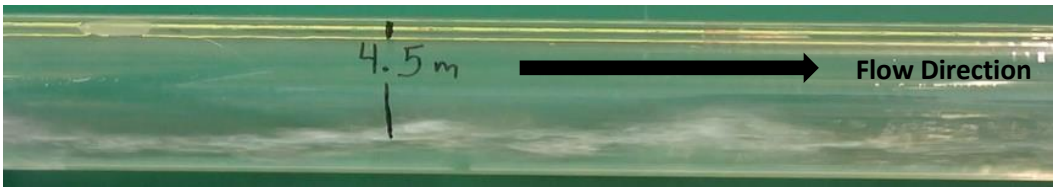

Figure 5.11 Stratified-Wavy Flow for Downwards Inclination Angle

5.2. Single-Phase Water Pressure drop

A set of six tests for measurement of water single-phase pressure drop between ports 2 and 5 of the acrylic section have been carried out. Liquid flow rates ranged from 5 to 30 gpm. It is recommended to choose port 2 instead of port 1 because a fully

developed flow can be achieved and entrance effects are minimized. Results measured by the DP Transmitter and the predicted ones (from the calculation procedure of the last chapter) are shown in the next plot and table:

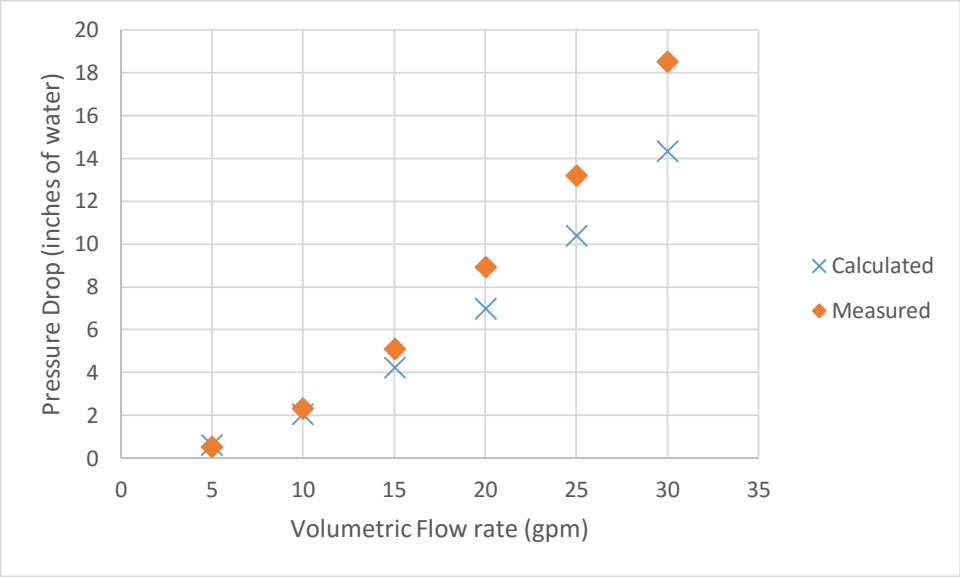

Figure 5.12 Single-Phase Pressure Drop Results

Table 8 Single-Phase Water Pressure Drop Summary Results

Liquid Flowrate (gpm)	Calculated Pressure Drop (in of water)	Measured Pressure Drop (in of water)	Discrepancy (%)
5	0.6	0.5	-22.08%
10	2.0	2.3	10.94%
15.05	4.2	5.1	17.49%
20.04	7.0	8.9	21.52%
25.04	10.4	13.2	21.41%
30	14.3	18.5	22.65%

It is possible to note that the results collected through the facility match pretty good with the ones calculated from single-phase pressure drop equation shown in the last chapter. It should be taken into account an accuracy of +/- 0.04% provided by the

DP Transmitter. The majority of the discrepancy can be related to the additional pressure drop caused by the several flow restrictions existing along the test section (five tees and two ball valves). Thus, it is expected that the measured pressure drop is higher than the calculated one, which is confirmed from the results above. This discrepancy becomes higher as liquid flow rates increase because the pressure drop due to the flow restrictions increases as well.

Another interesting feature was obtained when measuring pressure drop along different ports along the pipe. The next graph shows that pressure drop is higher close to the outlet than next to the inlet of the pipe as expected. Furthermore, results confirmed that as liquid flowrate increases, pressure drop also goes up.

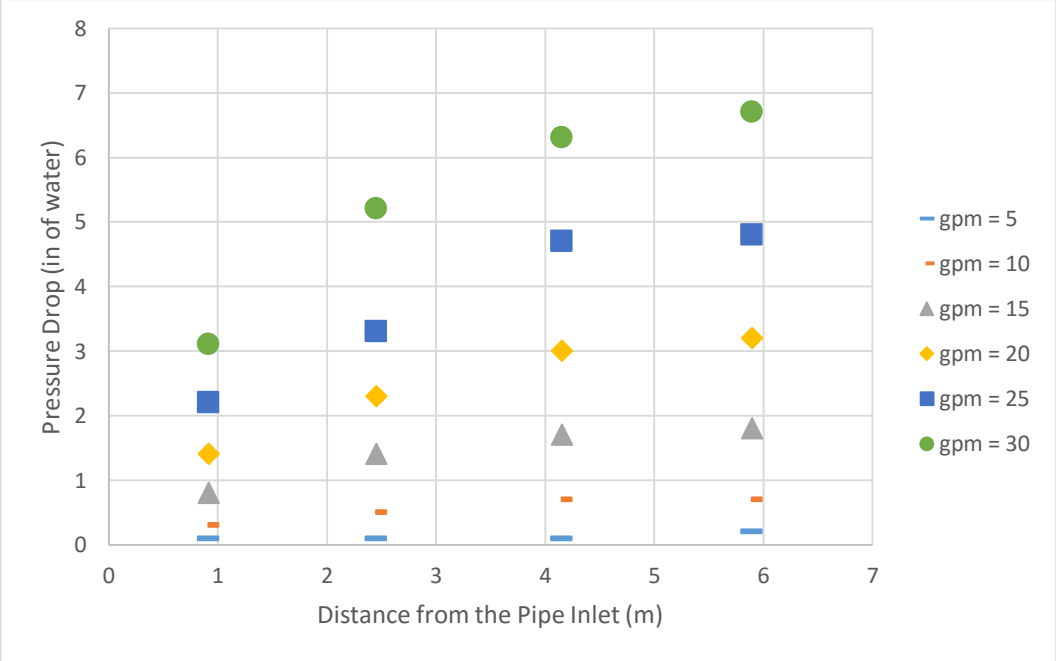

Figure 5.13 Pressure Drop Measured at Different Ports along the Pipe

5.3. Typical Errors for Models Prediction

Prediction of gas-liquid two-phase through models and correlations existent in the literature poses a high uncertainty since this kind flow is too complex. The following

tables show the order of magnitude of the errors typically found when comparing some existing models against experimental data. The average percent error (ε_2) should be taken into account because it represents better the errors obtained through experimental work. Data of stratified flow and slug flow pressure drops are shown to put things into perspective. The reader can understand that the discrepancies observed in the experiment of this work are acceptable when they fall in the range of errors shown on the tables below:

Table 9. Models and Correlations Typical Errors for Stratified Flow Pressure Drop. Developed by Xiao et al.[85]

No.	Model or Correlation	No. of Data Points	Statistical Parameters					
			ε_1 (%)	ε_2 (%)	ε_3 (%)	ε_4 $\times 10^4$ (Pa)	ε_5 $\times 10^4$ (Pa)	ε_6 $\times 10^4$ (Pa)
1	**This Model**	89	-18.0	34.6	49.1	-3.2	8.1	14.3
2	Beggs & Brill	86	-9.0	34.9	53.7	6.6	9.0	16.2
3	Muk. & Brill	83	16.7	66.9	79.0	16.0	19.3	19.4
4	Dukler	86	32.1	59.2	80.8	21.1	22.5	25.1
5	Dukler-Eaton	86	23.1	54.4	78.8	17.4	19.0	23.1

Table 10. Models and Correlations Typical Errors for Slug Flow Pressure Drop. Developed by Xiao et al.[85]

No.	Model or Correlation	No. of Data Points	Statistical Parameters					
			ε_1 (%)	ε_2 (%)	ε_3 (%)	ε_4 $\times 10^4$ (Pa)	ε_5 $\times 10^4$ (Pa)	ε_6 $\times 10^4$ (Pa)
1	**This Model**	121	-18.9	22.7	19.8	-8.7	9.3	12.6
2	Beggs & Brill	129	23.3	31.6	33.0	7.9	9.6	13.9
3	Muk. & Brill	127	27.1	40.0	54.7	4.8	10.1	15.7
4	Dukler	128	28.5	34.4	35.5	10.5	11.4	16.5
5	Dukler-Eaton	129	22.5	29.9	32.4	9.6	10.7	18.2

5.4. Pressure Drop and Liquid Holdup for Water-Gas Stratified Flow

Pressure drop between ports 1 and 5 was measured for stratified-smooth and stratified-wavy flows in horizontal pipe. Moreover, for the horizontal configuration, average liquid holdup was obtained as well. Liquid superficial velocity was fixed at 0.03 m/s (0.09 ft/s). Gas superficial velocities ranged from 0.24 to 13.04 m/s (0.79 to 42.78 ft/s). Results collected through the facility were compared to the ones from the calculation procedure detailed in the last chapter. The next graph and table summarize the results obtained:

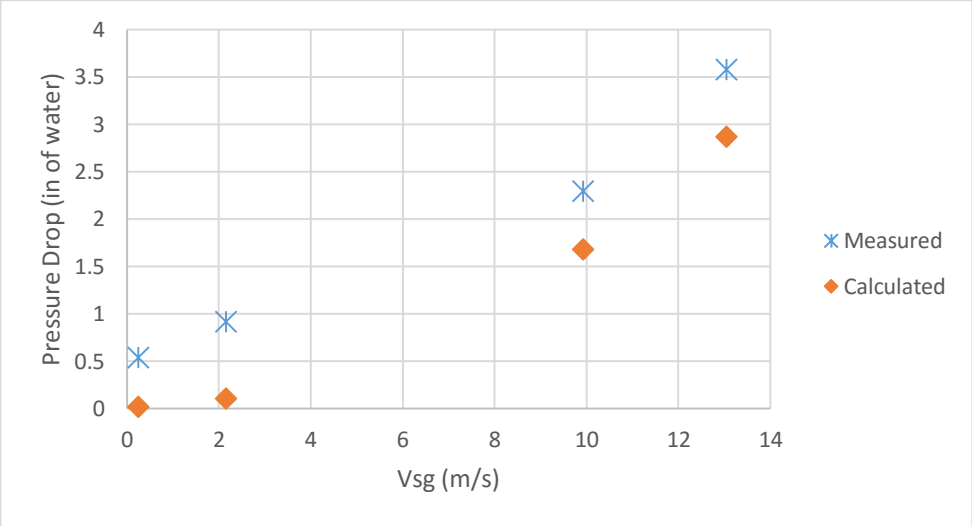

Figure 5.14 Stratified Pressure Drop Results

Table 11. Stratified Pressure Drop Summary Table

Flow Pattern	v_{SG} (m/s)	Pressure Drop Measured (in of water)	Pressure Drop Calculated (in of water)	Discrepancy (%)
Stratified Smooth	0.24	0.54	0.02	96.30%
Stratified Smooth	2.15	0.92	0.11	88.04%
Stratified Wavy	9.92	2.3	1.68	26.96%
Stratified Wavy	13.04	3.58	2.87	19.83%

Results suggest that pressure drop measured increases as gas superficial velocity increases. It was expected due to the higher frictional losses caused by the greater gas velocities. Discrepancy between measured and calculated values are high for stratified-smooth flow because the DP Transmitter is not accurate for very low liquid and gas velocities. This discrepancy becomes much more acceptable as gas velocities go up and flow becomes stratified-wavy. In this case, predicted and measured values agree pretty well. In addition, like single-phase pressure drop, calculated values do not take into account pressure losses caused by flow restrictions along the pipe. It makes them to be lower than the measured values.

Liquid holdup measurement was performed by suddenly closing both valves at the inlet and at the outlet of the acrylic test section during stratified flow regime. All liquid trapped inside the pipe was drained out through the drain valve. Then, its volume was recorded using a graduated cylinder. Average liquid holdup for a given set of flow conditions could be obtained by dividing the drained volume of liquid by the total volume of the acrylic pipe.

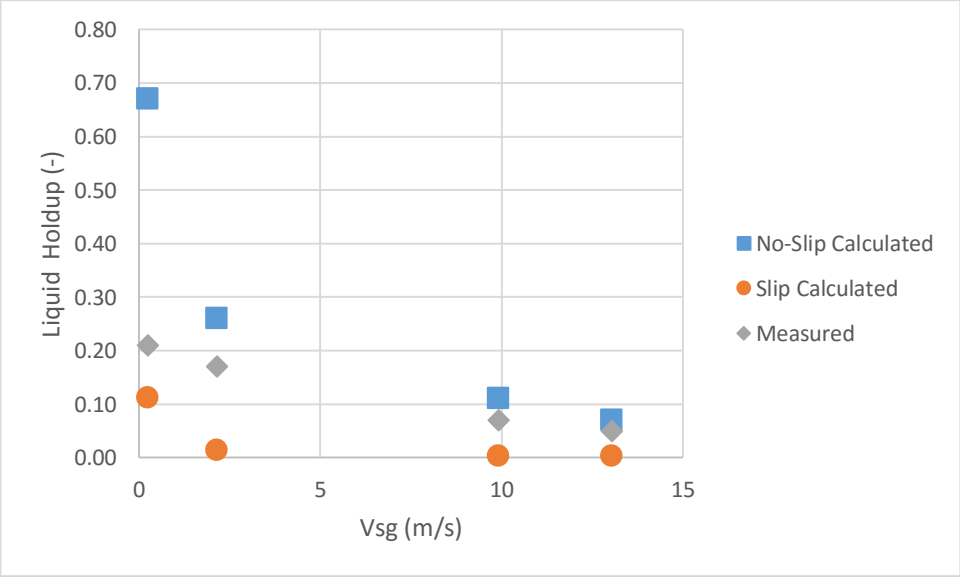

Figure 5.15 Stratified Liquid Holdup Results

Table 12. Stratified Liquid Holdup Summary Table

Flow Pattern	Vsg (m/s)	Measured Holdup (-)	Calculated No-Slip Holdup (-)	Calculated Slip Liquid Holdup (-)
Stratified Smooth	0.24	0.21	0.67	0.112
Stratified Smooth	2.15	0.17	0.26	0.013
Stratified Wavy	9.92	0.07	0.11	0.003
Stratified Wavy	13.04	0.05	0.07	0.002

Experimental results show that as gas velocity increases (leading to a higher area of the pipe occupied by that phase) liquid holdup decreases. It occurs because there is less area available for liquid to flow. Discrepancy in liquid holdup is quite large for stratified-smooth flows as the table above shows. This can be explained by the differences between the liquid level at the inlet and at the outlet of the pipe for that kind of flow. This behavior was not observed for stratified-wavy flow.

The next two pictures show that, at the inlet, liquid height is much higher than at the outlet. It takes some distance for the liquid holdup inside the pipe to be fully developed. Commonly, the no-slip liquid holdup is observed at the pipe inlet. This is because there is not enough length for the liquid holdup to reach the fully developed slip liquid holdup value. Thus, the flow loop test section may not be long enough for the fully developed slip liquid holdup value to be reached, for the case of stratified smooth. Furthermore, calculated values do not consider the in-situ holdup differences because an equilibrium liquid height was assumed throughout the pipe.

It is complicated to precise accurately at which location slip and no-slip conditions take place on the flow. Thus, what is indeed important for validation purposes of the data acquired through the facility is that the measured value for liquid holdup must fall between the range of no-slip and slip holdups. That is exactly what happens with the results collected.

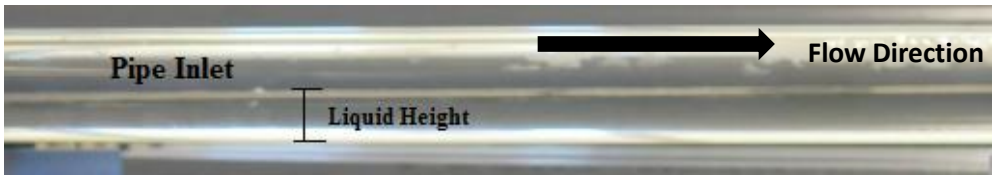

Figure 5.16 Liquid Height at the Inlet

Figure 5.17 Liquid Height at the Outlet

5.5. Slug Flow Pressure Drop

Pressure drop tests have been carried out for water and air slug flow for 1 degree upwards pipe. Measurement were taken between ports 1 and 5. Moreover, average liquid holdup data was also collected for the same set of flow conditions. Pressure drop and liquid holdup behavior versus gas velocity have been plotted for two different liquid flow rates as shown in the next figures and tables:

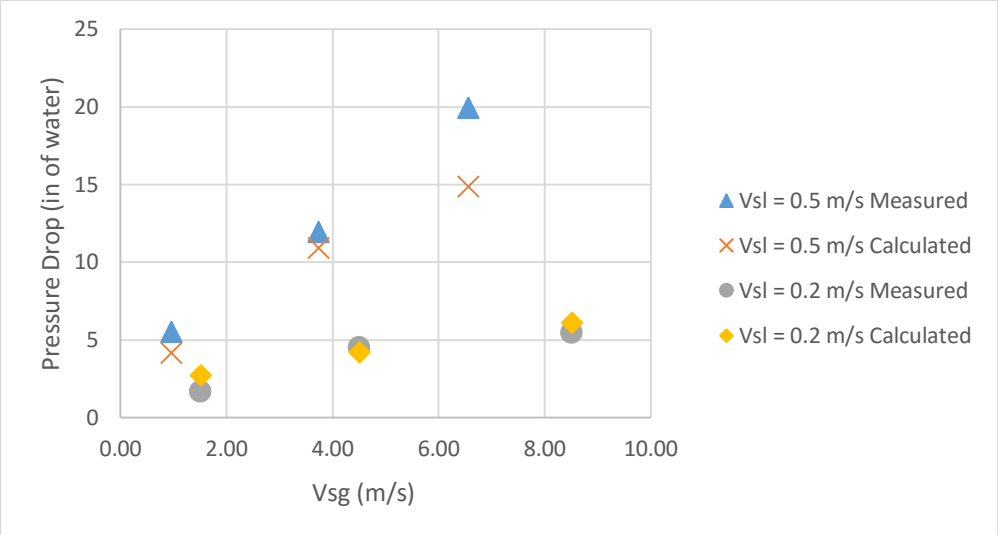

Figure 5.18 Slug Flow Pressure Drop Results

Table 13 Pressure Drop for Slug Flow Summary Table

v_{SL} (m/s)	v_{SG} (m/s)	Calculated (in of water)	Measured (in of water)	Discrepancy (%)
0.5	0.97	4.18	5.53	24.41%
	3.74	10.94	11.95	8.45%
	6.56	14.87	19.94	25.43%
0.2	1.52	2.72	1.65	-64.85%
	4.51	4.22	4.5	6.22%
	8.52	6.09	5.42	-12.36%

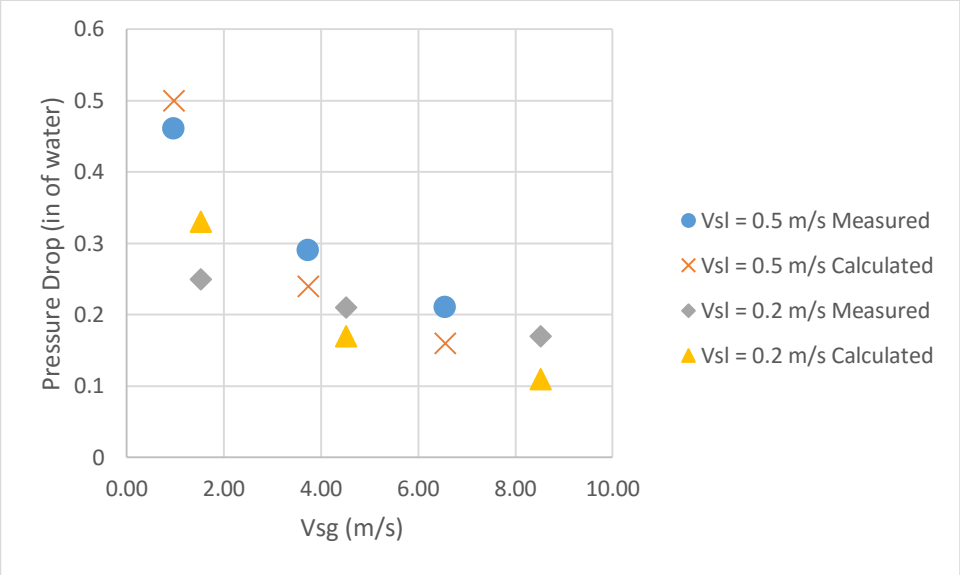

Figure 5.19 Slug Flow Average Liquid Holdup Results

Table 14. Slug Flow Slug Liquid Holdup Summary Table Results

v_{SL} (m/s)	v_{SG} (m/s)	Calculated (-)	Measured (-)	Discrepancy (%)
0.5	0.97	0.5	0.46	-8.70%
	3.74	0.24	0.29	17.24%
	6.56	0.16	0.21	23.81%
0.2	1.52	0.33	0.25	-32.00%
	4.51	0.17	0.21	19.05%
	8.52	0.11	0.17	35.29%

Results gathered through the facility match pretty well with the calculated ones as it can be noted. Pressure drop increased as gas velocity increased for the same liquid velocity. This trend was expected because frictional pressure losses should go up. Similarly, pressure drop goes up as liquid velocity increases for the same gas velocity.

On the other hand, liquid holdup decreases as gas velocities increases (for the same liquid velocity). It is explained by the shrinking in the area available for the liquid phase to flow. Moreover, an increase in liquid velocity leads to an increase in liquid holdup, for the same gas velocity, as expected.

Thus, the facility proves to produce good quality data for both parameters measured. Comparison with the calculated results and the low discrepancy between them show that the results obtained experimentally are reliable.

5.6. Slug Length

Twelve slug length were measured in horizontal pipe for superficial velocities of liquid and gas of 0.50 m/s (1.6 ft/s) and 1.83 m/s (6.0 ft/s), respectively. The recorded video file was uploaded to a computer and analyzed. Slug length could be measured with the aid of a measuring tape placed above the pipe.

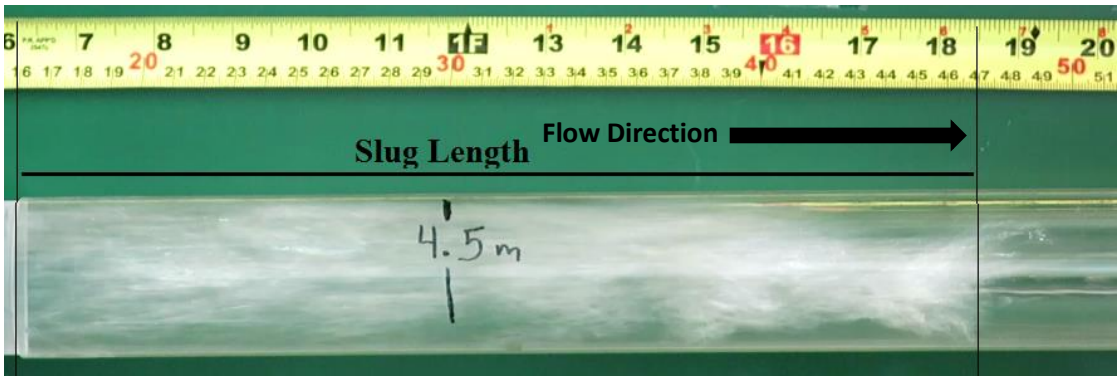

Figure 5.20 Slug Length Measurement

The number of occurrences of each slug length range is depicted in the histogram as follows:

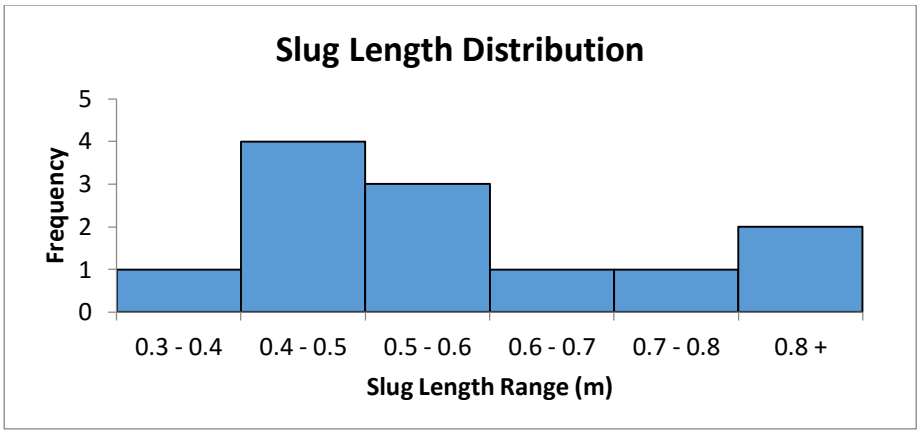

Figure 5.21 Slug Length Histogram

Three different correlations (shown in the last chapter) have been used to predict the average slug length for water and air slug flow. The next table shows the results comparing the measured and the calculated values for this parameter:

Table 15. Slug Length Results

Measured(m)	Brill et al. (1981) (m)	Scott et al. (1987) (m)	Marcano (1998) (m)
0.588	0.768	0.569	0.464
Discrepancy (%)	23.39%	-3.49%	-26.90%

Among all models, Scott et al.[34] is the one that better predicts the result obtained through the facility. More accurate results along with a lognormal probability distribution of slug length would be possible if more data was collected. However, it could not be accomplished due to the lack of time to finish this work. Even so, the reliability of the flow loop for slug length measurement is proved because results match pretty well with the correlations.

5.7. Translational Velocity

Results for translational velocity were obtained from the same test performed to measure slug length. Superficial velocities of liquid and gas were 0.50 m/s (1.6 ft/s) and 1.83 m/s (6.0 ft/s), respectively. Totally, 20 slugs from this test were analyzed to get the

results. The test video file was uploaded to a computer. The interface velocity of each slug was tracked in low-motion. The time taken for the interface between the tail of the Taylor bubble and front of the slug body to travel between two points was recorded. Translational velocity is calculated by dividing the distance between these two points by the time recorded. This process was repeated for 20 different slugs on the same test. Thus, several values for translational velocity were produced and then, averaged.

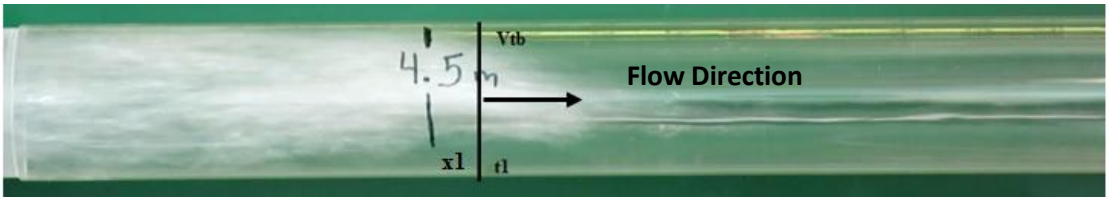

Figure 5.22 Translational Velocity Measurement Point 1

Figure 5.23 Translational Velocity Measurement Point 2

Measured values were compared to the calculated ones obtained from Bendiksen[61] approach for drift velocity as described in the calculation procedure of the last chapter. The next table summarizes the results obtained:

Table 16. Translational Velocity Results

Measured (m/s)	Bendiksen Approach (1984) (m/s)	Discrepancy (%)	Avg. SD (m)
2.697	3.126	13.73%	0.630

The measured value for translational velocity matches pretty well with the calculated one. They fall in the same range when the average standard deviation calculated is considered. Thus, the facility proofs to produce good quality data for this parameter as well.

5.8. Slug Frequency

Three tests in the horizontal pipe configuration have been conducted to obtain slug frequency. Gas superficial velocities were 1.84 (6.0), 7.04 (23.09), and 8.68 (28.48) m/s (ft/s). Liquid superficial velocity was set to remain constant at 0.5 m/s (1.6 ft/s). The video files (lasting approximately one minute each) were recorded close to the acrylic test section's outlet, where the slug flow was more developed. The number of times that a slug body passed over a fixed location was counted, so that slug frequency could be measured. Two correlations (shown in last chapter) have been used for testing the reliability of the facility. The measured and calculated values are compared as next table shows:

Table 17. Slug Frequency Summary Table

v_{SG} (m/s)	Measured (Hz)	Heywood and Richardson (1979) (Hz)	Discrepancy (%)	Zhao et al. (2015) (Hz)	Discrepancy (%)
1.84	0.633	0.663	-4.74%	0.885	28.47%
7.04	0.95	0.622	34.57%	0.736	-29.08%
8.68	1.016	0.695	31.59%	0.7248	-40.18%

Heywood and Richardson[86] correlation showed to match better the experimental results Discrepancy in this work can be credited to the counting of some incomplete slugs (slugs that are not fully developed). It is likely that the correlations tested above did not consider them. Even so, the state-of-the-art multiphase flow loop shows that it is capable of producing good slug frequency data.

5.9. Film Shape

The film profile in the stratified region of the slug flow can be calculated through two different methods: Dukler and Hubbard[27] and Taitel and Barnea.[31] Pictures of a slug test for horizontal flow, with a gas superficial velocity of 1.83 m/s (6.0 ft/s) and a liquid

superficial velocity of 0.5 m/s (1.6 ft/s) were taken. The film shape was analyzed in the computer. The next figure shows the film profile obtained:

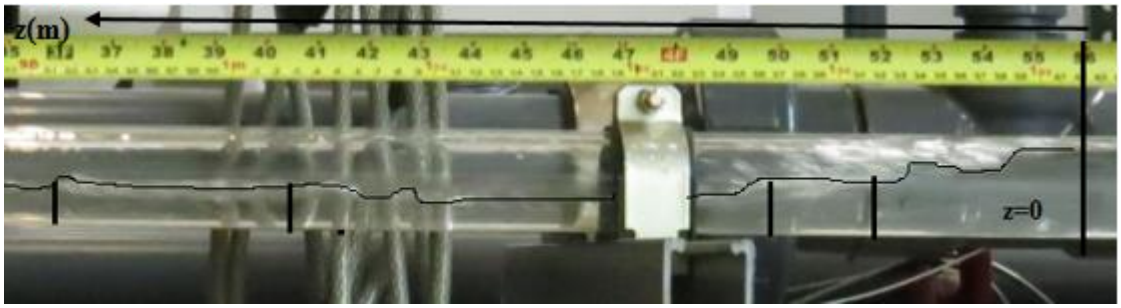

Figure 5.24 Picture of Film Profile

A region of 1 meter long was analyzed. The liquid height across that zone was measured with aid of a measuring tape and a Paint™ software. The point corresponding to $z = 0$ is the liquid height at the front of the Taylor bubble. The measured and the calculated values (obtained from the VBA code provided in Appendix C) of the film profile are represented in the dimensionless form in the next graph:

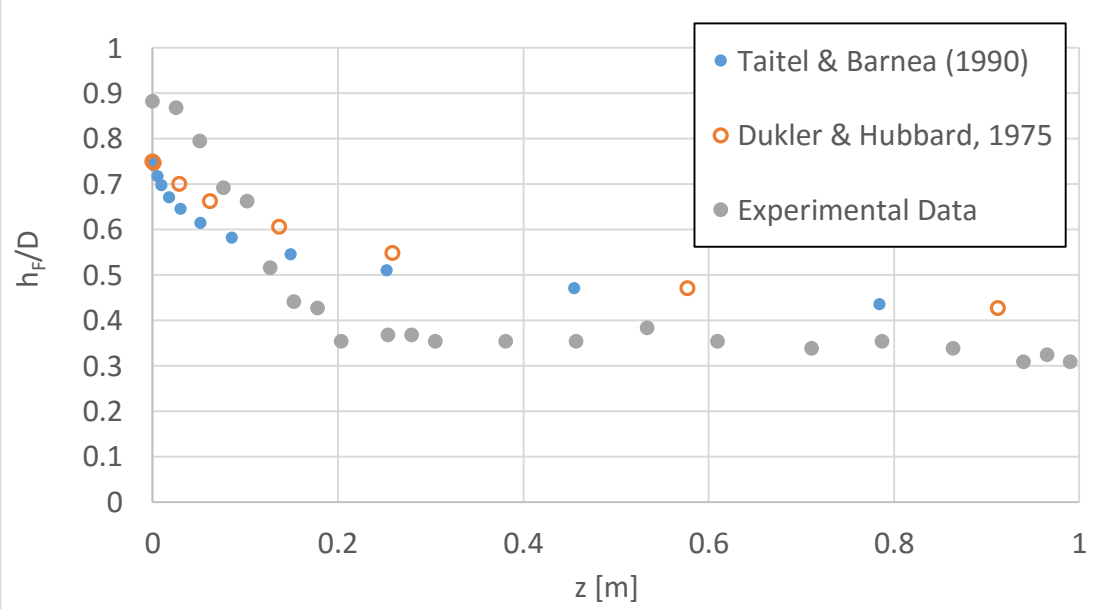

Figure 5.25 Film Shape Results

Analysys of the results suggest that both calculated and measured values are close and in the same order of magnitude. Next to Taylor bubble's front, measurement

of the liquid height was complicated because it was hard to exactly precise the gas-liquid interface.

5.10. Drift velocity

Pictures taken from the facility experiment and from CFD for three different inclination angles (0°, 1° and 5°) are shown next in Figures 5.26 through 5.31. It can be noticed, in all of them, a big similarity of the Taylor bubble shape and liquid height between the simulations and the experiment.

Several pen marks on the acrylic pipe (five in total, one meter away of each other) have been made. First, it was allowed the entrance of the Taylor bubble into the column of stagnant liquid. Then, the time taken by the bubble to travel between two consecutive marks was recorded with a stopwatch. Thus, drift velocity could be obtained by simply dividing the distance between two marks by the time taken by the bubble to flow between them.

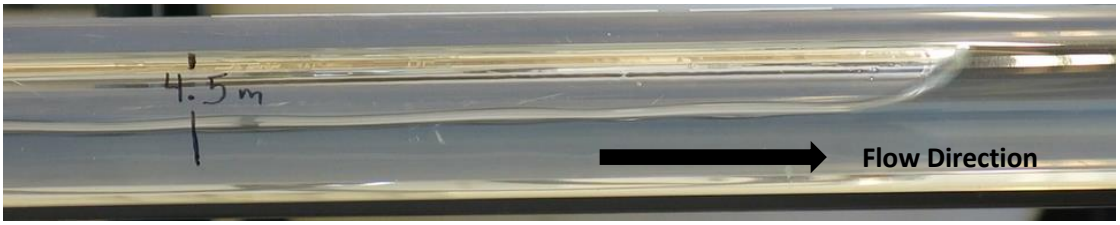

Figure 5.26 Taylor Bubble in Drift Velocity Measurement for 1 degrees upwards pipe

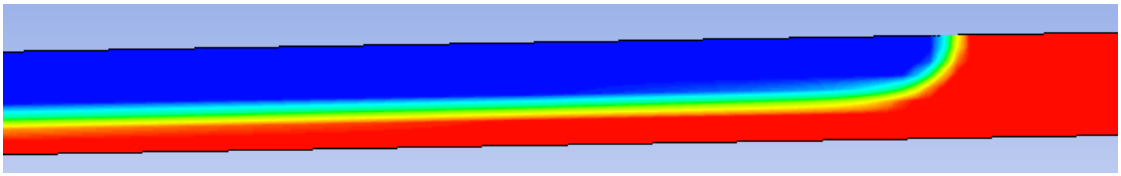

Figure 5.27 Taylor Bubble in Drift Velocity CFD Simulation for 1 degrees upwards pipe

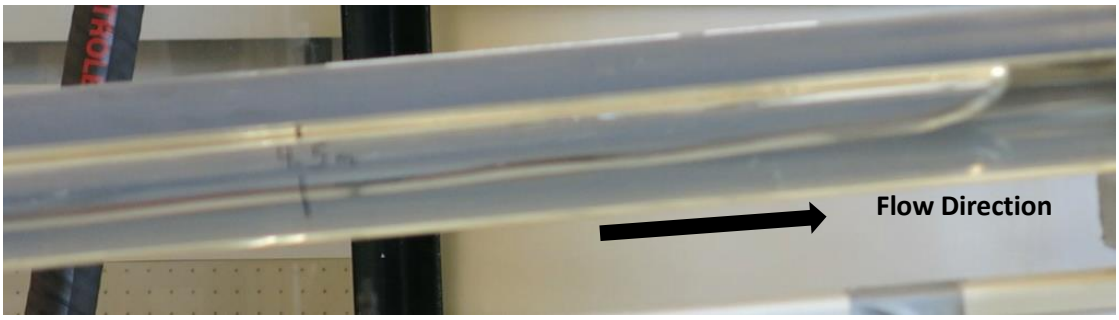

Figure 5.28 Taylor Bubble in Drift Velocity Measurement for 5 degrees upwards pipe

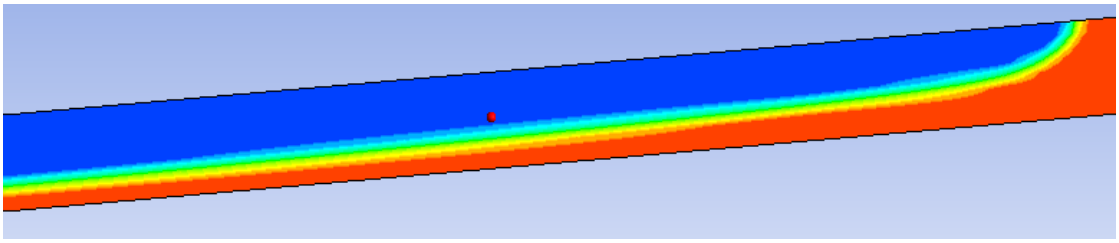

Figure 5.29 Taylor Bubble in Drift Velocity CFD Simulation for 5 degrees upwards pipe

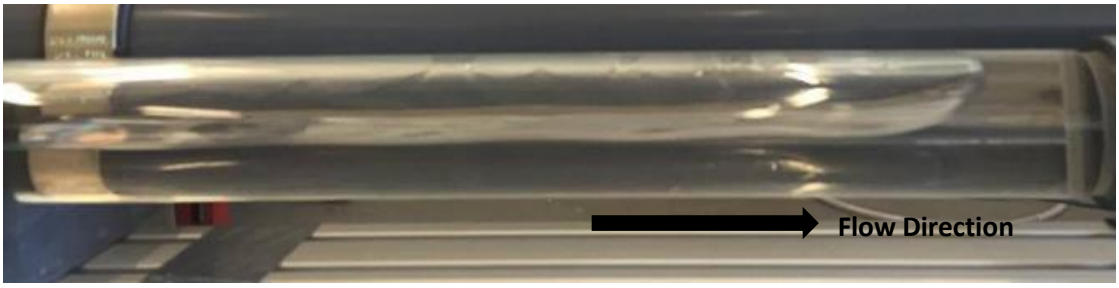

Figure 5.30 Taylor Bubble in Drift Velocity Measurement for Horizontal pipe

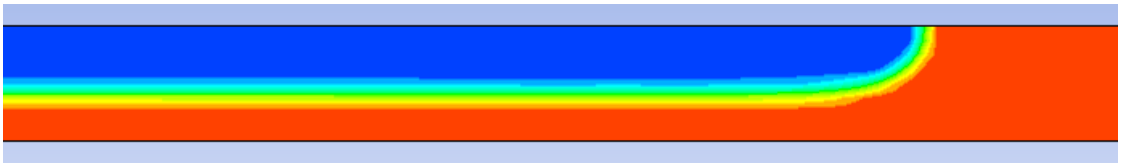

Figure 5.31 Taylor Bubble in Drift Velocity CFD Simulation for 1 degrees upwards pipe

The next graphs and table show the results obtained with experiment, Bendiksen[61] correlation and simulations for drift velocity:

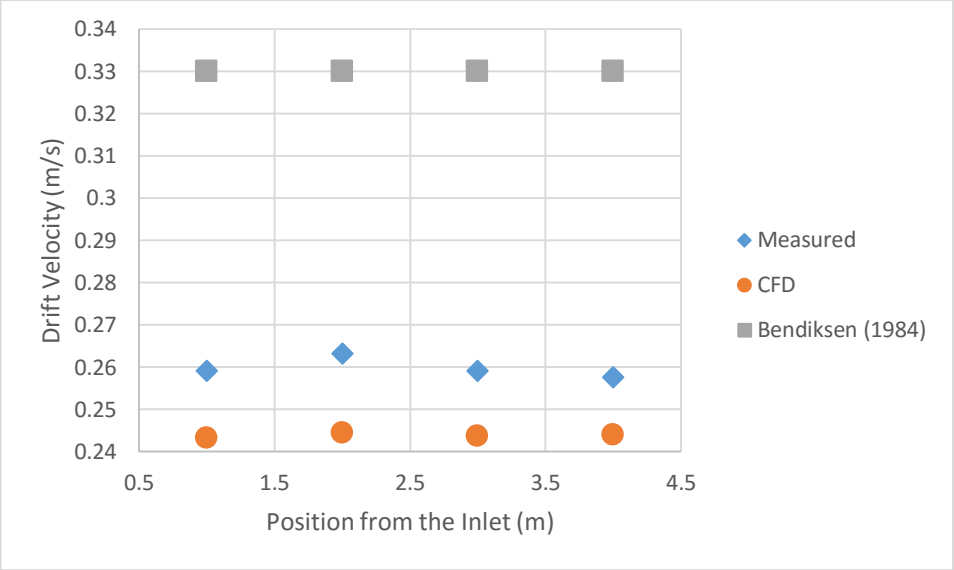

Figure 5.32 Drift Velocity Results for Horizontal Pipe

Table 18. Drift Velocity Results for Horizontal Pipe

Pipe Extension (m/s)	Calculated Drift Velocity (m/s)	Measured Drift Velocity (m/s)	CFD Drift Velocity (m/s)	Calculated Discrepancy (%)	CFD Discrepancy (%)
1	0.3301	0.2591	0.2432	21.52%	6.14%
2	0.3301	0.2632	0.2444	20.27%	7.14%
3	0.3301	0.2591	0.2437	21.52%	5.94%
4	0.3301	0.2577	0.2440	21.94%	5.32%

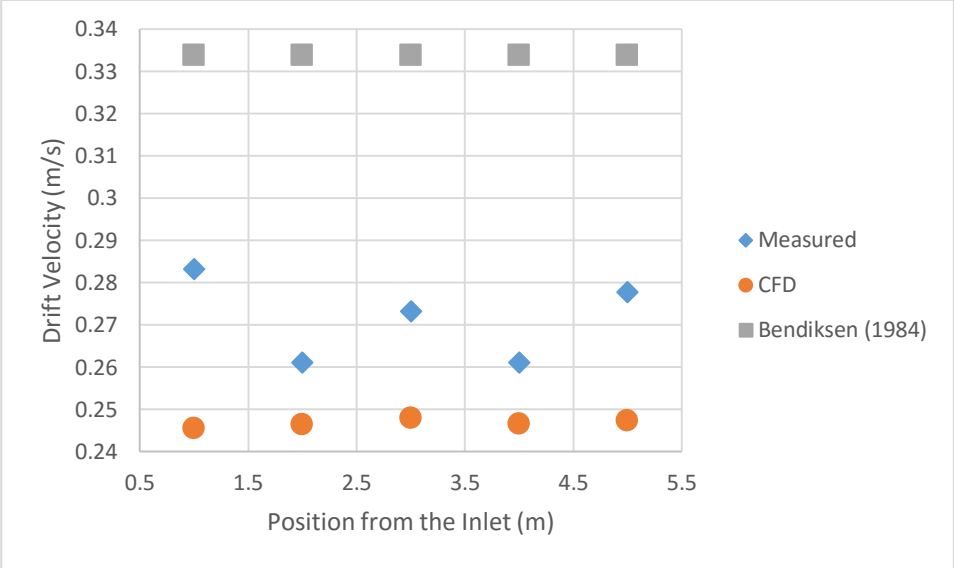

Figure 5.33. Drift Velocity Results for 1 degree upwards pipe

Table 19. Drift Velocity Results Summary Table for 1° Upwards Pipe

Pipe Extension (m/s)	Calculated Drift Velocity (m/s)	Measured Drift Velocity (m/s)	CFD Drift Velocity (m/s)	Calculated Discrepancy (%)	CFD Discrepancy (%)
1	0.3338	0.2833	0.2455	15.14%	13.34%
2	0.3338	0.2611	0.2464	21.79%	5.64%
3	0.3338	0.2732	0.2480	18.16%	9.24%
4	0.3338	0.2611	0.2466	21.79%	5.55%
5	0.3338	0.2778	0.2473	16.79%	10.97%

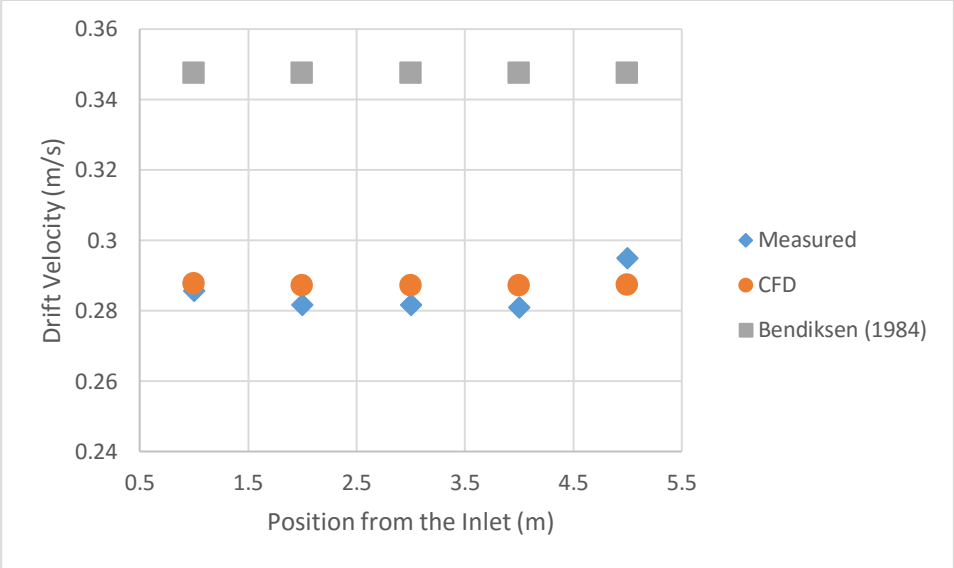

Figure 5.34. Drift Velocity Results for 5 degrees Upwards Pipe

Table 20. Drift Velocity Results for 5 degrees Upwards Pipe

Pipe Extension (m/s)	Calculated Drift Velocity (m/s)	Measured Drift Velocity (m/s)	CFD Drift Velocity (m/s)	Calculated Discrepancy (%)	CFD Discrepancy (%)
1	0.3476	0.2857	0.2876	17.81%	-0.67%
2	0.3476	0.2817	0.2872	18.97%	-1.95%
3	0.3476	0.2817	0.2871	18.97%	-1.92%
4	0.3476	0.2809	0.2872	19.20%	-2.24%
5	0.3476	0.2950	0.2874	15.14%	2.59%

As it can be observed, results agreed pretty well, especially when compared to CFD simulations. The relative discrepancy for all results falls within a range of +/- 22%. Moreover, drift velocity followed the expected behavior. Its value increases as pipe inclination angle goes up from the horizontal to 5°. It happens because the gravitational potential for liquid drainage increases as well.

One more interesting phenomenon to report is related to the experimental procedure to obtain drift velocity measurements. It was not clear in the literature whether the drain valve should remain open or not after trapping gas inside the trap section. Both tests were performed in order to clarify this question. In the first one, the

drain valve was left open throughout the test. In the second one, the drain valve was immediately closed after trapping gas. Both approaches yields the same results. Therefore, closing the drain valve or leaving it opened should not affect the drift velocity measured value at all.

CHAPTER VI

CONCLUSIONS AND RECOMMENDATIONS

The main objective of this work was to present to the reader an overall of the process of designing, building and commissioning a state-of-the art multiphase flow loop. Equipment used and operational procedures were described in detail to show how each parameter could be experimentally measured. Challenges faced throughout the process have been discussed. Moreover, several flow pattern videos were uploaded to a Youtube channel to encourage students and researchers around the world to understand better the Multiphase Flow phenomenon.

In addition, an in-depth literature review on slug flow and its main hydrodynamics parameters was detailed. It showed that the status of the research for low viscous liquids is well developed. The recent effort towards the production of non-conventional fields around the world reinforces the need of a better analysis of medium/high viscous liquid. Recently, much has been done on the high-viscosity/gas two-phase flow field. However, the majority of the correlations and models existent are inaccurate when applied to a wider range of viscosities. It becomes still more inaccurate when it comes to medium viscous liquid and higher inclination angles. The facility built will provide means to fill those data gaps in the future.

The reliability of the data produced was assessed by carrying out two-phase water and air experiment and by comparing them against calculated results from correlations and models existing in the literature. Several tests have been conducted, such as single-phase and two-phase pressure drop, liquid holdup, slug length and frequency, translational, drift velocity and film shape analysis. All of them prove to produce good quality data.

Moreover, CFD simulations were conducted for validation purposes of the data acquired through the facility for drift velocity. Numerical analyses and the bubble shape confirm that both ways yield similar results.

Some future recommendations are given in order to improve the performance and applicability of the flow loop for the next tests to be conducted with medium and high viscous oils:

- An automatic control of the pipe-supporting beam inclination angle could be implemented instead of the jack used, which hinders the application for inclination angles higher than 5° upwards;
- Installation of the optical sensors bought (not installed due to time limitation) can improve the accuracy of the data for slug flow measurements. Those sensors should be connected to the pipe and work by sending light, and receiving signal back. Depending on the kind of fluid passing through them (liquid or gas), the signal will be different. This way, tracking of the gas-liquid interface is improved;
- For multiphase flow measurements, the DP Transmitter used is not appropriate because gas bubbles were found constantly along the capillary tubing connecting the test section to the device. That line must be always liquid full for accurate pressure drop prediction. The solution found for that was to open the bleeding valve at the DP side every time before conducting gas-liquid tests. It allows the bubbles to come out of the line. Otherwise, misleading results are obtained. A DP Transmitter which has a mechanism to remove those bubbles from the line is more recommended;
- A small pipe or capillary tubing is highly recommended to connect between the DP Transmitter's bleeding valve and the lab's drain. This would avoid wetting the floor with any leaking fluid (especially for oils in the future);
- For liquid holdup experiment, it is suggested to trap the flow between valves 3 and 4, rather than between valves 2 and 4. This would provide more reliable results because the flow next to the outlet approaches to a

fully developed profile (the pipe inlet is dominated by non-developed flow). When flow in the entire pipe is trapped, the effect of the developing region (between valves 2 and 3) might contribute to less accurate results;

- More CFD simulations could not be accomplished in this work because the computational time to run simulations is extremely extensive using just one computer, especially for transient flows. Simulations of slug flow through CFD is highly recommended to compare against the results obtained experimentally in the facility (slug frequency, slug length, translational velocity and pressure drop);
- A Steel-made pipe should replace the PVC plastic capillary tubing used for the DP line in the future, even though they proved to work. Plastic was selected in this work to fit in the budget available. Steel is more appropriate to connect with the brass valves than plastic. After some time, there is a high chance that the PVC tubing will no longer support the weight of the fluid inside and it might fall down, causing some leaking.

REFERENCES

1. Shoham O. *Mechanistic Modeling of Gas-Liquid Two-Phase Flow in Pipes*.; 2006.
2. Hossein Alboudwarej; John Felix; Shawn Taylor. Highlighting Heavy Oil. *Summer Oilf Rev*. 2006.
3. Gomes TS. Multiphase Flow Loop for the Near Horizontal Hydrodynamics Parameters Measurement: Design, Construction, and Commissioning. 2016. https://drive.google.com/file/d/0BwMN-JpifGJ9XzZGdW5HSnhQWTA/view
4. Gomes TS. Excel Calculations. 2016. https://drive.google.com/file/d/0BwMN-JpifGJ9bkx1ejNKWWN3OGs/view?usp=sharing
5. Brunetti F. Escoamento permanente de fluido incompressível em condutos forçados. *Mecânica dos Fluidos*. 2008:163-205.
6. Bird RB, Stewart WE, Lightfoot EN. *Transport Phenomena*.; 2002.
7. Ansys Fluent Tutorial. https://www.sharcnet.ca/Software/Fluent6/html/ug/node462.htm.
8. Sverdrup HU, Johnson MW, Fleming RH. *The Oceans Their Physics, Chemistry, and General Biology*. New York: Prentice-Hall, Inc.; 1942.
9. Ove Bratland. *Single-Phase Flow Assurance*.; 2009.
10. Bertani C, Salve M De. State-of-Art and selection of techniques in multiphase flow measurement. *Ital Natl agency …*. 2010. http://www.sede.enea.it/attivita_ricerca/energia/sistema_elettrico/Nuovo-nucleare-fissione/LP2/LP2-033-1255-CIRTEN_POLITO_RL.pdf.
11. Hewitt GF. Gas-Liquid Flow. http://www.thermopedia.com/content/2/. Accessed May 26, 2016.
12. França PFDA. Modelagem de Escoamentos Multifásicos.
13. Brill JP. Modeling Multiphase Flow in Pipes. *Production*. 2010:16-17.

14. Kolev NI. Multiphase Flow Dynamics 4: Turbulence, Gas Adsorption and Release, Diesel Fuel Properties. In: Berlin, Heidelberg: Springer Berlin Heidelberg; 2012:39-65. doi:10.1007/978-3-642-20749-5_2.

15. Ansys Fluent Tutorial 6.3. https://www.sharcnet.ca/Software/Fluent6/html/ug/node910.htm.

16. Motion M, Paper W. Understanding the Challenges of Two-Phase Flow.

17. Paladino EE. Estudo do Escoamento Multifásico em Medidores de Vazão do tipo Pressão Diferencial. 2005:263.

18. Ghajar AJ. Non-boiling heat transfer in gas-liquid flow in pipes – a tutorial. *J Braz Soc Mech Sci Eng Rio Janeiro*. vol.27 no. doi:http://dx.doi.org/10.1590/S1678-58782005000100004.

19. Ramdin M. Benchmarking of Computational Fluid Dynamics for multiphase flows in pipelines Delft University of Technology. *Fluid Dyn*. 2010.

20. Taitel Y, Dukler AE. MODEL FOR PREDICTING FLOW REGIME TRANSITIONS IN HORIZONTAL AND NEAR HORIZONTAL GAS-LIQUID FLOW. *AIChE J*. 1976;22(1):47-55.

21. Souza RGS. Escoamento bifásico líquido-gás: previsão de gradientes de pressão com a correlação de Lockhart & Martinelli e fluidodinâmica computacional. 2009:74.

22. Benjamin TB. Gravity currents and related phenomena. *J Fluid Mech*. 1968;31(02):209-248. doi:10.1017/S0022112068000133.

23. R.H. Bonnecaze, W. Erskine EJG. Holdup and Pressure Drop for Two-Phase Slug Flow in Inclined Pipelines. *Esso Math Syst*. 1971.

24. Brill JP, Schmidt Z, Coberly WA, Herring JD, Moore DW. ANALYSIS OF TWO-PHASE TESTS IN LARGE-DIAMETER FLOW LINES IN PRUDHOE BAY FIELD. *Soc Pet Eng J*. 1981;21(3):363-378.

25. Bratland O. *Pipe Flow 2 Flow Assurance*.; 2010.

26. Lu M. Experimental and computational study of two-phase slug flow. 2015;(June).

27. Dukler, A.E., Hubbard MG. A model for gas-liquid slug flow in horizontal and near horizontal tubes. *Ind Eng Chem Fundam*. 1975;Volume 14(Issue 4):Pages 337-347.

28. M.C. Cook, C.H. Newton MB. Experimental Investigtion of Air-Water Slug Flow in Horizontal Pipes and Comparison with Existing Models. *Twefth Aust Fluids Mech Conf*. 1995.

29. Scott S, Shoham O, Brill J. Prediction of Slug Length in Horizontal, Large-Diameter Pipes. *SPE Prod Eng*. 1989;4(August):335-340. doi:10.2118/15103-PA.

30. Nicholson MK, Aziz K, Gregory GA. INTERMITTENT TWO PHASE FLOW IN HORIZONTAL PIPES: PREDICTIVE MODELS. *Can J Chem Eng*. 1978;56(6):653-663.

31. Taitel Y, Barnea D. A consistent approach for calculating pressure drop in inclined slug flow. *Chem Eng Sci*. 1990;45(5):1199-1206. doi:10.1016/0009-2509(90)87113-7.

32. Xiao JJ, Shonham O, Brill JP. A Comprehensive Mechanistic Model for Two-Phase Flow in Pipelines. *SPE Annu Tech Conf Exhib*. 1990:167-180. doi:10.2118/20631-MS.

33. Norris L. Correlation of Prudhoe Bay Liquid Slug Lengths and Holdups Including 1981 Large Diameter Flow Line Tests. *Intern Report, Exxon Prod Res Co*. 1982.

34. Scott, S. L., Shoham, O., and Brill JP. Modelling Slug Growth in Large Pipe Diameter Pipes. *Pap B2, Present 3rd Int Conf Multiph Flow, Hague*. 1987.

35. Nydal OJ, Pintus S, Andreussi P. Statistical characterization of slug flow in

horizontal pipes. *Int J Multiph Flow*. 1992;18(3):439-453. doi:10.1016/0301-9322(92)90027-E.

36. Marcano R, Chen XT, Sarica C, Brill JP. Study of slug characteristics for two-phase horizontal flow. *Proc SPE Int Pet Conf Exhib Mex*. 1998:213-219. doi:10.1016/S0920-5489(99)92000-7.

37. Siddiqui MI, Munir S, Heikal MR, Rashid Aziz AA, Dass SC. Slug Dynamics in a Nearly Horizontal Pipe Using Non-Invasive Measurement Techniques. *Mod Appl Sci*. 2015;9(9):50-57. doi:10.5539/mas.v9n9p50.

38. Gokcal B. AN EXPERIMENTAL AND THEORETICAL INVESTIGATION OF SLUG FLOW FOR HIGH OIL VISCOSITY IN HORIZONTAL PIPES. 2008.

39. Al-safran, Gokcal B, Cem Sarica, Sarica C. Investigation and Prediction of High-Viscosity Liquid Effect on Two-Phase Slug Length in Horizontal Pipelines. *SPE Prod Oper*. 2013;28(3):12-14. doi:10.2118/150572-PA.

40. Taitel Y, Bornea D, Dukler AE. Modelling flow pattern transitions for steady upward gas-liquid flow in vertical tubes. *AIChE J*. 1980;Volume 26(Issue 3):Pages 345-354. doi:10.1002/aic.690260304.

41. Barnea D, Brauner N. Holdup of the liquid slug in two phase intermittent flow. *Int J Multiph Flow*. 1985;11(1):43-49. doi:10.1016/0301-9322(85)90004-7.

42. Jeyachandra BC. EFFECT OF PIPE INCLINATION ON FLOW CHARACTERISTICS OF HIGH VISCOSITY OIL-GAS TWO-PHASE FLOW. 2011.

43. Brito R. EFFECT OF MEDIUM OIL VISCOSITY ON TWO-PHASE OIL-GAS FLOW BEHAVIOR IN HORIZONTAL PIPES. 2012.

44. Al-Safran EM. Probabilistic modeling of slug frequency in gas/liquid pipe flow using the Poisson probability theory. *J Pet Sci Eng*. 2016;138:88-96. doi:10.1016/j.petrol.2015.12.008.

45. Gregory, Scott. CORRELATION OF LIQUID SLUG VELOCITY AND FREQUENCY IN HORIZONTAL COCURRENT GAS-LIQUID SLUG FLOW. *AIChE J*. 1969;15(6):933-935.

46. Greskovich EJ, Shrier AL. Slug frequency in horizontal gas-liquid slug flow. *Ind Eng Chem Process Des Dev*. 1972;11(2):317-318.

47. Heywood NI, Richardson JF. Slug flow of air-water mixtures in a horizontal pipe: Determination of liquid holdup by ??-ray absorption. *Chem Eng Sci*. 1979;34(1):17-30. doi:10.1016/0009-2509(79)85174-X.

48. Hill TJ, Wood DG. New approach to the prediction of slug frequency. In: *Proceedings - SPE Annual Technical Conference and Exhibition*. Vol Pi. Publ by Soc of Petroleum Engineers of AIME; 1990:141-149.

49. Hill TJ, Wood DG. Slug flow: Occurrence, consequences, and prediction. In: *Proceedings of the University of Tulsa Centennial Petroleum Engineering Symposium*. Society of Petroleum Engineers (SPE); 1994:53-62.

50. Zabaras GJ. Prediction of slug frequency for gas-liquid flows. In: *Proceedings - SPE Annual Technical Conference and Exhibition*. Vol 1. ; 1999.

51. Al-Safran E. Investigation and prediction of slug frequency in gas/liquid horizontal pipe flow. *J Pet Sci Eng*. 2009;69(1-2):143-155. doi:10.1016/j.petrol.2009.08.009.

52. Marcano R, Chen XT, Sarica C, Brill JP. Study of slug characteristics for two-phase horizontal flow. In: *Proceedings of the SPE International Petroleum Conference & Exhibition of Mexico*. Soc Pet Eng (SPE); 1998:213-219.

53. Hernandez-Perez V, Abdulkadir M, Azzopardi BJ. Slugging Frequency Correlation for Inclined Gas-liquid Flow. *World Acad Sci, Eng*. 2010;2(5):44-51. http://www.waset.ac.nz/journals/waset/v61/v61-8.pdf.

54. Okezue CN. Application of the gamma radiation method in analysing the effect of liquid viscosity and flow variables on slug frequency in high viscosity oil-gas

horizontal flow. *WIT Trans Eng Sci*. 2013;79(4):447-461. doi:10.2495/MPF130371.

55. Schulkes R. Slug Frequencies Revisited. *15th Int Conf Multiph Prod Technol*. 2011;(1969):311-325.

56. Zhao Y, Yeung H, Lao L. Slug Frequency in High Viscosity Liquid and Gas Flow in Horizontal Pipes. 2013:105-117.

57. Nicklin DJ. Two-phase bubble flow. *Chem Eng Sci*. 1962;17(9):693-702.

58. Colmenares J, Ortega P, Padrino J, Trallero JL. Slug Flow Model for the Prediction of Pressure Drop for High Viscosity Oils in a Horizontal Pipeline. *Proc SPE Int Therm Oper Heavy Oil Symp*. 2001. doi:10.2523/71111-MS.

59. Zukoski EE. Influence of viscosity, surface tension, and inclination angle on motion of long bubbles in closed tubes. *J Fluid Mech*. 1966;25(04):821. doi:10.1017/S0022112066000442.

60. Davies RM, Taylor GI. The Mechanics of Large Bubbles Rising through Extended Liquids and through Liquids in Tubes. *Proc R Soc A Math Phys Eng Sci*. 1950;200(1062):375-390. doi:10.1098/rspa.1950.0023.

61. Bendiksen KH. An experimental investigation of the motion of long bubbles in inclined tubes. *Int J Multiph Flow*. 1984;10(4):467-483. doi:10.1016/0301-9322(84)90057-0.

62. Weber ME, Alarie A, Ryan ME. Velocities of extended bubbles in inclined tubes. *Chem Eng Sci*. 1986;41(9):2235-2240. doi:10.1016/0009-2509(86)85073-4.

63. Hasan AR, Kabir CS. Predicting multiphase flow behavior in a deviated well. *SPE Prod Eng*. 1989;3(4):474-482. doi:10.2118/15449-PA.

64. Carew PS, Thomas NH, Johnson AB. A physically based correlation for the effects of power law rheology and inclination on slug bubble rise velocity. *Int J Multiph Flow*. 1995;21(6):1091-1106. doi:10.1016/0301-9322(95)00047-2.

65. Alves IN, Shoham O, Taitel Y. Drift velocity of elongated bubbles in inclined pipes. *Chem Eng Sci*. 1993;48(17):3063-3070. doi:10.1016/0009-2509(93)80172-M.

66. Moreiras J, Pereyra E, Sarica C, Torres CF. Unified drift velocity closure relationship for large bubbles rising in stagnant viscous fluids in pipes. *J Pet Sci Eng*. 2014;124:359-366. doi:10.1016/j.petrol.2014.09.006.

67. Ben-Mansour R, Al-Sarkhi AS, Sarica C. Effects of high oil viscosity on drift velocity for horizontal pipes. *BHR Gr - 6th North Am Conf Multiph Technol*. 2008;(1962):207-214. doi:10.2118/115342-PA.

68. Andreussi P, Bonizzi M, Vignali A. Motion of elongated gas bubbles over a horizontal liquid layer. *14th Int Conf Multiph Prod Technol*. 2009:309-318.

69. Ramdin M. Benchmarking of Computational Fluid Dynamics for multiphase flows in pipelines. 2010.

70. Ramdin M, Henkes R. Computational Fluid Dynamics Modeling of Benjamin and Taylor Bubbles in Two-Phase Flow in Pipes. *J Fluids Eng*. 2012;134(4):41303. doi:10.1115/1.4006405.

71. Kroes RF, Henkes RAWM. CFD for the motion of elongated gas bubbles in viscous liquid. *BHR Gr - 9th North Am Conf Multiph Technol 2014*. 2014;(1):283-298. http://www.scopus.com/inward/record.url?eid=2-s2.0-84907059424&partnerID=tZOtx3y1.

72. Gregory GA, Nicholson MK, Aziz K. Correlation of the liquid volume fraction in the slug for horizontal gas-liquid slug flow. *Int J Multiph Flow*. 1978;4(1):33-39. doi:10.1016/0301-9322(78)90023-X.

73. Barnea D, Brauner N. Holdup of the liquid slug in two phase intermittent flow. *Int J Multiph Flow*. 1985;11(1):43-49. doi:10.1016/0301-9322(85)90004-7.

74. Gomez L., Shoham O, Taitel Y. Prediction of slug liquid holdup: horizontal to upward vertical flow. *Int J Multiph Flow*. 2000;26(3):517-521.

doi:10.1016/S0301-9322(99)00025-7.

75. Abdul-Majeed GH. Liquid slug holdup in horizontal and slightly inclined two-phase slug flow. *J Pet Sci Eng*. 2000;27(1-2):27-32. doi:10.1016/S0920-4105(99)00056-X.

76. Kora C, Sarica C, Zhang H-Q, Al-sarkhi A, Fahd K, Alsafran EM. Effects of High Oil Viscosity on Slug Liquid Holdup in Horizontal Pipes. *SPE Can Unconvetional Resour Conf 2011*. 2011;(November):1-15. doi:10.2118/102727-MS.

77. Al-safran E, Kora C, Sarica C. Prediction of liquid volume fraction in slugs in two-phase horizontal pipe flow with high viscosity liquid. *Int Conf Multiph Prod Technol*. 2013:415-428.

78. Rosa E. Flow structure in the horizontal slug flow. *9th BRAZILIAN Congr Therm Eng Sci*. 2004;3(2):1-11. http://www.abcm.org.br/pt/wp-content/anais/encit/2002/Paper-title/10/CIT02-0143.PDF.

79. Gokcal B, Wang Q, Zhang H, Sarica C, Tulsa U. Effects of High Oil Viscosity on Oil / Gas Flow Behavior in Horizontal Pipes. *SPE Annu Tech Conf Exhib*. 2006. doi:10.2118/102727-PA.

80. Hanratty LSCJ. Effect of Waves at a Gas-Liquid Interface on a Turbulent Air Flow. *J Fluid Mech*. 1968;31(03):467-479.

81. Zhao Y, Lao L, Yeung H. Investigation and prediction of slug flow characteristics in highly viscous liquid and gas flows in horizontal pipes. *Chem Eng Res Des*. 2015;102:124-137. doi:10.1016/j.cherd.2015.06.002.

82. ANSYS Fluent Tutorial Guide 16.0. https://www.google.com.br/url?sa=t&rct=j&q=&esrc=s&source=web&cd=5&cad=rja&uact=8&ved=0ahUKEwjczN-c0bnNAhXGh5AKHT5mDhcQFgg1MAQ&url=http://148.204.81.206/Ansys/150/ANSYS%20Fluent%20Tutorial%20Guide.pdf&usg=AFQjCNGrQYr956Lx

ci_I46MMzAU4ul7T. Published 2015.

83. Carestiato GL. Multiphase Flow Loop for the Near Horizontal Heat Transfer Parameters Measurement: Design, Construction, and Commissioning. 2016.

84. Gomes T, Carestitato G. Flow Patterns Videos. https://www.youtube.com/channel/UCF1-HmnUErXNHTJKrNcKu5g Published 2016.

85. Xiao JJ, Shoham O, Brill JP. Comprehensive mechanistic model for two-phase flow in pipelines. In: *Proceedings - SPE Annual Technical Conference and Exhibition*. Vol Pi. Publ by Soc of Petroleum Engineers of AIME; 1990:167-180.

86. Heywood NI, Richardson JF. Slug flow of air—water mixtures in a horizontal pipe: Determination of liquid holdup by γ-ray absorption. *Chem Eng Sci*. 1979;34(1):17-30. doi:10.1016/0009-2509(79)85174-X.

APPENDIX A

TWO-PHASE FLOW VARIABLES

The mixture mass flow rate (W [kg/s]) and the volumetric flow rate (q [m^3/s] can be obtained as follows:

$$W = W_L + W_G \tag{A.1}$$

$$q = q_L + q_G \tag{A.2}$$

Where W_L, q_L, W_G *and* q_G are the liquid mass and volumetric flowrate and the gas liquid mass and volumetric flowrate.

A.1 Liquid Holdup and Gas Void Fraction

Shoham[1] defines liquid hold up as the fraction of a volume element in a two-phase flow occupied by the liquid phase. In the same way, the gas void fraction is the fraction of the volume element occupied by the gas phase. For two phase flow, $0<H_L$ or $\alpha<1$ and $H_L + \alpha = 1$. Both are found at a given time and position in the pipe. The instantaneous average liquid holdup average can be found from the following integration of time and space simultaneously:

$$H_L = \frac{\iint H_L(r,t)drdt}{\int dr \int dt} \tag{A.3}$$

A.2 Superficial Velocity of the Phases

The superficial velocity of a phase is the velocity which would occur if that phase alone flows in the pipe.[1] Therefore, the gas superficial velocity (v_{GS}) and the liquid superficial velocity (v_{LS}) are given by:

$$v_{SG} = \frac{q_G}{A} \quad v_{SL} = \frac{q_L}{A} \tag{A.4}$$

Where A is the cross sectional area of the pipe.

A.3 Mixture Velocity

The total volumetric flow rate of both phases per unit of area is called mixture velocity [v_m] and it is given by:

$$v_m = \frac{q_G + q_L}{A} = v_{SG} + v_{SL} \tag{A.5}$$

When a no-slip condition of the phases is assumed, which means, gas and liquid are travelling at the same speed ($v_G = v_L$), the ratio of the liquid volumetric flow rate to the total volumetric flow rate is named no-slip liquid holdup:

$$\lambda_L = \frac{q_L}{q_G + q_L} = \frac{v_{SL}}{v_{SG} + v_{SL}} \tag{A.6}$$

A.4 Actual Velocity

Because each phase does not occupy the whole pipe cross sectional area, the superficial velocities are not the actual velocity of the phases, which are given by:

$$v_L = \frac{q_L}{A_L} = \frac{v_{SL}}{H_L} \quad and \quad v_G = \frac{q_G}{A_G} = \frac{v_{SG}}{1 - H_L} \tag{A.7}$$

A.5 Slip Velocity

As the actual velocities of the phases are not usually the same, the slip velocity represents the relative velocity between them:

$$v_{SLIP} = v_G - v_L \tag{A.8}$$

A.6 Average Density and Viscosity

The average density and viscosity of the mixture are based on each gas and liquid density and viscosity taking the holdup effect as a weighting criteria as the following equations show:

$$\rho_M = \rho_L H_L + \rho_G (1 - H_L) \tag{A.9}$$

$$\mu_M = \mu_L H_L + \mu_G (1 - H_L)$$

A.7 Slippage and Holdup

For no-slip conditions (gas and liquid with the same velocity), the in-situ liquid holdup is equal to the no-slip liquid holdup:

$$\lambda_L = \frac{q_L}{q_{G+}q_L} = H_L \tag{A.10}$$

This condition occurs in homogeneous flow or dispersed-bubble flow with high-liquid and low-gas flow rates. Due to the high liquid flow rate, the gas bubbles are carried out by the liquid phase at the same velocity, causing zero slippage.[1]

However, in most of the cases, the gas moves at a much greater speed than the liquid phase because of the buoyancy and lower frictional forces, which make slippage to take place. From the continuity equation, a higher gas velocity will cause its cross-sectional area to shrink while the cross-sectional are of liquid will increase. Therefore, liquid tend to accumulate in the pipe and the in-situ liquid holdup will be greater than for the no-slip liquid holdup: $H_L > \lambda_L$.[1]

APPENDIX B
PRESSURE DROP CALCULATION FOR TWO-PHASE GAS-LIQUID SLUG FLOW

The Taitel and Barnea[31] model has been chosen for calculating the slug flow pressure gradient in horizontal and inclined pipes. This section presents the main steps taken in order to obtain the pressure gradient for this flow pattern.

For a given set of known flow conditions, including the gas and liquid flow rates, gas and liquid properties, pipe geometry, Taitel and Barnea[31] model along with some closure relationships can be solved to predict the pressure gradient. This work considers the equilibrium liquid-film thickness case.

Additional input parameters are needed for the model and they come from closure relationships: slug liquid holdup, from Gomez et al.;[74] slug length and frequency, from Zabaras[50] and translational velocity, based on Bendiksen[61] approach for drift velocity:

$$H_{LLS} = \exp -(0.45\theta + 2.481 * 10^{-6} Re_S) \tag{B.1}$$

$$\frac{L_S}{D} = (32.0\cos^2\theta + 16.0\sin^2\theta)$$

$$f_s = 0.0226\left(\frac{v_{SL}}{gD}\right)^{1.2}\left(\frac{212.6}{v_m} + v_m\right)^{1.2}[0.836 + 2.75(sin\theta)^{0.25}]$$

$$Re_S = \frac{\rho_L v_m D}{\mu_L}$$

$$v_{TB} = 1.2 * v_M + 0.54 * \sqrt{gD} * \cos(\theta) + 0.35 * \sqrt{gD} * \sin(\theta)$$

Where θ is given in radians.

Having all those parameters calculated, the slug unit length and period- time taken for a slug unity to pass over a fixed location in the pipe- and film length can be calculated respectively as follows:

$$L_U = \frac{v_{TB}}{f_S} \tag{B.2}$$

$$T_U = \frac{1}{f_S}$$

$$L_F = L_U - L_S$$

Next, a mass balance applied on a control volume bounded by the front of the slug body and a plane in the back of the liquid film zone yields the pickup/shedding rate, *x*- amount of particles from the slow liquid film ahead of the slug body scooped/shed by it over time. Application of the continuity equation on the liquid phase results in:

$$x_L = (v_{TB} - v_{LLS})\rho_L A_P H_{LLS} \tag{B.3}$$

The model applied in this work considered a homogeneous no-slip holdup in the slug body. In others words, gas and liquid travels at the same speed- as dispersed bubble flow in a pseudo single-phase approach. Hence:

$$v_{LLS} = v_{GLS} = v_S = v_m = v_{LS} + v_{GS} \tag{B.4}$$

An overall mass balance applied over a slug unity yields:

$$w_L = \frac{\rho_L L_S A_p H_{LLS} + \int_0^{L_F} \rho_L A_p H_{LTB}\, dL}{T_U} - x_L \tag{B.5}$$

Assuming equilibrium/constant film thickness, the equation above is simplified to:

$$w_L = \frac{\rho_L L_S A_p H_{LLS} + \rho_L A_p H_{LTB} L_F}{T_U} - x_L \tag{B.6}$$

The only unknown is the liquid holdup in the stratified region, H_{LTB}. Solving for it, the equation is given as:

$$H_{LTB} = \frac{(w_L + x_L)T_U - \rho_L L_S A_p H_{LLS}}{\rho_L A_p L_F} \tag{B.7}$$

The liquid velocity in the Taylor bubble region is obtained from a similar procedure performed previously when the continuity equation for the liquid phase was applied on the slug body to find the pickup rate. Now doing the same technique for the Taylor bubble side:

$$x_L = (v_{TB} - v_M)\rho_L A_P H_{LLS} = (v_{TB} - v_{LTB})\rho_L A_P H_{LTB} \tag{B.8}$$

Rearranging and isolating the only unknown of the equation above, the liquid velocity in the stratified zone is obtained:

$$v_{LTB} = v_{TB} - (v_{TB} - v_M)\frac{H_{LLS}}{H_{LTB}} \tag{B.9}$$

Next, doing the same mass balance for gas phase to calculate the velocity of the gas phase inside the Taylor bubble, yields:

$$(v_{TB} - v_M)\rho_G A_P \alpha_{LLS} = x_G = (v_{TB} - v_{GTB})\rho_G A_P \alpha_{LTB} \tag{B.10}$$

$$\alpha = 1 - H_{LTB}$$

$$v_{GTB} = v_{TB} - \frac{(v_{TB} - v_M)\alpha_{LLS}}{\alpha_{LTB}}$$

The only unknown is v_{GTB} and it can be calculated from the above equations. After that, it is possible to calculate the slug unit liquid holdup (H_{LSU}) from:

$$H_{LSU} = \frac{H_{LLS}L_S + H_{LTB}L_F}{L_U} \tag{B.11}$$

Finally, the next step is to calculate pressure drop. Its components are split in two. For stratified region and slug body region (pseudo-single-phase approach), it can be calculated respectively as follows:

$$|-\Delta p_F| = L_F * \frac{\tau_F S_F + \tau_G S_G}{A_P} \tag{B.12}$$

$$|-\Delta p_S| = \rho_U g * \sin\theta * L_U + \frac{\tau_S \pi D}{A_p} \tag{B.13}$$

The first step is to calculate pressure drop for Taylor bubble region in slug flow. Treating Taylor bubble region as it was stratified flow, it is necessary to obtain the following geometry parameters- S_I, S_G, S_L, A_L, and A_G- to calculate the pressure drop for stratified flow case. All of them depends on the dimensionless equilibrium liquid level ($\tilde{h}_L$), which can be found iteratively through Newton numerical method based on the liquid holdup in the film region (H_{LTB}):

$$\tilde{A}_L = \frac{A_L}{D^2} = 0.25\left(\pi - arccos(2\tilde{h}_L - 1) + (2\tilde{h}_L - 1)\sqrt{1-(2\tilde{h}_L-1)^2}\right) \tag{B.14}$$

$$\begin{aligned} H_L = \frac{A_L}{0.25 * \pi D^2} &= \frac{\tilde{A}_L}{0.25 * \pi} \\ &= \frac{1}{\pi}\left(\pi - arccos\left(2\tilde{h}_L - 1\right) + \left(2\tilde{h}_L - 1\right)\sqrt{1-\left(2\tilde{h}_L-1\right)^2}\right) \end{aligned} \tag{B.15}$$

The dimensionless liquid level obtained is used then to calculate the geometrical parameters left:

$$\tilde{S}_I = \frac{S_I}{D} = \sqrt{1-\left(2\tilde{h}_L - 1\right)^2} \tag{B.16}$$

$$\tilde{S}_G = \frac{S_G}{D} = \arccos\left(2\tilde{h}_L - 1\right)$$

$$\tilde{S}_L = \frac{S_L}{D} = \pi - arccos\left(2\tilde{h}_L - 1\right)$$

$$A_L = H_{LTB} * A_p$$

$$A_G = A_p - A_L$$

$$d_L = \frac{4A_L}{S_L}$$

$$d_G = \frac{4A_G}{S_G + S_I}$$

After that, the actual Reynolds number in the Taylor bubble region for each phase considering turbulent flow for both can be calculated as follows:

$$Re_L = \frac{\rho_L |v_{LTB}| d_L}{\mu_L} \quad \text{(B.17)}$$

$$Re_G = \frac{\rho_G v_{GTB} d_G}{\mu_G} \quad \text{(B.18)}$$

Friction Factor is calculated from Blasius-type correlation for both phases:

$$f_L = 0.046 * {Re_L}^{-0.2} \quad \text{(B.19)}$$

$$f_G = 0.046 * {Re_G}^{-0.2} \quad \text{(B.20)}$$

The gas-liquid interface in the Taylor-bubble region is considered to be wavy, so the friction factor is approximately:

$$f_I = 0.0142 \quad \text{(B.21)}$$

Now shear stress in each phase is calculated from:

$$\tau_G = \frac{1}{2} f_G \rho_G v_{GTB}^2 \quad \text{(B.22)}$$

$$\tau_I \approx -\frac{1}{2} f_I \rho_I (v_{GTB} - v_{LTB})^2 \tag{B.23}$$

$$\tau_L = \frac{1}{2} f_L \rho_L |v_{LTB}| * v_{LTB} \tag{B.24}$$

Averaging ρ in the Taylor bubble zone (or film zone):

$$\rho_{TB} = H_{LTB} * \rho_L + (1 - H_{LTB}) * \rho_G \tag{B.25}$$

Gravitational pressure gradient and pressure loss in film zone (due to both gas and liquid phases) are obtained, respectively, from:

$$-\left.\frac{dp}{dz}\right|_g = \rho_{TB}\, g \sin\theta \tag{B.26}$$

$$-\Delta p_g = -\left.\frac{dp}{dz}\right|_g * L_F$$

Frictional pressure loss in the film zone is calculated as follows:

$$-\left.\frac{dp}{dz}\right|_F = \frac{\tau_L S_L + \tau_G S_G}{A_P} = -\left.\frac{dp}{dz}\right|_{LF} * L_F + -\left.\frac{dp}{dz}\right|_{GF} * L_F \tag{B.27}$$

$$-\Delta p_F = -\left.\frac{dp}{dz}\right|_F * L_F$$

Now pressure drop in the slug body is calculated:

$$-\Delta p_S = \rho_S g * \sin\theta * L_S + \frac{\tau_S \pi D}{A_p} \tag{B.28}$$

Averaging the slug density based on the liquid holdup in the slug body yields:

$$\rho_S = \rho_L * H_{LLS} + \rho_G * (1 - H_{LLS}) \tag{B.29}$$

Gravitational pressure loss in the slug body is:

$$-\Delta P_{S,gravity} = \rho_S g * \sin\theta * L_S \tag{B.30}$$

Frictional pressure loss in the slug body is obtained from:

$$\frac{\tau_S \pi D}{A_p} = \frac{2 f_s \rho_S v_s^2}{D} \tag{B.31}$$

Hence,

$$-\Delta P_{S,friction} = L_S * \frac{2 f_s \rho_S v_s^2}{D} \tag{B.32}$$

Averaging fluids properties allows calculation of slug body Reynolds number:

$$\mu_s = \mu_L * H_{LLS} + \mu_g (1 - H_{LLS}) \tag{B.33}$$

$$Re_s = \frac{\rho_s v_s D}{\mu_s} \tag{B.34}$$

Slug friction factor can be calculated now:

$$f_s = 0.046 * Re_s^{-0.2} \tag{B.35}$$

Total pressure loss in the slug body is obtained from adding up gravitational and frictional terms. To obtain total pressure drop per one slug unit, it just needs to add to this last amount calculated the pressure drop calculated previously due to the film zone. In the end, total pressure drop along the pipe is estimated as follows:

$$\Delta P = \left(\frac{-\Delta P_{s,total} + -\Delta P_{F,total}}{L_F + L_S} \right) * L_{pipe} \tag{B.36}$$

APPENDIX C
VBA CODE FOR FILM SHAPE CALCULATION

```
Option Explicit
Const Pi = 3.14159265358979
Const epsilon = 0.000001

Dim D As Double
Dim Ap As Double
Dim x As Double
Dim rho_L As Double
Dim rho_G As Double
Dim Mu_L As Double

Dim g As Double
Dim theta As Double
Dim v_SL As Double
Dim v_SG As Double
Dim v_TB As Double
Dim v_S As Double
Dim v_M As Double
Dim H_LLS As Double

Dim h_F As Double 'psig
Dim zLoop As Long
Dim TotalCount As Long
Dim SecondCondition As Integer

Dim debugVal As Double

Function Cal_HLTB(h_tilde As Double) As Double
    Dim hU As Double 'hU = 2 * h_tilde - 1
    hU = 2 * h_tilde - 1
    Cal_HLTB = 1 - 1 / Pi * (ArcCos(hU) - hU * (1 - hU ^ 2) ^ 0.5)
End Function
Function f_inv_HLLS(ht As Double, HLLS As Double) As Double
    Dim hU As Double 'hU = 2 * h_tilde - 1
    hU = 2 * ht - 1
    f_inv_HLLS = 1 - 1 / Pi * (ArcCos(hU) - hU * (1 - hU ^ 2) ^ 0.5)_
- HLLS
End Function

Function Cal_Inv_HLLS(ht As Double, HLLS As Double) As Double
Dim i As Double
Dim epsilon As Double
Dim slope As Double
Dim error As Double
'ht is the h_tilde that make HLTB = target HLTB
```

```
epsilon = 0.0000000001
For i = 1 To 100
    slope = (f_inv_HLLS(ht + epsilon / 2, HLLS) - _
        f_inv_HLLS(ht - epsilon / 2, HLLS)) / epsilon
    ht = ht - f_inv_HLLS(ht, HLLS) / slope
    error = Abs(f_inv_HLLS(ht, HLLS))
    If (error < epsilon) Then
        Exit For
    End If
Next i
Cal_Inv_HLLS = ht
End Function

Function Cal_HLTB_prime(h_tilde As Double, D As Double) As Double
    Dim hU As Double
    hU = 2 * h_tilde - 1
    Cal_HLTB_prime = 4 / Pi / D * (1 - (2 * h_tilde - 1) ^ 2) ^ 0.5
End Function

Function ArcCos(x As Double) As Double
    ArcCos = WorksheetFunction.Acos(x)
End Function
Function f_h_c(h_tilde As Double, x As Double, rho As Double, g As
Double, Ap As Double, D As Double, theta As Double) As Double
    'theta is in radiant
    f_h_c = x ^ 2 / rho / Ap * Cal_HLTB_prime(h_tilde, D) /_
(Cal_HLTB(h_tilde)) ^ 2 - Ap * Cal_HLTB(h_tilde) * rho * g *_
Cos(theta)
End Function

Function Cal_hCrit(guess As Double, x As Double, rho As Double, g As
Double, Ap As Double, D As Double, theta As Double) As Double
    Dim i As Integer
    Dim hh As Double
    Dim slope As Double
    Dim f_hh As Double
    Dim epsilon As Double
    epsilon = 0.0000001

    hh = guess

    For i = 1 To 100
        f_hh = f_h_c(hh, x, rho, g, Ap, D, theta)
        If Abs(f_hh) < epsilon Then
            Exit For
        End If
        slope = (f_h_c(hh + epsilon, x, rho, g, Ap, D, theta) -_
f_h_c(hh, x, rho, g, Ap, D, theta)) / epsilon
        hh = hh - f_hh / slope
    Next i
Cal_hCrit = hh
End Function
```

```
Function Cal_dh_f_dz(ht As Double, D As Double, _
Ap As Double, x As Double, rho_L As Double, Mu_L As Double _
, g As Double, theta As Double, v_SL As Double _
, v_TB As Double, v_S As Double, H_LLS As Double) As Double


Dim At_L As Double
Dim At_G As Double
Dim St_L As Double
Dim St_G As Double
Dim St_I As Double
Dim vt_L As Double
Dim vt_G As Double
Dim dt_L As Double
Dim dt_G As Double

Dim D_F As Double
Dim v_LTB As Double
Dim f_F As Double
Dim Tau_F As Double
Dim Re_F As Double
Dim v_F As Double
Dim S_F As Double
Dim H_LTB As Double
Dim H_LTB_prime As Double

St_I = (1 - (2 * ht - 1) ^ 2) ^ 0.5
St_G = ArcCos(2 * ht - 1)
St_L = Pi - St_G
At_G = 0.25 * (St_G - (2 * ht - 1) * St_I)
At_L = Pi / 4 - At_G
vt_L = Pi / 4 / At_L
vt_G = Pi / 4 / At_G
dt_L = 4 * At_L / St_L
dt_G = 4 * At_G / (St_G + St_I)
S_F = St_L * D

D_F = dt_L * D
v_F = (v_TB - v_S) * H_LLS / Cal_HLTB(ht)
v_LTB = v_TB - v_F
Re_F = rho_L * v_LTB * D_F / Mu_L
f_F = 0.046 * Re_F ^ (-0.2)
Tau_F = 0.5 * f_F * rho_L * v_LTB * v_LTB
H_LTB = Cal_HLTB(ht)
H_LTB_prime = Cal_HLTB_prime(ht, D)

Cal_dh_f_dz = (-Tau_F * S_F - Ap * H_LTB * rho_L * g * Sin(theta)) _
/ (x ^ 2 * H_LTB_prime / rho_L / Ap / H_LTB ^ 2 - Ap * H_LTB * rho_L_
* g * Cos(theta))


End Function
```

```
Function FSlope(h_F As Double) As Double

Dim At_L As Double
Dim At_G As Double
Dim St_L As Double
Dim St_G As Double
Dim St_I As Double
Dim vt_L As Double
Dim vt_G As Double
Dim dt_L As Double
Dim dt_G As Double

Dim D_F As Double
Dim v_LTB As Double
Dim f_F As Double
Dim Tau_F As Double
Dim Re_F As Double
Dim v_F As Double
Dim S_F As Double
Dim H_LTB As Double
Dim H_LTB_prime As Double
Dim ht As Double
Dim BackFlow As Double

BackFlow = 0

ht = h_F / D

St_I = (1 - (2 * ht - 1) ^ 2) ^ 0.5
St_G = ArcCos(2 * ht - 1)
St_L = Pi - St_G
At_G = 0.25 * (St_G - (2 * ht - 1) * St_I)
At_L = Pi / 4 - At_G
vt_L = Pi / 4 / At_L
vt_G = Pi / 4 / At_G
dt_L = 4 * At_L / St_L
dt_G = 4 * At_G / (St_G + St_I)
S_F = St_L * D

D_F = dt_L * D
v_F = (v_TB - v_S) * H_LLS / Cal_HLTB(ht)
v_LTB = v_TB - v_F
If v_LTB <= 0 Then
    BackFlow = 1
End If
Re_F = rho_L * Abs(v_LTB) * D_F / Mu_L
If Re_F > 2100 Then
    f_F = 0.046 * Re_F ^ (-0.2)
Else
    f_F = 16 / Re_F
End If
Tau_F = 0.5 * f_F * rho_L * Abs(v_LTB) * v_LTB
H_LTB = Cal_HLTB(ht)
```

```
H_LTB_prime = Cal_HLTB_prime(ht, D)

FSlope = (-Tau_F * S_F - Ap * H_LTB * rho_L * g * Sin(theta)) _
/ (x ^ 2 * H_LTB_prime / rho_L / Ap / H_LTB ^ 2 - Ap * H_LTB * rho_L_
* g * Cos(theta))

End Function
Function f_h_E(h_tilde As Double, x As Double, rho_L As Double, Mu_L
As Double, g As Double, Ap As Double, _
D As Double, theta As Double, v_TB As Double, v_S As Double, H_LLS As
Double) As Double
    'theta is in radiant

Dim At_L As Double
Dim At_G As Double
Dim St_L As Double
Dim St_G As Double
Dim St_I As Double
Dim vt_L As Double
Dim vt_G As Double
Dim dt_L As Double
Dim dt_G As Double

Dim D_F As Double
Dim v_LTB As Double
Dim f_F As Double
Dim Tau_F As Double
Dim Re_F As Double
Dim v_F As Double
Dim S_F As Double
Dim H_LTB As Double
Dim H_LTB_prime As Double
Dim ht As Double
Dim BackFlow As Double
ht = h_tilde

St_I = (1 - (2 * ht - 1) ^ 2) ^ 0.5
St_G = ArcCos(2 * ht - 1)
St_L = Pi - St_G
At_G = 0.25 * (St_G - (2 * ht - 1) * St_I)
At_L = Pi / 4 - At_G
vt_L = Pi / 4 / At_L
vt_G = Pi / 4 / At_G
dt_L = 4 * At_L / St_L
dt_G = 4 * At_G / (St_G + St_I)
S_F = St_L * D

D_F = dt_L * D
v_F = (v_TB - v_S) * H_LLS / Cal_HLTB(ht)
v_LTB = v_TB - v_F
If v_LTB <= 0 Then
    BackFlow = 1
End If
Re_F = rho_L * Abs(v_LTB) * D_F / Mu_L
```

```
If Re_F > 2100 Then
    f_F = 0.046 * Re_F ^ (-0.2)
Else
    f_F = 16 / Re_F
End If

Tau_F = 0.5 * f_F * rho_L * Abs(v_LTB) * v_LTB
H_LTB = Cal_HLTB(ht)

f_h_E = (-Tau_F * S_F - Ap * H_LTB * rho_L * g * Sin(theta))



End Function
Sub RKF45()
'Application.Calculation = xlCalculationManual
'Application.ScreenUpdating = False
Dim fa As Double 'take answer from FSlope function
Dim X3(1 To 13) As Double
Dim KK(1 To 6) As Double

Dim i As Integer
Dim h As Double
Dim RKFLoop As Long

Dim xx As Double
Dim E_RKF As Double 'RKF error (4th order - 5th order)
Dim E_RKFVal As Double
Dim XxAtZ As Double
Dim StepRatio As Double
Dim RKFEps As Double

Dim hMax As Double
Dim hMin As Double
Dim hminCondition As Integer
Dim Totalz As Double 'Total length [m]
Dim z As Double 'axial location [m]

Dim v_F As Double
Dim v_LTB As Double
Dim NextExit As Integer
NextExit = 0
SecondCondition = 0
'<Set Initial Values>
zLoop = 0
RKFEps = 0.00001

D = Cells(9, 7)
Ap = Cells(10, 7)
x = Cells(36, 7)
rho_L = Cells(14, 7)
Mu_L = Cells(15, 7)
g = Cells(6, 7)
```

```
theta = Cells(7, 7)
v_SL = Cells(11, 7)
v_TB = Cells(35, 7)
v_S = Cells(29, 7)
H_LLS = Cells(31, 7)


z = 0
h = 0.001
h_F = Cells(55, 7)
Totalz = Cells(48, 7) 'm
StepRatio = 1
hMax = 2 'm
hMin = 0.00001 'm
TotalCount = 0

v_F = (v_TB - v_S)
v_LTB = v_TB - v_F

'<zLoop>
For zLoop = 1 To 1000
    v_F = (v_TB - v_S) * H_LLS / Cal_HLTB(h_F / D)
    v_LTB = v_TB - v_F


    Cells(55 + zLoop, 10) = z
    Cells(55 + zLoop, 11) = h_F
    Cells(55 + zLoop, 13) = v_LTB
    If (z >= Totalz) Then Exit For
    XxAtZ = h_F

    fa = FSlope(h_F)

    hminCondition = 0
    For RKFLoop = 1 To 1000
        h = h * StepRatio

        If (h > hMax) Then h = hMax
        If (h < hMin) Then
        h = hMin
        hminCondition = 1
        End If

        If (z + h >= Totalz) Then
        h = Totalz - z
        End If



        'Cal KK1
        xx = h_F

        fa = FSlope(h_F)
```

```
        KK(1) = fa


        'Cal KK2

        xx = XxAtZ + h / 4# * KK(1)

        fa = FSlope(xx)

        KK(2) = fa

        'Cal KK3
        xx = XxAtZ + h * (3# / 32# * KK(1) + 9# / 32# * KK(2))

        fa = FSlope(xx)

        KK(3) = fa

        'Cal KK4
            xx = XxAtZ + h * (1932# / 2197# * KK(1) - 7200# / 2197#*_
KK(2) + 7296# / 2197# * KK(3))
        fa = FSlope(xx)

            KK(4) = fa


        'Cal KK5

            xx = XxAtZ + h * (439# / 216# * KK(1) - 8# * KK(2) + _
3680# / 513# * KK(3) - 845# / 4104# * KK(4))

        fa = FSlope(xx)

            KK(5) = fa


        'Cal KK6

            xx = XxAtZ + h * (-8# / 27# * KK(1) + 2# * KK(2) - 3544#_
/ 2565# * KK(3) + 1859# / 4104# * KK(4) - 11# / 40# * KK(5))

        fa = FSlope(xx)

            KK(6) = fa



            E_RKF = Abs(h * (KK(1) / 360# - 128# / 4275# * KK(3) -_
2197# / 75240# * KK(4) + KK(5) / 50# + 2# / 55# * KK(6)))

        E_RKFVal = E_RKF

        If (E_RKFVal <> 0#) Then
            StepRatio = (Abs(RKFEps * h / 2# / E_RKFVal)) ^ 0.25
```

```
        Else
            StepRatio = 1.25
        End If

        If (StepRatio < 0.05) Then StepRatio = 0.05
        If (StepRatio >= 1) Then
            Exit For
        End If

        If (RKFLoop > 999) Then
            MsgBox "error in RKF calculation"
        End If
    Next RKFLoop


    XxAtZ = XxAtZ + h * (16# / 135# * KK(1) + 6656# / 12825# * KK(3)_
+ 28561# / 56430# * KK(4) - 9# / 50# * KK(5) + 2# / 55# * KK(6))

    h_F = XxAtZ

    z = z + h
Next zLoop
'</zLoop>
Cells(54, 10) = TotalCount
'Application.ScreenUpdating = True
'Application.Calculation = xlCalculationAutomatic
End Sub


Function Cal_hE(guess As Double, x As Double, rho_L As Double, Mu_L
As Double, g As Double, Ap As Double, _
D As Double, theta As Double, v_TB As Double, v_S As Double, H_LLS As
Double) As Double
    Dim i As Integer
    Dim hh As Double
    Dim slope As Double
    Dim f_hh As Double
    Dim epsilon As Double
    epsilon = 0.0000001

    hh = guess

    For i = 1 To 100
        f_hh = f_h_E(hh, x, rho_L, Mu_L, g, Ap, D, theta, v_TB, v_S,_
H_LLS)
        If Abs(f_hh) < epsilon Then
            Exit For
        End If
        slope =(f_h_E(hh + epsilon, x, rho_L, Mu_L, g, Ap, D, theta,_
v_TB, v_S, H_LLS) _
        - f_h_E(hh, x, rho_L, Mu_L, g, Ap, D, theta, v_TB, v_S, _
H_LLS)) / epsilon
        hh = hh - f_hh / slope
    Next i
```

```
Cal_hE = hh
End Function



Function Cal_hC_TTBN(h_F As Double) As Double

Dim At_L As Double
Dim At_G As Double
Dim St_L As Double
Dim St_G As Double
Dim St_I As Double
Dim vt_L As Double
Dim vt_G As Double
Dim dt_L As Double
Dim dt_G As Double

Dim D_F As Double
Dim v_LTB As Double
Dim v_LLS As Double
Dim v_GLS As Double
Dim f_F As Double
Dim Tau_F As Double
Dim Re_F As Double
Dim v_F As Double
Dim S_F As Double
Dim H_LTB As Double
Dim H_LTB_prime As Double
Dim ht As Double
Dim v_G As Double

D = Cells(9, 7)
Ap = Cells(10, 7)
x = Cells(53, 7)
rho_L = Cells(14, 7)
rho_G = Cells(23, 7)
Mu_L = Cells(15, 7)
g = Cells(6, 7)
theta = Cells(7, 7)
v_SL = Cells(11, 7)
v_SG = Cells(16, 7)
v_TB = Cells(35, 7)
v_M = Cells(29, 7)
H_LLS = Cells(31, 7)
v_GLS = Cells(51, 7)
v_LLS = Cells(52, 7)

ht = h_F / D

St_I = (1 - (2 * ht - 1) ^ 2) ^ 0.5
St_G = ArcCos(2 * ht - 1)
St_L = Pi - St_G
```

```
At_G = 0.25 * (St_G - (2 * ht - 1) * St_I)
At_L = Pi / 4 - At_G
vt_L = Pi / 4 / At_L
vt_G = Pi / 4 / At_G
dt_L = 4 * At_L / St_L
dt_G = 4 * At_G / (St_G + St_I)
S_F = St_L * D

D_F = dt_L * D

H_LTB = Cal_HLTB(ht)
H_LTB_prime = Cal_HLTB_prime(ht, D)
v_F = (v_TB - v_LLS) * H_LLS / H_LTB
v_LTB = v_TB - v_F

'Re_F = rho_L * v_LTB * D_F / Mu_L
'f_F = 0.046 * Re_F ^ (-0.2)
'Tau_F = 0.5 * f_F * rho_L * v_LTB * v_LTB


v_G = (v_TB - v_GLS) * (1 - H_LLS) / (1 - H_LTB)

Cal_hC_TTBN = (rho_L - rho_G) * g * Cos(theta) - rho_L * v_F*(v_TB -_
v_LLS) * H_LLS / H_LTB ^ 2 * H_LTB_prime _
- rho_G * v_G * (v_TB - v_GLS) * (1 - H_LLS) / (1 - H_LTB) ^ 2 * _
H_LTB_prime


End Function


Function FSlope2(h_F As Double) As Double
Dim Denominator_TTBN As Double
Dim Numerator_TTBN As Double
Dim At_L As Double
Dim At_G As Double
Dim St_L As Double
Dim St_G As Double
Dim St_I As Double
Dim vt_L As Double
Dim vt_G As Double
Dim dt_L As Double
Dim dt_G As Double

Dim S_F As Double
Dim S_G As Double
Dim S_I As Double
Dim A_G As Double
Dim A_F As Double

Dim D_F As Double
Dim D_G As Double
Dim v_LTB As Double
Dim v_LLS As Double
```

```
Dim v_GLS As Double
Dim v_GTB As Double
Dim f_F As Double
Dim f_G As Double
Dim f_I As Double
Dim Tau_F As Double
Dim Tau_G As Double
Dim Tau_I As Double
Dim Re_F As Double
Dim Re_G As Double
Dim v_F As Double
Dim v_G As Double

Dim H_LLS As Double
Dim H_LTB As Double
Dim H_LTB_prime As Double
Dim ht As Double
Dim v_TB As Double
Dim v_M As Double

Dim rho_L As Double
Dim rho_G As Double
Dim Mu_L As Double
Dim Mu_G As Double
Dim x As Double
Dim g As Double
Dim theta As Double
Dim v_SL As Double
Dim v_SG As Double


D = Cells(9, 7)
Ap = Cells(10, 7)
x = Cells(53, 7)
rho_L = Cells(14, 7)
rho_G = Cells(23, 7)
Mu_L = Cells(15, 7)
Mu_G = Cells(24, 7)

g = Cells(6, 7)
theta = Cells(7, 7)
v_SL = Cells(11, 7)
v_SG = Cells(16, 7)
v_TB = Cells(35, 7)
v_M = Cells(29, 7)
H_LLS = Cells(31, 7)
v_GLS = Cells(51, 7)
v_LLS = Cells(52, 7)

ht = h_F / D

St_I = (1 - (2 * ht - 1) ^ 2) ^ 0.5
St_G = ArcCos(2 * ht - 1)
St_L = Pi - St_G
```

```
At_G = 0.25 * (St_G - (2 * ht - 1) * St_I)
At_L = Pi / 4 - At_G
vt_L = Pi / 4 / At_L
vt_G = Pi / 4 / At_G
dt_L = 4 * At_L / St_L
dt_G = 4 * At_G / (St_G + St_I)
S_F = St_L * D
D_F = dt_L * D
A_G = At_G * D ^ 2
A_F = At_G * D ^ 2
S_G = St_G * D
S_I = St_I * D

D_G = 4 * A_G / (S_G + S_I)

H_LTB = Cal_HLTB(ht)
H_LTB_prime = Cal_HLTB_prime(ht, D)
v_F = (v_TB - v_LLS) * H_LLS / H_LTB
v_LTB = v_TB - v_F
v_G = (v_TB - v_GLS) * (1 - H_LLS) / (1 - H_LTB)
v_GTB = v_TB - v_G

Denominator_TTBN = (rho_L - rho_G) * g * Cos(theta) _
- rho_L * v_F * (v_TB - v_LLS) * H_LLS / H_LTB ^ 2 * H_LTB_prime _
- rho_G * v_G * (v_TB - v_GLS) * (1 - H_LLS) / (1 - H_LTB) ^ 2 *_
H_LTB_prime

Re_F = rho_L * Abs(v_LTB) * D_F / Mu_L
Re_G = rho_G * Abs(v_GTB) * D_G / Mu_G

If (Re_F > 2100) Then
    f_F = 0.046 * Re_F ^ (-0.2)
Else
    f_F = 16 / Re_F
End If

If (Re_G > 2100) Then
    f_G = 0.046 * Re_G ^ (-0.2)
Else
    f_G = 16 / Re_G
End If

f_I = 0.014 'f_G
Tau_F = 0.5 * f_F * rho_L * Abs(v_LTB) * v_LTB
Tau_G = 0.5 * f_G * rho_G * Abs(v_GTB) * v_GTB
Tau_I = 0.5 * f_I * rho_G * Abs(v_GTB - v_LTB) * (v_GTB - v_LTB)

Numerator_TTBN = Tau_F * S_F / A_F - Tau_G * S_G / A_G - Tau_I * S_I
_
* (1 / A_F + 1 / A_G) + (rho_L - rho_G) * g * Sin(theta)
debugVal = Sin(theta)

FSlope2 = Numerator_TTBN / Denominator_TTBN
End Function
```

```
Sub RKF45_TTBN()
'Application.Calculation = xlCalculationManual
'Application.ScreenUpdating = False
Dim fa As Double 'take answer from FSlope function
Dim X3(1 To 13) As Double
Dim KK(1 To 6) As Double

Dim i As Integer
Dim h As Double
Dim RKFLoop As Long

Dim xx As Double
Dim E_RKF As Double 'RKF error (4th order - 5th order)
Dim E_RKFVal As Double
Dim XxAtZ As Double
Dim StepRatio As Double
Dim RKFEps As Double

Dim hMax As Double
Dim hMin As Double
Dim hminCondition As Integer
Dim Totalz As Double 'Total length [m]
Dim z As Double 'axial location [m]
SecondCondition = 0
'<Set Initial Values>
zLoop = 0
RKFEps = 0.00001


z = 0
h = 0.001
h_F = Cells(55, 7)
Totalz = Cells(48, 7) 'm
StepRatio = 1
hMax = 2 'm
hMin = 0.00001 'm
TotalCount = 0
'<zLoop>
For zLoop = 1 To 1000

    Cells(55 + zLoop, 17) = z
    Cells(55 + zLoop, 18) = h_F
    If (z >= Totalz) Then Exit For
    XxAtZ = h_F

    fa = FSlope2(h_F)

    hminCondition = 0
    For RKFLoop = 1 To 1000
        h = h * StepRatio

        If (h > hMax) Then h = hMax
        If (h < hMin) Then
```

```
        h = hMin
        hminCondition = 1
        End If

        If (z + h >= Totalz) Then
        h = Totalz - z
        End If



        'Cal KK1
        xx = h_F

        fa = FSlope2(h_F)

        KK(1) = fa


        'Cal KK2

        xx = XxAtZ + h / 4# * KK(1)

        fa = FSlope2(xx)

        KK(2) = fa

        'Cal KK3
        xx = XxAtZ + h * (3# / 32# * KK(1) + 9# / 32# * KK(2))

        fa = FSlope2(xx)

        KK(3) = fa

        'Cal KK4
            xx = XxAtZ + h * (1932# / 2197# * KK(1) - 7200# / 2197#*_
KK(2) + 7296# / 2197# * KK(3))
        fa = FSlope2(xx)

            KK(4) = fa


        'Cal KK5

            xx = XxAtZ + h * (439# / 216# * KK(1) - 8# * KK(2) +_
3680# / 513# * KK(3) - 845# / 4104# * KK(4))

        fa = FSlope2(xx)

            KK(5) = fa


        'Cal KK6
```

```
            xx = XxAtZ + h * (-8# / 27# * KK(1) + 2# * KK(2) - 3544#_
/ 2565# * KK(3) + 1859# / 4104# * KK(4) - 11# / 40# * KK(5))

        fa = FSlope2(xx)

            KK(6) = fa



            E_RKF = Abs(h * (KK(1) / 360# - 128# / 4275# * KK(3) -_
2197# / 75240# * KK(4) + KK(5) / 50# + 2# / 55# * KK(6)))

        E_RKFVal = E_RKF

        If (E_RKFVal <> 0#) Then
            StepRatio = (Abs(RKFEps * h / 2# / E_RKFVal)) ^ 0.25
        Else
            StepRatio = 1.25
        End If

        If (StepRatio < 0.05) Then StepRatio = 0.05
        If (StepRatio >= 1) Then
            Exit For
        End If

        If (RKFLoop > 999) Then
            MsgBox "error in RKF calculation"
        End If
    Next RKFLoop


    XxAtZ =XxAtZ + h * (16# / 135# * KK(1) + 6656# / 12825# * KK(3)+_
28561# / 56430# * KK(4) - 9# / 50# * KK(5) + 2# / 55# * KK(6))

    h_F = XxAtZ

    z = z + h
Next zLoop
'</zLoop>
Cells(52, 17) = TotalCount
'Application.ScreenUpdating = True
'Application.Calculation = xlCalculationAutomatic
End Sub

Function TTBN_Numerator(h_F As Double) As Double
Dim Denominator_TTBN As Double
Dim Numerator_TTBN As Double
Dim At_L As Double
Dim At_G As Double
Dim St_L As Double
Dim St_G As Double
Dim St_I As Double
Dim vt_L As Double
Dim vt_G As Double
```

```
Dim dt_L As Double
Dim dt_G As Double

Dim S_F As Double
Dim S_G As Double
Dim S_I As Double
Dim A_G As Double
Dim A_F As Double

Dim D_F As Double
Dim D_G As Double
Dim v_LTB As Double
Dim v_LLS As Double
Dim v_GLS As Double
Dim v_GTB As Double
Dim f_F As Double
Dim f_G As Double
Dim f_I As Double
Dim Tau_F As Double
Dim Tau_G As Double
Dim Tau_I As Double
Dim Re_F As Double
Dim Re_G As Double
Dim v_F As Double
Dim v_G As Double

Dim H_LLS As Double
Dim H_LTB As Double
Dim H_LTB_prime As Double
Dim ht As Double
Dim v_TB As Double
Dim v_M As Double

Dim rho_L As Double
Dim rho_G As Double
Dim Mu_L As Double
Dim Mu_G As Double
Dim x As Double
Dim g As Double
Dim theta As Double
Dim v_SL As Double
Dim v_SG As Double


D = Cells(9, 7)
Ap = Cells(10, 7)
x = Cells(53, 7)
rho_L = Cells(14, 7)
rho_G = Cells(23, 7)
Mu_L = Cells(15, 7)
Mu_G = Cells(24, 7)

g = Cells(6, 7)
theta = Cells(7, 7)
```

```
v_SL = Cells(11, 7)
v_SG = Cells(16, 7)
v_TB = Cells(35, 7)
v_M = Cells(29, 7)
H_LLS = Cells(31, 7)
v_GLS = Cells(51, 7)
v_LLS = Cells(52, 7)

ht = h_F / D

St_I = (1 - (2 * ht - 1) ^ 2) ^ 0.5
St_G = ArcCos(2 * ht - 1)
St_L = Pi - St_G
At_G = 0.25 * (St_G - (2 * ht - 1) * St_I)
At_L = Pi / 4 - At_G
vt_L = Pi / 4 / At_L
vt_G = Pi / 4 / At_G
dt_L = 4 * At_L / St_L
dt_G = 4 * At_G / (St_G + St_I)
S_F = St_L * D
D_F = dt_L * D
A_G = At_G * D ^ 2
A_F = At_G * D ^ 2
S_G = St_G * D
S_I = St_I * D

D_G = 4 * A_G / (S_G + S_I)

H_LTB = Cal_HLTB(ht)
H_LTB_prime = Cal_HLTB_prime(ht, D)
v_F = (v_TB - v_LLS) * H_LLS / H_LTB
v_LTB = v_TB - v_F
v_G = (v_TB - v_GLS) * (1 - H_LLS) / (1 - H_LTB)
v_GTB = v_TB - v_G

Denominator_TTBN = (rho_L - rho_G) * g * Cos(theta) _
- rho_L * v_F * (v_TB - v_LLS) * H_LLS / H_LTB ^ 2 * H_LTB_prime _
- rho_G * v_G * (v_TB - v_GLS) * (1 - H_LLS) / (1 - H_LTB) ^ 2 *_
H_LTB_prime

Re_F = rho_L * Abs(v_LTB) * D_F / Mu_L
Re_G = rho_G * Abs(v_GTB) * D_G / Mu_G

If (Re_F > 2100) Then
    f_F = 0.046 * Re_F ^ (-0.2)
Else
    f_F = 16 / Re_F
End If

If (Re_G > 2100) Then
    f_G = 0.046 * Re_G ^ (-0.2)
Else
    f_G = 16 / Re_G
End If
```

```
f_I = f_G
Tau_F = 0.5 * f_F * rho_L * Abs(v_LTB) * v_LTB
Tau_G = 0.5 * f_G * rho_G * Abs(v_GTB) * v_GTB
Tau_I = 0.5 * f_I * rho_G * Abs(v_GTB - v_LTB) * (v_GTB - v_LTB)

Numerator_TTBN = Tau_F * S_F / A_F - Tau_G * S_G / A_G - Tau_I *S_I _
_
* (1 / A_F + 1 / A_G) + (rho_L - rho_G) * g * Sin(theta)

TTBN_Numerator = Numerator_TTBN
End Function
```